

**Molecular mechanisms controlling
feeding state-dependent behavioral choice
in zebrafish**

Inaugural-Dissertation
to obtain the academic degree
Doctor rerum naturalium (Dr. rer. nat.)

submitted to the Department of Biology, Chemistry, Pharmacy
of Freie Universität Berlin

by

Margherita Zaupa

2023

The present work was carried out under the supervision of Dr. Suphansa Sawamiphak at the Max Delbrück Center for Molecular Medicine in the Helmholtz Association between October 2018 and December 2023.

1st reviewer: Dr. Suphansa Sawamiphak

2nd reviewer: Prof. Dr. Peter Robin Hiesinger

Date of defense: 15.07.2024

Acknowledgements:

I would like to thank Dr. Alessandro Filosa for his continued support throughout my doctoral studies. Thank you for maintaining an open and positive attitude and believing in the project even during the most challenging times. I would also like to thank Dr. Suphansa Sawamiphak for the supervision. I have a profound respect for your knowledge and sharp thinking.

I would like to extend my appreciation to Prof. Dr. Peter Robin Hiesinger, Prof. Dr. Ruben Portugues and Dr. Niccolò Zampieri for participating in my thesis advisory committee meetings. Your insightful inputs greatly helped me in improving the project.

I would also like to thank the Advanced Light Microscopy platform and the caretakers of the Zebrafish facility at the MDC for the technical support in carrying out my experiments.

Thank you to Anne, not only for the technical assistance but also for helping me with all kinds of personal problems.

A big thank you to all my colleagues: Laura, Dilem, Onur, Paul, Bhakti, Ilan, Akerke, Seulki, Anna, Tara, Clara and Giovanni for making the lab a warm place to work in. All the lively discussions (scientific and not) have greatly expanded my thinking. I will fondly remember all the moments spent together inside and outside the lab.

Last but not least, I will be forever grateful to my family for always being there for me, supporting me during good and hard days. Thank you for being a rock throughout my whole life.

Herewith I certify that I have prepared and written my thesis independently and that I have not used any sources and aids other than those indicated by me.

The results and the figures in this dissertation will be published in the paper: 'The Calmodulin-interacting peptide Pcp4a regulates feeding state-dependent behavioral choice in zebrafish'; Margherita Zaupa, Nagarjuna Nagaraj, Anna Sylenko, Herwig Baier, Suphansa Sawamiphak, Alessandro Filosa (currently under review).

The data presented in section 1.3.1. were generated by Nagarjuna Nagaraj (Biochemistry Core Facility, Max Planck Institute of Biochemistry, Martinsried, Germany. Current affiliation: Evotec München GmbH).

Table of contents:

Summary	1
Zusammenfassung	5
1. Introduction	9
1.1. <i>Decision-making behavior</i>	9
1.1.1. Ethological importance of decision-making.....	9
1.1.2. Neurotransmitters regulating decision-making.....	10
1.1.3. Modulation of sensorial processing for decision-making.....	11
1.1.4. Decision-making during foraging behavior.....	12
1.2. <i>Behavioral choice in zebrafish</i>	14
1.2.1. Zebrafish as a model in neuroscience.....	14
1.2.2. Behavioral choice during foraging behavior in zebrafish.....	17
1.2.3. Metabolic modulation of behavioral choice.....	21
1.3. <i>Molecular mechanisms regulating behavioral choice</i>	22
1.3.1. Proteomic screen.....	22
1.3.2. Pcp4a.....	23
2. Aims	25
3. Materials and Methods	26
3.1. <i>Zebrafish lines</i>	26
3.2. <i>Oligonucleotides</i>	26
3.3. <i>Antibodies</i>	27
3.4. <i>Chemicals and reagents</i>	27
3.5. <i>Solutions and buffers</i>	29
3.6. <i>Kits</i>	31
3.7. <i>Consumables</i>	31
3.8. <i>Equipment</i>	32
3.9. <i>Softwares and algorithms</i>	33
3.10. <i>Zebrafish lines and maintenance</i>	34
3.11. <i>Feeding protocol</i>	35
3.12. <i>Behavioral assays</i>	36
3.12.1. Spontaneous locomotion.....	36
3.12.2. Behavioral choice.....	37

3.12.3. Optomotor response (OMR).....	38
3.13. <i>qRT-PCR</i>	39
3.14. <i>Pharmacology</i>	40
3.15. <i>In situ hybridization</i>	41
3.16. <i>Immunohistochemistry</i>	42
3.17. <i>In vivo calcium imaging</i>	43
3.18. <i>Statistical analysis</i>	46
3.19. <i>Graphics</i>	47
4. Results	48
4.1. <i>pcp4a</i> expression.....	48
4.2. <i>Role of pcp4a in the modulation of behavioral choice</i>	50
4.3. <i>Tectal pcp4a+ neurons activity</i>	54
4.3.1. <i>Modulation of pcp4a+ tectal neurons activity by feeding state</i>	54
4.3.2. <i>Role of pcp4a in modulation of tectal neurons activity</i>	59
4.4. <i>Neuromodulation upstream pcp4a</i>	64
4.4.1. <i>Neurotransmitter systems upstream pcp4a</i>	64
4.4.2. <i>Food-dependent activation of dopaminergic neurons</i>	65
4.4.3. <i>Molecular signaling upstream pcp4a</i>	67
4.5. <i>Effect of dopaminergic signaling on tectal neurons activity</i>	69
5. Discussion	80
5.1. <i>A model of the pcp4a pathway for feeding state-dependent modulation of behavioral choice</i>	80
5.2. <i>Neuromodulatory systems regulating behavioral choice</i>	84
5.3. <i>Mechanisms for Pcp4a-dependent regulation of neuronal activity and behavioral switch</i>	86
5.4. <i>Translational potential of this study</i>	88
6. Bibliography	90
List of abbreviations	103
List of figures	105

Summary:

Animals need to switch behavioral strategies to adapt to changing environmental conditions. The ability to choose the most advantageous response to a situation is crucial for survival. These decisions are influenced by environmental factors and internal signals such as physiological needs.

During foraging behavior, larval zebrafish approach potential preys and avoid potential predators. The choice is influenced by external factors, such as the size of the object they are interacting with: small visual stimuli are perceived as preys while large objects are considered predators. Moreover, it was previously shown that behavioral choice during feeding behavior is modulated by metabolic state: food-deprived larvae are more likely to take risks during hunting and approach small, prey-like objects compared to fed fish. It was also demonstrated that this modulation is mediated by a differential processing of visual stimuli. In zebrafish the visual information is relayed from the retina to a midbrain structure, the optic tectum, where sensory inputs are integrated. Distinct downstream motor centers are subsequently activated to perform either an approach or an escape. This makes the optic tectum a major center for decision-making. In food-deprived larvae, tectal neurons respond preferentially to small visual stimuli compared to fed siblings, showing a shift of the tuning towards cues important for survival. These results suggest feeding induces a change in the excitability of tectal neurons to modulate behavioral choice, however the molecular mechanisms underlying this phenomenon are still unclear.

To fill the gap by investigating the molecular pathways mediating the influence of metabolic state on behavioral choice, a proteomic study was performed to identify proteins differentially abundant in fed versus food-deprived larvae. Among all the hits, an especially interesting candidate was selected: a small peptide known to modulate neuronal excitability, Pcp4a, which was less abundant in fed larvae compared to food-deprived fish. *pcp4a* mRNA levels were also found to be lower in brain samples from fed larvae, suggesting that feeding modulates its expression through a transcriptional mechanism. PCP4, the mammalian ortholog of Pcp4a is known to bind to calmodulin, a molecule

involved in several processes during neuronal activation, and to inhibit its target enzymes such as CaMKII. This results in modulation of neuron excitability *in vivo*. Since *pcp4a* is expressed in the optic tectum in zebrafish, we hypothesized that it may play a role in the regulation of tectal neurons excitability by feeding state.

To test this hypothesis, I first looked at the role of *pcp4a* in the modulation of behavioral choice by feeding state using a loss-of-function model. Food-deprived larvae lacking Pcp4a show increased avoidance of small objects in a size discrimination assay, thus phenocopying behavioral choice of fed larvae. To understand if the effect was due to modulation of tectal neurons excitability, I investigated the response to visual stimuli of different size in tectal neurons expressing *pcp4a* (*pcp4a*⁺). Tectal *pcp4a*⁺ neurons in fed larvae responded preferentially to large objects compared to starved siblings; the same response profile was observed in larvae lacking Pcp4a, suggesting that Pcp4a mediates the effect of feeding on tectal neurons excitability. I then looked into the neuromodulatory mechanisms mediating the influence of metabolic signals on *pcp4a* expression. I found that feeding increased activity of dopaminergic neurons in the pretectum and hypothalamus, which could exert an effect on tectal *pcp4a*⁺ neurons through their direct and indirect projections to the optic tectum. Indeed, pharmacological activation of dopaminergic signaling through D2 receptors decreased *pcp4a* expression in food-deprived larvae, mimicking the effect of feeding. Dopamine controls *pcp4a* transcription through the D2 receptor - cAMP signaling cascade. Pharmacological activation of dopaminergic signaling induced a shift of the response profile of *pcp4a*⁺ tectal neurons towards large stimuli by altering the tuning properties of individual neurons.

In this study we elucidate a novel molecular mechanism mediating the effect of metabolic state on behavioral choice in zebrafish. In our model, feeding activates dopaminergic neurons in the pretectum and hypothalamus, which project to the optic tectum. Dopaminergic signaling through D2 receptors induces a decrease of *pcp4a* expression through a transcriptional mechanism, which results in a shift of the response profile of *pcp4a*⁺ tectal neurons towards large visual stimuli through a cell-autonomous mechanism. This ultimately leads to increased avoidance of small stimuli during foraging behavior.

This study advances our knowledge of the molecular mechanisms mediating neuromodulation of decision-making behavior.

Zusammenfassung:

Tiere müssen ihre Verhaltensstrategien ändern, um sich an veränderte Umweltbedingungen anzupassen. Die Fähigkeit, die vorteilhafteste Reaktion auf eine Situation zu wählen, ist entscheidend für das Überleben. Diese Entscheidungen werden durch Umweltfaktoren und interne Signale (wie physiologische Bedürfnisse) beeinflusst.

Bei der Nahrungssuche nähern sich die Zebrafisch-Larven potenziellen Beuten und meiden potenzielle Räuber. Die Entscheidung wird durch Außenfaktoren beeinflusst, u.a. durch die Größe des Objekts, mit dem sie interagieren: kleine visuelle Reize werden als Beute wahrgenommen, während große Objekte als Räuber angesehen werden. Eine frühere Studie hat außerdem gezeigt, dass das Verhalten während der Nahrungssuche durch den Stoffwechszustand moduliert wird. Nahrungsdeprivierte Larven sind bei der Jagd risikofreudiger und nähern sich kleinen, beuteartigen Objekten eher als gefütterte Fische. Es wurde auch nachgewiesen, dass diese Modulation durch eine unterschiedliche Verarbeitung visueller Reize ausgelöst wird. Bei Zebrafischen werden die visuellen Informationen von der Netzhaut an eine Mittelhirnstruktur, den Tectum Opticum, weitergeleitet, wo die sensorischen Inputs integriert werden. Anschließend werden die respektiven nachgeschaltete motorische Zentren aktiviert, um entweder eine Annäherung oder eine Flucht durchzuführen. Damit ist der Tectum Opticum ein wichtiges Zentrum für die Entscheidungsfindung. Bei Larven, denen die Nahrung entzogen wurde, reagieren die Tectum-Neuronen häufiger auf kleine visuelle Reize im Vergleich zu gefütterten Geschwistern, was eine Verschiebung der Abstimmung in die Richtung überlebenswichtiger Signale zeigt. Diese Ergebnisse deuten darauf hin, dass die Fütterung eine Veränderung der Erregbarkeit von Tectum-Neuronen bewirkt, um das Verhalten zu beeinflussen. Die molekulare Mechanismen, die das Phänomen bestimmen, sind allerdings noch unklar.

Um diese Lücke zu schließen, wurden die molekularen Signalwege untersucht, die den Einfluss des Stoffwechszustands auf das Verhalten vermitteln. Und zwar wurde eine Proteomstudie durchgeführt, um Proteine zu identifizieren, die in gefütterten Larven unterschiedlich häufig vorkommen als in

nahrungsdeprivierten Larven. Unter den Treffern wurde ein besonders interessanter Kandidat ausgewählt: ein kleines Peptid, von dem man weiß, dass es die neuronale Erregbarkeit moduliert, Pcp4a. Dies kam in gefütterten Larven weniger häufig vor als in nahrungsdeprivierten Fischen. Die mRNA-Spiegel von *pcp4a* waren in Gehirnproben von gefütterten Larven ebenfalls niedriger, was darauf hindeutet, dass die Fütterung die Expression von diesem Peptid durch einen Transkriptionsmechanismus moduliert. PCP4, das Säugetierortholog von Pcp4a, bindet bekanntermaßen an Calmodulin, ein Molekül, das an mehreren Prozessen während der neuronalen Aktivierung beteiligt ist, und inhibiert seine Zielenzyme (wie z.B. CaMKII). Dies führt zu einer Modulation der neuronalen Erregbarkeit *in vivo*. Da *pcp4a* im Tectum Opticum des Zebrafisches exprimiert wird, stellten wir die Hypothese auf, dass es eine Rolle bei der Regulierung der Erregbarkeit von Tectum-Neuronen durch den Fütterungszustand spielen könnte.

Um diese Hypothese zu testen, erforschte ich zunächst die Rolle von *pcp4a* bei der Modulation des Verhaltens durch den Fütterungszustand anhand von einem Loss-of-Function-Modell. Nahrungsdeprivierte Larven, denen Pcp4a fehlt, zeigen in einem Größendiskriminierungstest eine erhöhte Meidung kleiner Objekte, und phänokopieren damit das Verhalten gefütterter Larven. Um herauszufinden, ob dieser Effekt auf eine Modulation der Erregbarkeit der Tectum-Neuronen zurückzuführen ist, habe ich die Reaktion auf visuelle Reize unterschiedlicher Größe in Tectum-Neuronen untersucht, die *pcp4a* exprimieren (*pcp4a+*). *pcp4a+*-Tectum-Neuronen in gefütterten Larven reagierten häufiger auf große Objekte im Vergleich zu nahrungsdeprivierten Geschwistern. Das gleiche Reaktionsprofil wurde bei Larven ohne Pcp4a beobachtet, was darauf hindeutet, dass Pcp4a die Wirkung der Fütterung auf die Erregbarkeit der Tectum-Neuronen beeinflusst. Anschließend untersuchte ich die neuromodulatorischen Mechanismen, die den Einfluss von Stoffwechselsignalen auf die *pcp4a*-Expression vermitteln. Ich fand heraus, dass die Fütterung die Aktivität dopaminerger Neuronen im Prätektum und im Hypothalamus erhöht. Diese Neuronen könnten, über ihre direkten und indirekten Projektionen in den Tectum Opticum, eine Wirkung auf *pcp4a+*-Tectum-Neuronen ausüben. In der Tat verringerte die pharmakologische Aktivierung der Signalübertragung durch D2-Rezeptoren die *pcp4a*-Expression

in nahrungsdeprivierten Larven, und ahmte somit die Wirkung der Fütterung nach. Dopamin steuert die *pcp4a*-Transkription über die Signalkaskade D2-Rezeptor - cAMP. Die pharmakologische Aktivierung der dopaminergen Signalübertragung führte zu einer Verschiebung des Reaktionsprofils von *pcp4a*+Tectum-Neuronen auf große Reize, indem die Abstimmungseigenschaften einzelner Neuronen verändert wurden.

In dieser Studie klären wir einen neuen molekularen Mechanismus auf, der die Auswirkung des Stoffwechszustands auf das Verhalten bei Zebrafischen steuert. In unserem Modell aktiviert die Fütterung dopaminerge Neuronen im Prätektum und Hypothalamus, die in den Tectum Opticum projizieren. Die dopaminerge Signalübertragung durch D2-Rezeptoren führt anhand von einem Transkriptionsmechanismus zu einem Rückgang der *pcp4a*-Expression, was eine Veränderung des Reaktionsprofils von *pcp4a*+Tectum-Neuronen auf große visuelle Reize durch einen zellautonomen Mechanismus auslöst. Dies führt letztendlich dazu, dass kleine Reize bei der Nahrungssuche vermehrt gemieden werden.

Diese Studie erweitert unser Wissen über den molekularen Mechanismus, der die Neuromodulation der Entscheidungsfindung steuert.

1. Introduction

1.1. Decision-making behavior

1.1.1. Ethological importance of decision-making

Historically, the majority of studies in behavioral neuroscience have focused on the neural substrates underlying a specific behavior. This has led to substantial progress in understanding the neural circuits mediating the response to an environmental cue. However, in natural conditions, animals do not always react in the same way to a similar stimulation. The behavioral response is heavily influenced by the presence of contrasting cues or conspecifics, richness of the environment and internal state of the individual. As the environment is ever-changing, animals need to switch behavioral strategy to adapt to external and internal conditions. While some environmental variables, such as seasonal climate or food resources availability, may change slowly, others (presence of preys, predators or conspecifics) operate on much shorter timescales. Hence, making fast and accurate decisions on what is the most fitting behavioral strategy is crucial for survival. Moreover, it needs to be attuned to the animal's physiological needs: for example, the most advantageous foraging strategy for a hungry animal may not be optimal for a well-fed one. Internal states, such as hunger, arousal or stress, strongly influence decision-making, favoring behavioral strategies that maintain the body homeostasis.

Studying how internal states affect behavioral choice is fundamental to understand animal behavior in a natural environment. Thus, elucidating the neural circuits for decision-making and how they are influenced by internal signals is a topic of major interest in neuroscience.

1.1.2. Neurotransmitters regulating decision-making

Efforts to identify the neural substrates for decision-making in mammals have highlighted the key role of modulatory neurotransmitters. Neuromodulators like dopamine, serotonin, acetylcholine and norepinephrine have been shown to regulate different aspects of decision-making.

Dopamine is a neurotransmitter that has long been known to be important in motivation. It has been shown to be involved in effort discounting, the willingness to expend more effort to obtain larger rewards (Kurniawan et al., 2011).

Dopamine receptors can be divided in two classes: D1-like receptors, activating adenylate cyclase, and D2-like receptors, inhibiting adenylate cyclase (Beaulieu & Gainetdinov, 2011). The different isoforms are expressed in distinct neural circuits to regulate specific aspects of decision-making, which in mammals is heavily influenced by learning from previous experiences. Dopamine is involved in learning from positive outcomes through the striatal direct pathway, expressing D1 receptors, and negative outcomes through the striatal indirect pathway, expressing D2 receptors (Frank & O'Reilly, 2006). Inhibition of D2 receptors increases risky behavior due to attributing less weight to bad outcomes (Rogers, 2011).

Serotonin has been shown to be involved in delay discounting, the willingness to wait longer for larger rewards, thus playing a role in impulsive behavior (Wogar et al., 1993). Serotonergic neurons in the dorsal raphe exhibit tonic firing in the delay period waiting for a reward, with higher serotonin levels facilitating longer waiting periods (Miyazaki et al., 2011). Moreover, serotonin is involved in learning from delayed negative outcomes (Tanaka et al., 2009). Dopamine and serotonin have long been formulated to be in general opposition in controlling decision-making, in particular in their role to initiate or inhibit a behavioral response. This can be explained by studies showing that serotonin from the raphe nucleus negatively regulates dopamine release. However, increasing evidence suggests that the relationship between serotonin and dopamine may not be so straightforward, with the two systems cooperating in the regulation of certain behaviors. More recent studies suggest that the two neuromodulators rather play a complementary role in the modulation of

decision-making, controlling different aspects through specific mechanisms (Boureau & Dayan, 2011).

Norepinephrine, produced by the locus coeruleus, is implicated in regulating the choice to exploit known resources versus exploring the environment to look for alternatives. Increased noradrenergic tonic firing facilitates a change in behavior if the current task is not remunerative anymore or if the environment has changed (Aston-Jones & Cohen, 2005).

Acetylcholine has been shown to regulate the effect of dopamine on specific aspects of decision-making, in particular increasing sensitivity to reward (Kenny & Markou, 2006).

The activity of neuromodulatory systems is strongly influenced by internal states. For example, dopaminergic signaling is activated by food intake (Zhang et al., 2022) and is thus closely related to the metabolic state. The serotonergic system is downregulated by the hypothalamic-pituitary-adrenal gland (HPA) axis and thus inhibited in chronic stress conditions (Leonard, 2007). Cholinergic and noradrenergic signaling show strong variation during the sleep-wake cycle (Becchetti & Amadeo, 2016).

Hence, neuromodulators play a central role in mediating the effect of internal signals on decision-making, tuning behavior to the physiological needs.

1.1.3. Modulation of sensorial processing for decision-making

Internal states often modulate decision-making by regulating the processing of task-related sensorial inputs. Metabolic or arousal state changes the tonic firing of modulatory neurons, expressing neurotransmitters such as dopamine, serotonin, norepinephrine or acetylcholine. These neurons project to areas processing sensory stimuli and alter the representation of task-relevant cues in the brain (Lee & Dan, 2012). This mechanism is evolutionary conserved, as it has been observed in both invertebrates and vertebrates models.

In flies, metabolic state changes the valence attributed to certain odors through dopaminergic modulation of neuronal activity in the mushroom bodies, the region processing olfactory stimuli. Hungry flies display attraction towards CO₂

instead of the typical avoidance, allowing energy-deprived animals to approach new food sources like fermenting fruits (Siju et al., 2021).

In mice, thirst regulates performance in a two-whisker discrimination task by changing activity in cortical neurons so that whisker stimuli are better decoded in water-deprived mice (Matteucci et al., 2022).

In humans, arousal state affects the secretion of norepinephrine from the locus coeruleus, thus improving the performance in an object recognition task by optimizing visual processing of task-relevant information (Sørensen et al., 2022).

Neuromodulation of the sensory processing of environmental cues has the benefit to be fairly rapid, allowing for fast changes in behavior (Gaudry & Kristan, 2009). This constitute an advantage in a natural environment, where circumstances can quickly vary and decisions concerning survival, like whether to approach a prey or escape from a predator, need to be taken fast.

1.1.4. Decision-making during foraging behavior

Foraging behavior is crucial for survival and entails animals making decisions about whether to approach a possible food source, escape from potential predators, explore a larger area or choosing between different food sources. It also needs to be tuned down to prioritize other behaviors, like mating in the presence of a potential reproductive partner or defending the territory against a potential rival. It is a complex behavior that needs to be tightly regulated and attuned to the metabolic state of the animal to acquire enough food to ensure survival. Given the key importance of foraging behavior for all species, the modulation of feeding by metabolic state has been investigated in several animal models, from invertebrates to humans.

In the sea slug *Pleurobranchaea*, appetitive state, encoded in the excitation of the feeding network, regulates a switch between approach and avoidance behavior (Hirayama & Gillette, 2012). In the same animal, hunger replace avoidance responses with orienting turns (Gillette et al., 2000).

In flies, starvation induces an increased preference for sweetness and a decreased sensitivity to bitterness. Higher sugar sensitivity precedes lower

bitterness sensitivity as its pathway is recruited at lower hunger levels, allowing for adaptive feeding decisions based on the intensity of the starvation state (Inagaki et al., 2014).

In mice, hunger bias neurons in the postrhinal association cortex and lateral amygdala to food-related cues. Such bias is abolished by satiation (C. R. Burgess et al., 2016). Hunger also increases activity of agouti-related peptide (AgRP) neurons in the hypothalamus, promoting feeding (Laing et al., 2018). This leads to mice foraging in areas more susceptible to predators and reduced aggression within a territory depleted in nutrients (Padilla et al., 2016). Moreover, hunger increases the capacity of AgRP neurons to suppress competitive motivational systems, like thirst, innate fear, anxiety and social behaviors (Burnett et al., 2016). AgRP neurons thus integrate internal metabolic signals with contextual environmental cues to modulate behavioral strategies (Deem et al., 2022).

In monkeys, hunger increases the response to sugar in the caudolateral orbitofrontal cortex secondary taste area. Responses decreased to zero with satiety and the behavior switched from acceptance to active rejection (Rolls et al., 1989).

In humans, hunger increases responses to food-related stimuli in the amygdala and associated inferotemporal regions (LaBar et al., 2001).

All these examples in a wide variety of animals, from simple invertebrates to primates and humans, paint a clear picture of the role that appetitive state play in regulating decision-making during foraging behavior, often by altering the representation of food-related cues in the neural networks dedicated to feeding.

1.2. Behavioral choice in zebrafish

1.2.1. Zebrafish as a model in neuroscience

Progress has been made in identifying neural substrates and neurotransmitter systems involved in decision-making, however information about the molecular mechanisms underlying this phenomenon are still scarce. In attempt to fill this gap, we designed a study investigating decision-making in zebrafish.

Zebrafish (*Danio rerio*) is a model organism that has gained popularity in neuroscience research in the last decade thanks to its numerous advantages. It has high fecundity, a female laying up to 300 eggs at a time, and fast development, ideal for high-throughput studies. External development allows for easy manipulation at early stages. At larval stages, its transparency and small size allow to image simultaneously the entire brain using non-invasive techniques. The brain of a 5 days-post-fertilization (dpf) larva is around 1.5 mm long and only 500 μm deep, making imaging of the whole brain volume feasible at relatively high speed. Calcium imaging is the preferred method to measure neuronal activity, using lines expressing genetically encoded calcium sensors (GECI), such as GCaMP, in neuronal populations (Kettunen, 2020). This technique allows to monitor simultaneously the activity of a large number of neurons. Using techniques like lightsheet microscopy permits fast imaging of the entire larval brain at a cell resolution, crucial for network studies (Vladimirov et al., 2014). Mounting the fish under the microscope in a head-fixed and tail-free preparation makes it possible to monitor simultaneously neuronal activity and motor behavior, associating specific active neurons to a particular behavior.

Genetic tools are well established in zebrafish: the genome, which share 70% of homology with humans, was sequenced in 2013 and it is well annotated (Howe et al., 2013). Targeted mutagenesis techniques like CRISPR/Cas9 are widely used and relatively easy to employ thanks to external development and high fecundity (Li et al., 2016). Moreover, numerous mutant lines have been generated during early chemical mutagenesis screens (Mullins et al., 1994). A

large number of transgenic lines labeling specific neuronal populations are available. The Gal4/UAS system, derived from yeast, is widely used to express a protein of interest in a particular cell population (Asakawa & Kawakami, 2008). A 'driver' line, expressing the transcription factor Gal4 under the control of a cell-specific promoter, is crossed with a 'reporter' line, containing the protein of interest under the control of the UAS sequence. Gal4 binds to the UAS sequence and drive the expression of the protein of interest only in the specific cells where it is produced (Figure 1).

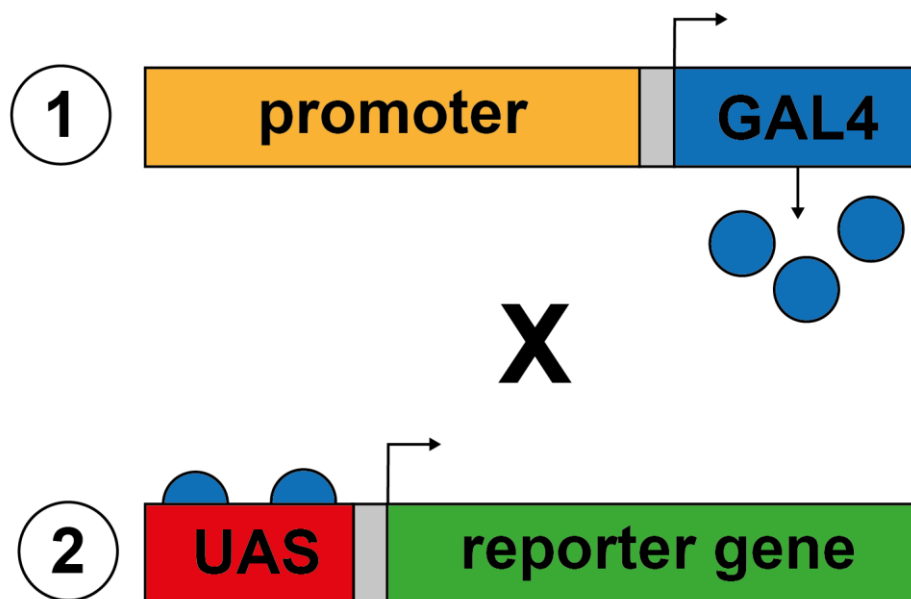


Figure 1: Gal4/UAS system

Schematic representation of how the Gal4/UAS system works. A transgenic line containing a construct expressing Gal4 under the control of a cell-specific promoter ('driver') (1) is crossed with a transgenic line expressing a reporter gene under the control of a UAS sequence ('reporter') (2). The transcription factor Gal4 binds to the UAS sequence and drive expression of the reporter gene only in the specific cell population where it is produced.

Zebrafish brain presents some differences in anatomical organization compared to mammals, due to the absence of a cortex and because in teleost development the anterior neural tube undergoes eversion instead of evagination like in most vertebrates, resulting in an anatomical displacement of

homologous forebrain regions (Wullimann & Mueller, 2004). Despite these anatomical differences, many of the homologous structures in zebrafish possess the same function and neurotransmitter identity of their mammalian counterparts. Neurotransmitter systems are conserved and often control similar behaviors.

For example, the serotonergic system, comprised of neurons located in the pretectum, hypothalamus and raphe, is involved in arousal, stress responses, aggressivity and anxiety (Lillesaar, 2011).

Likewise, the dopaminergic system, comprised of distinct nuclei in the telencephalon, pretectum, posterior tuberculum and hypothalamus, has been shown to regulate motivation, reward and locomotion (Irons et al., 2013; Scerbina et al., 2012; van Staden et al., 2020).

These observations suggest that, although the neuroanatomy and the neural circuits involved may differ, the molecular mechanisms employed are likely conserved (Ek et al., 2016). This makes zebrafish an attractive model to study the molecular basis of behavior due to the simplicity of genetic manipulation.

Zebrafish possess an extended behavioral repertoire already at early developmental stages: larvae start to hunt autonomously for food at 5 dpf, displaying a stereotypical prey capture sequence (Muto & Kawakami, 2013). They also show phototaxis and respond to optic flow by swimming following the direction of the flow (optomotor response, OMR) (Brockerhoff et al., 1995; Maaswinkel & Li, 2003). They display startle response to aversive stimuli such as a loud sound, electric shock, vibration, touch or a rapidly expanding dark circle (looming stimulus), characterized by a stereotypical bending of the body (C-turn) mediated by the activation of specific premotor neurons (Mauthner cells) (H. A. Burgess & Granato, 2007). Although there is conflicting evidence for associative learning at early developmental stages, primitive forms of learning such as habituation are present already as early as 4 dpf (Beppi et al., 2021).

The richness in behavioral paradigms, coupled with the simplicity of imaging neuronal activity and genetic manipulation, make zebrafish a very attracting model for the study of molecular mechanisms underlying behavioral flexibility.

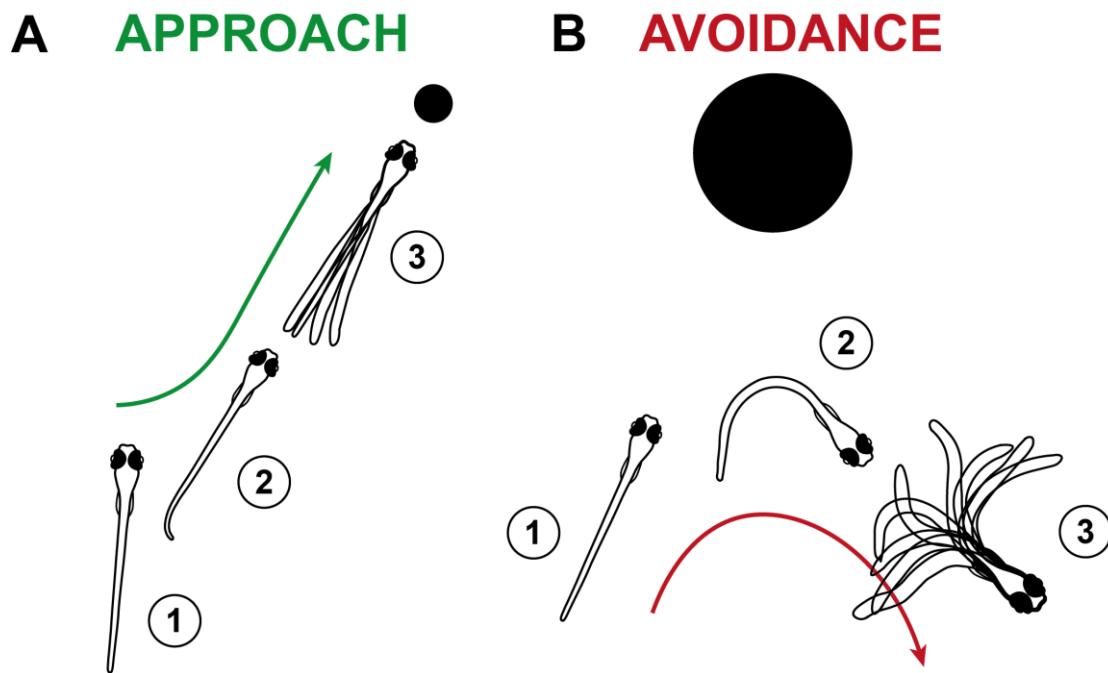


Figure 2: Approach and avoidance behavior in zebrafish

Schematic representation of the locomotor sequence during approach and avoidance of visual stimuli. **A.** Approach: when the fish detects a prey-like visual stimulus (1), it performs J-turns to reorient itself towards the stimulus (2) and then it approaches the object with slow swimming bouts (3). **B.** Avoidance: when the fish detects a predator-like visual stimulus (1), it performs a C-turn in the opposite direction of the stimulus (2) and then escapes away from the object with fast, vigorous swimming bouts (3).

1.2.2. Behavioral choice during foraging behavior in zebrafish

During foraging behavior, zebrafish larvae switch between approaching potential preys and escaping from potential predators. Approach and active avoidance are two opposite and mutually exclusive behaviors, each involving a stereotypical and well recognizable locomotor sequence. During approach, the eyes converge to focus on the object and the larva orients itself towards the visual cue, bending the caudal part of the tail to one side (J-turn). The fish then performs short forward swimming bouts to reach and capture the prey (Figure 2A) (Muto & Kawakami, 2013). During active avoidance, the fish instead perform a fast, stereotypical turn away from the stimulus, bending the whole body (C-turn). This is followed by fast, vigorous swim bouts to escape in the opposite direction from the object (Figure 2B) (Dunn et al., 2016).

These two behaviors are mediated by distinct and opposite neural pathways, so it is a simple paradigm to study behavioral choice. The decision to perform an approach or an escape is mainly influenced by the size of the object the fish is interacting with: small visual cues are perceived as preys and pursued, while large objects are seen as predators and avoided. The choice is computed in the optic tectum, a brain region processing and integrating visual cues (Barker & Baier, 2015).

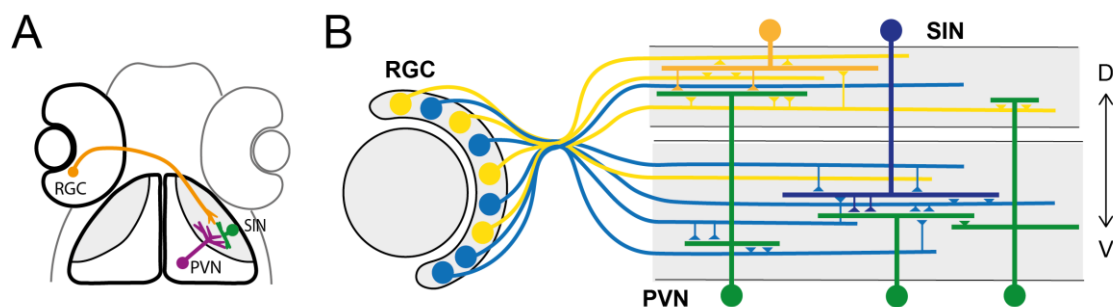


Figure 3: Neuronal circuits in the optic tectum in zebrafish

A. Schematic representation of the optic tectum and its neuronal classes: the tectum receives inputs from RGCs in the retina, which projects to the tectum neuropil. SINS have their soma in the superficial layers of the neuropil, while PVNs have their soma in the PVL and their dendrites arborize in the neuropil. **B.** Schematic representation of how size selectivity is acquired in the tectal circuits. Size-selective RGCs project to different layers in the tectum neuropil: small-selective RGCs (labeled in yellow) mainly project to the superficial layers, while large-selective RGCs (labeled in blue) mainly project to the deeper neuropil layers. SINS acquire their tuning size depending on the neuropil layer they arborize to and thus on the RGCs input they receive. PVNs acquire their tuning size from the the RGCs and the SINS they receive input from. PVNs are also connected to other PVNs to form complex intratectal circuits.

The optic tectum is a structure located in the mesencephalon and it is homologous to the mammalian superior colliculus. It is composed by a periventricular layer (PVL), containing the majority of neuronal somas, and a neuropil containing dendrites of periventricular neurons (PVNs) and axonal projections from the afferents. In the neuropil are also located the somas of a particular class of neurons called superficial interneurons (SINs). The optic

tectum receives mainly visual inputs from the retina, with projections from retinal ganglion cells (RGCs) arborizing in the tectum neuropil (Robles et al., 2014) (Figure 3A). However, the optic tectum does not receive exclusively visual inputs but also afferents from other sensory areas, including the lateral line. Indeed, some subsets of tectal neurons respond to auditory and water flow stimuli (Thompson et al., 2016). The tectum also receives projections from the hypothalamus (Heap et al., 2018), suggesting it receives information about internal states. Neuronal circuits in the optic tectum integrate all the stimuli from different sensory modalities and periventricular projection neurons (PVPNs) send projections through the ipsilateral tectobulbar tract (iTB) to activate downstream reticulospinal neurons to perform either an approach or an escape (Helmbrecht et al., 2018). Indeed, the tectum has been shown to be important in both prey capture (Gahtan et al., 2005) and avoidance behavior (Temizer et al., 2015). This ability to induce different behavioral responses depending on the sensory information makes the optic tectum a major center for decision-making during foraging behavior in zebrafish.

Tectal neurons show size selectivity, partially determined by the retinal inputs they receive. The neuropil is organized in laminae along the dorso-ventral axis and RGCs project to specific layers depending on their size-selectivity: RGCs responding to small stimuli project preferentially to superficial layers, while RGCs selective for large stimuli project to deeper layers in the neuropil (Preuss et al., 2014). SInNs have distinct size tuning properties depending on which class of RGCs they receive inputs from, based on their arborization pattern (Preuss et al., 2014). PVNs size tuning is partially determined by the inputs from size-selective RGCs, depending on which neuropil layers PVNs dendrites arborize (Förster et al., 2020), and it is refined by feedforward inhibition from SInNs (Del Bene et al., 2010) (Figure 3B). However, the inputs can only partially predict the size tuning of PVNs, which is fine-tuned by computation in the intratectal circuits (Förster et al., 2020).

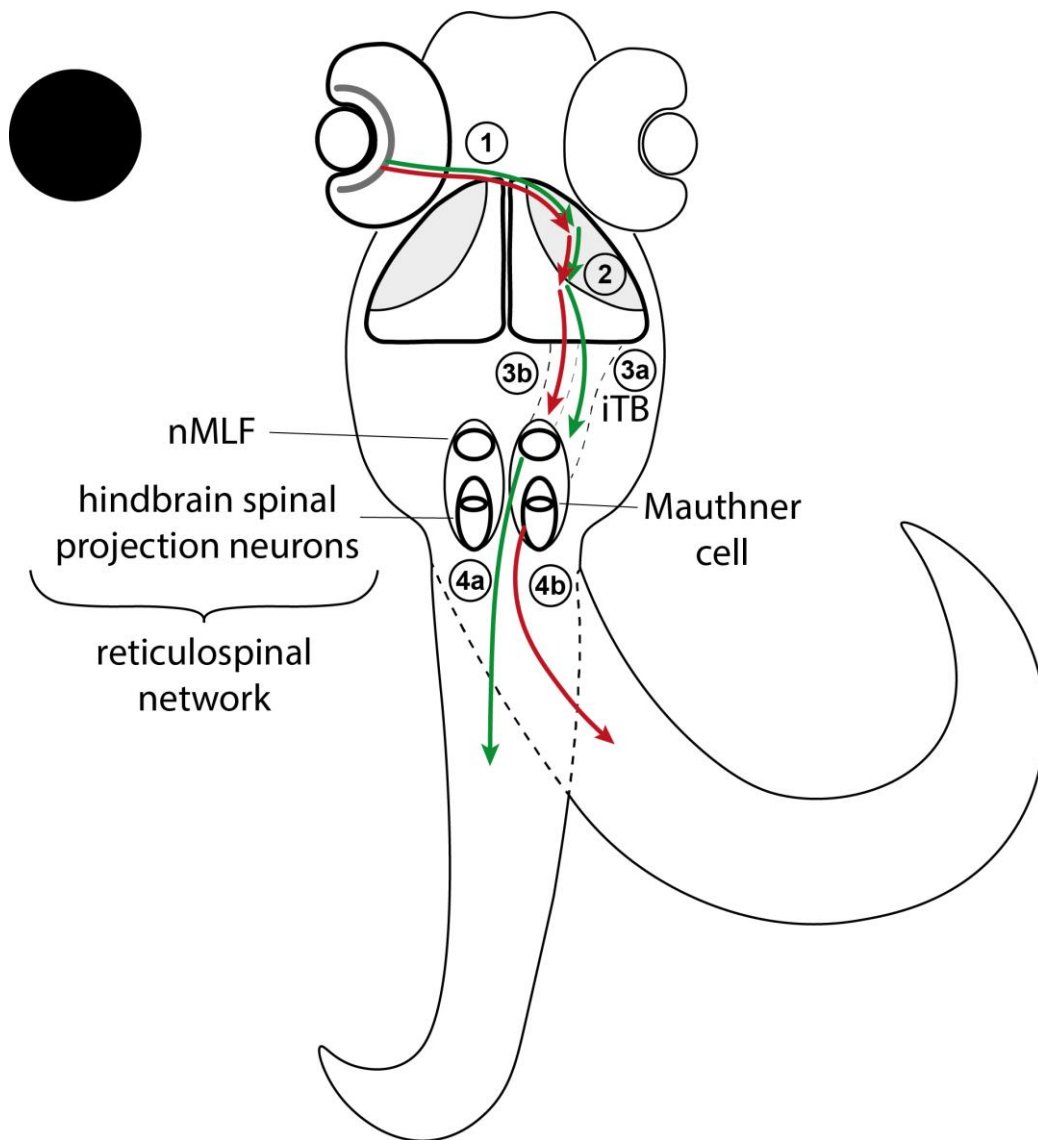


Figure 4: Visuomotor transformations underlying approach and avoidance

Schematic representation of the neuronal circuits for approach and avoidance, from the detection of the visual stimulus to the locomotor response. Visual inputs are relayed from the retina to the optic tectum neuropil (1), where they are integrated and projection PVNs are activated (2) to initiate either an approach or an avoidance. PVPNs mediating approach send projections to the reticulospinal network through the lateral iTB (iTBL) (3a), while PVPNs mediating avoidance send projections to the reticulospinal network through the medial iTB (iTBM) (3b). In the premotor areas, neurons of the nMLF induce the J-turn typical of approaches (4a), while the Mauthner cells mediate the C-turn typical of escapes (4b).

In response to moving objects, the optic tectum activates premotor neurons in the reticulospinal networks, which send projections to the spinal cord to elicit a

motor response. The reticulospinal system is composed of neurons of the medial longitudinal fasciculus (nMLF) in the midbrain and hindbrain spinal projection neurons, which include the Mauthner cells. In response to small visual stimuli, the optic tectum activates the nMLF, which mediate the small turning movement to orient towards the prey (J-turn) (Gahtan et al., 2005). In response to large visual stimuli, the optic tectum activates the Mauthner cells and other spinal projection neurons in the hindbrain, mediating the fast, stereotypical escape turn (C-turn) (Dunn et al., 2016) (Figure 4).

1.2.3. Metabolic modulation of behavioral choice

Since hunting preys and escaping from predators accurately is crucial for survival, behavioral choice during feeding must be tightly regulated. As previously mentioned, it is mainly influenced by the size of the object the fish is interacting with: large moving objects are perceived as predators and avoided, while small visual cues are perceived as preys and approached (Barker & Baier, 2015). However, decision making needs to take into account the physiological needs of the animal: is it worth it to take risks and approach an object resembling a prey if hungry? Or would it be better to employ a safer strategy and avoid all objects if there is no immediate need for energy? Indeed, it has been shown that metabolic state modulates behavioral choice during foraging behavior: 7 dpf food-deprived larvae approach more small and intermediate objects compared to fed siblings in a size discrimination assay, suggesting that hunger induce zebrafish larvae to take more risks during hunting (Filosa et al., 2016). The behavioral strategy is chosen based on the relative costs and benefits: a starving fish is more willing to take risks and approach a potential prey since there is an urgent need for energy, contrary to fed fish that can afford to take a more conservative approach.

Feeding state regulates decision-making through a differential representation of visual cues in the optic tectum. In food-deprived larvae there is an increased number of tectal neurons responding to small-size stimuli, tuning the response profile of tectal neurons to visual cues important for survival (Filosa et al., 2016).

The shift in the response profile is the result of feeding state-dependent neuromodulation: in food-deprived fish there is a decreased activation of the stress axis (hypothalamic-pituitary-interrenal, HPI). This leads to increased activity of serotonergic neurons in the raphe nucleus, which project to the optic tectum neuropil, resulting in modulation of PVNs responses. Serotonergic signaling recruits additional tectal neurons responding to small visual stimuli, tuning PVNs' response profile to prey-like cues (Filosa et al., 2016).

Feeding state-dependent regulation of behavioral choice through serotonergic modulation of tectal responses to visual cues is a great example of how internal states control decision-making through neuromodulation of sensory inputs.

1.3. Molecular mechanisms regulating behavioral choice

1.3.1. Proteomic screen

Given the differential response profile of tectal neurons depending on metabolic state, it is reasonable to hypothesize that feeding induces changes in neuronal excitability and/or synaptic function in these neurons. However, the molecular mechanisms underlying this phenomenon are still unclear. In an effort to identify potential candidate proteins involved in this process, a proteomic study was conducted in fed versus food-deprived larvae (Zaupa et al, *(under review)* data generated by Nagarjuna Nagaraj). The entire proteome was extracted from whole 7 dpf fed zebrafish larvae and food-deprived siblings and analyzed by mass spectrometry. This screen identified 166 proteins having significantly different abundance (Figure 5A). A literature search showed that differentially expressed proteins are involved in several biological processes, such as metabolic function, interaction with nucleic acids, protein metabolism, signal transduction, endocytosis/exocytosis and regulation of cell cycle (Zaupa et al, *(under review)* data not shown). Only few hits were closely related to regulation of neuronal physiology.

Among them, the small cytoplasmic protein Pcp4a, known to modulate neuronal excitability, was 35% less abundant in fed larvae compared to food-deprived siblings (Figure 5B) and was chosen for functional validation.

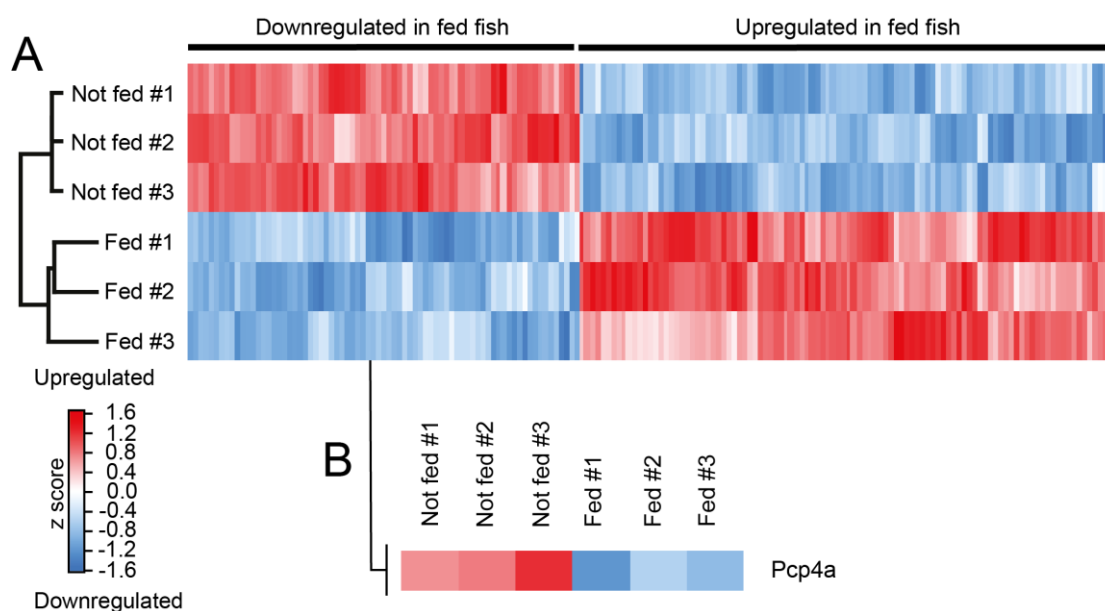


Figure 5: Feeding decrease abundance of Pcp4a

A. Heat map of proteins significantly differentially abundant in fed versus food-deprived 7 dpf larvae. **B.** Detail from the heat map in 5A, showing 35% reduction in Pcp4a abundance in fed larvae compared to food-deprived fish.

Data in Figure 5 were generated by Nagarjuna Nagaraj (Biochemistry Core Facility, Max Planck Institute of Biochemistry, Martinsried, Germany. Current affiliation: Evotec München GmbH).

1.3.2. *Pcp4a*

Purkinje cell protein 4a (Pcp4a) is a 63-aa peptide, homologous to the mammalian PCP4 (also called PEP-19). It belongs to a family of proteins containing a domain for binding to calmodulin (CaM) characterized by a conserved IQ motif (consensus: [I,L,V]QxxxRGxxx[R,K]), which include also neuromodulin and neurogranin (Slemmon et al., 2000). This small cytoplasmic protein acts by binding to the Ca²⁺-free calmodulin and undergoing a

conformational change that exerts an allosteric effect, increasing dissociation rates of Ca^{2+} to calmodulin (Kleerekoper & Putkey, 2009). This results in inhibition of the activation of calmodulin-dependent enzymes, such as Ca^{2+} /calmodulin-dependent kinase II (CaMKII) (Xiong et al., 2010) and nitric oxide synthase (NOS) (Slemmon et al., 1996). Due to the role of calmodulin-dependent enzymes in signal transduction during neuronal activation, expression of PCP4 leads to decreased neuronal excitability *in vitro* (Slemmon et al., 2000). However, PCP4 does not seem to affect indiscriminately all calcium-dependent signaling pathways. It has been shown to block CaMKII activation when neurons are depolarized by high K^+ but not by ATP-induced calcium influx (Johanson et al., 2000). This suggests that PCP4 exerts its regulation on CaM depending on the stimulus inducing the calcium influx, allowing for fine modulation of neuronal excitability.

In mammals PCP4 is highly expressed in Purkinje neurons in the cerebellum and there is evidence of a role of PCP4 in regulating excitability in these cells *in vivo*. PCP4 knock-out mice have impaired locomotor learning due to alteration of synaptic plasticity at granule cell parallel fiber – Purkinje cell (PF-PC) synapses (Wei et al., 2011). A stimulation protocol that produces long-term depression (LTD) in wild-type mice, induce long-term potentiation (LTP) instead in the knock-out. Interestingly, basal synaptic transmission at PF-PC synapses is not altered in the knock-out, suggesting that changes in PCP4 levels *in vivo* results in subtle modulation of synaptic plasticity rather than general neuron excitability.

In zebrafish, *pcp4a* is expressed in the optic tectum and other brain regions involved in visual processing and decision-making, such as retina, pretectum and the reticulospinal network (Mione et al., 2006).

2. Aims

Given the known function of *pcp4a* in regulating neuronal excitability and its expression in the optic tectum, it is reasonable to hypothesize that food-dependent changes in Pcp4a levels modulate the response of tectal neurons to visual cues. This would result in tuning of decision-making during foraging behavior to the metabolic needs of the animal.

To prove this hypothesis, I first elucidated the role that *pcp4a* plays in the regulation of behavioral choice by feeding state. For this purpose, I used a loss-of-function model and looked at decision-making in a size discrimination assay mimicking foraging behavior in larval zebrafish.

I then investigated if *pcp4a* regulates behavioral choice through a differential processing of visual stimuli in the optic tectum. For this purpose, I characterized the tuning properties of *pcp4a*-expressing (*pcp4a+*) tectal neurons using *in vivo* calcium imaging and tested how feeding state alters their response to visual cues. I also tested how lack of Pcp4a affects their tuning properties in the loss-of-function model.

I then looked into the neuromodulatory systems mediating the effect of feeding state on Pcp4a levels by studying the result of a pharmacological activation of several neuromodulator signaling on *pcp4a* expression levels. Zooming in the molecular mechanisms downstream of neuromodulation, I elucidated the signal transduction cascade upstream Pcp4a.

Finally, I investigated how neuromodulation is influencing *pcp4a+* tectal neurons responses to visual cues, gaining insight into how Pcp4a is regulating their tuning properties.

This study aims to elucidate the Pcp4a pathway for regulation of feeding state-dependent decision-making in zebrafish, from a molecular to a behavioral level.

3. Materials and Methods

3.1. Zebrafish lines

	Origin	Identifier
Zebrafish: <i>Tg[elavl3:H2B-GCaMP6s]^{jf5}</i>	(Freeman et al., 2014)	ZFIN: ZDB-ALT-141023-2
Zebrafish: <i>Tg[elavl3:GAL4-VP16]^{nn6Tg}</i>	(Kimura et al., 2008)	ZFIN: ZDB-ALT-090116-2
Zebrafish: <i>Tg[14XUAS:GCaMP6s]^{mpn101}</i>	(Thiele et al., 2014)	ZFIN: ZDB-ALT-140811-3
Zebrafish: <i>Tg[-7atoh7:GAL4-VP16]^{s1992t}</i>	(Del Bene et al., 2010)	ZFIN: ZDB-ALT-110912-2
Zebrafish: <i>Tg[5XUAS:EGFP]^{nkuasgfp1a}</i>	(Asakawa et al., 2008)	ZFIN: ZDB-ALT-080528-1
Zebrafish: <i>Tg[th:GAL4-VP16]^{m1233}</i>	(Fernandes et al., 2012)	ZFIN: ZDB-ALT-130110-4
Zebrafish: <i>Tg[UAS:EGFP-CAAX]^{m1230}</i>	(Fernandes et al., 2012)	ZFIN: ZDB-ALT-130110-5
Zebrafish: <i>pcp4a^{md78}</i>	This study	N/A

3.2. Oligonucleotides

	Origin	Identifier
sgRNA <i>pcp4a^{md78}</i> : GGAAGCATCAAACCCTCAGGTGG	This study	N/A
Primer: genotyping <i>pcp4a</i> Forward GAAAACAGACATCCCCGCTGTG	This study	N/A
Primer: genotyping <i>pcp4a</i> Reverse CCCCACAAATCCAAAGACGTG	This study	N/A
Primer: qPCR <i>pcp4a</i> Forward CTCAGGTGGACAAGACCCATC	This study	N/A
Primer: qPCR <i>pcp4a</i> Reverse ATCCCCCTGCCCTAAATGTG	This study	N/A
Primer: qPCR β -actin Forward GTCCCTGTATGCCTCTGGT	This study	N/A
Primer: qPCR β -actin Reverse AAGTCCAGACGGAGGATG	This study	N/A

3.3. Antibodies

	Origin	Identifier
Chicken polyclonal anti-GFP	Thermo Fisher	Cat# A10262; RRID: AB_2534023
Mouse monoclonal anti- p44/42 MAPK	Cell Signaling	Cat# 4696; RRID: AB_390780
Rabbit monoclonal anti- phospho-p44/42 MAPK (Thr202/Tyr204)	Cell Signaling	Cat# 4370; RRID: AB_2315112
Goat polyclonal anti-chicken IgY, Alexa Fluor 488 conjugate	Thermo Fisher	Cat# A11039; RRID: AB_142924
Goat polyclonal anti-mouse IgG, Alexa Fluor 647 conjugate	Cell Signaling	Cat# 4410; RRID: AB_1904023
Goat anti-rabbit IgG, Alexa Fluor 555 conjugate	Cell Signaling	Cat# 4413; RRID: AB_10694110

3.4. Chemicals and reagents

	Origin	Identifier
Agarose, Low Melting Point	Roboklon	E0303-50
Agarose NEEO Ultra Qualität	Carl Roth	2267.3
Apomorphine hydrochloride	AbCam	ab269887
Bovine Serum Albumin	Serva	11943.02
Calcium nitrate (Ca (NO ₃) ₂)	Honeywell	C1396
Cas9 protein	MDC facility	N/A
Chloroform	Fisher Chemical	C/4960/15
Ddel	New England Biolabs	R0175L
Dimethyl sulfoxide (DMSO)	Th. Geyer	23419.3
DNase I	Thermo Fisher	EN0521
Donepezil hydrochloride	Thermo Fisher	458050010
Ethanol	Roth	9065.2

Fluoxetine hydrochloride	Sigma	PHR1394
Forskolin	Sigma	F6886
Gel Red Nucleic Acid Stain	Linaris	41003
GeneRuler 1kb+ DNA ladder	Thermo Fisher	SM1331
Glycogen	Serva	23550.02
Goat serum	Sigma	G6767
Hydrochloric acid (HCl)	Sigma	H1758
Hydrogen peroxide (H ₂ O ₂) 30%	ChemCruz	sc-203336A
(4-(2-hydroxyethyl) -1-piperazineethanesulfonic acid) (HEPES)	Roth	9105.4
Isopropanol	Carl Roth	7343.2
KN-93	Adooq Bioscience	A13276
Lithium chloride (LiCl)	Ambion	9480G
Loading dye (Orange G)	Carl Roth	0318.2
Magnesium sulfate (MgSO ₄)	ChemCruz	sc-211764
Master Mix Taq 2x	NEB	M0270
Methanol	Roth	4627.1
Pancuronium bromide	Sigma	P1918
Paraformaldehyde (PFA)	Sigma	P6148
Phenol-chloroform-isoamylalcohol	Roth	A156.2
Phenol Red	Sigma	P0290-100ml
Phosphate-buffered saline (PBS)	Sigma	P4417
Phusion High-Fidelity DNA Polymerase (2 U/μL)	LIFE Technologies	F530L
Potassium chloride (KCl)	ChemCruz	sc-203207
Potassium hydroxide (KOH)	Alfa Aesar	A16199
Proteinase K	Sigma	3115879001
Quinpirole hydrochloride	Sigma	Q102
RNase H	Life Technologies	EN0201
RNase inhibitor (40 U/μL)	Life Technologies	EO0381
Saline-sodium citrate (SSC) 20x	Sigma	S6639-1L
SDS-100 (dry food)	Special Diets Services	
SKF-38393 hydrochloride	MedChem Express	HY-12520A
Sodium acetate (NaOAc)	Calbiochem	567418- 500GM

Sodium chloride (NaCl)	Serva	39781.02
T4 DNA polymerase	New England Biolabs	M0203S
T7 polymerase	New England Biolabs	M0255AAVIAL (Kit: AM1340)
Tricaine (3-amino benzoic acidethylester)	PharmaQ	N/A
Tris	Sigma	T1503
Trizol	Thermo Fisher	15596026
Trypsin-EDTA	Sigma	T4299
Triton X 100	Roth	3051.3
Tween 20	Roth	9127.2
Water RNase/DNase free	LIFE Technologies	10977035

3.5. Solutions and buffers

1X PBS

Reagent	Final concentration	Amount
PBS	1X	5 tablets
MilliQ H ₂ O	N/A	Add to 1 L
Total		1 L

1X PBT

Reagent	Final concentration	Amount
1X PBS	1X	Add to 500 mL
Tween20	0.1%	50 µL
Total		500 mL

1X PBST

Reagent	Final concentration	Amount
1X PBS	1X	Add to 500 mL
Triton X 100	0.3%	1.5 mL
Total		500 mL

4% PFA/PBS

Reagent	Final concentration	Amount
1X PBS	1X	30 mL
PFA 16%	4%	10 mL
Total		40 mL

4% PFA/PBT

Reagent	Final concentration	Amount
1X PBT	1X	30 mL
PFA 16%	4%	10 mL
Total		40 mL

30X Danieau's medium

Reagent	Final concentration	Amount
NaCl	1740 mM	101.7 g
KCl	21 mM	1.56 g
MgSO ₄	12 mM	2.96 g
Ca(NO ₃) ₂	18 mM	4.25 g
HEPES	150 mM	35.75 g
MilliQ H ₂ O	N/A	Add to 1L
Total		1 L

10% KOH

Reagent	Final concentration	Amount
KOH	10%	10 g
MilliQ H ₂ O	N/A	Add to 100 mL
Total		100 mL

Immunostaining blocking solution

Reagent	Final concentration	Amount
Goat serum	5%	500 µL
BSA	1%	0.1 g
DMSO	1%	100 µL
PBT	1X	Add to 10 mL
Total		10 mL

1% low melting point agarose

Reagent	Final concentration	Amount
Agarose, low melting point	1%	1 g
1X Danieau's medium	1X	Add to 100 mL
Total		100 mL

Tricaine

Reagent	Final concentration	Amount
Tricaine	0.168 mg/ml	0.168 g
1X Danieau's medium	1X	Add to 1 L
Total		1 L

3.6. Kits

	Origin	Identifier
HCRv3 reagents	Molecular Instruments	https://www.molecularinstruments.com/
HiScribe T7 Quick Kit	New England Biolabs	E2050S
Luna Universal qPCR Master Mix	New England Biolabs	M3003L
NucleoSpin Gel and PCR Clean-up	Macherey-Nagel	740.609.250
SuperScript III First Strand Kit	Life Technologies	18080051

3.7. Consumables

	Origin	Identifier
Centrifuge tubes 15 ml, 50 ml	TPP	TPP91015, TPP91050
Glass capillaries	Science Products	GB120F-8P
Forceps	Dumont	
Microcentrifuge tubes 1.5 ml, 2.0 ml	Sarstedt	72.706.400, 72.695.400
Multi-well plates (6, 12, 24, 48, 96)	Falcon, Greiner	
Pellet Pestle, 1.5 ml	Fisher Scientific	11872913
Petri dish (60 mm)	Sarstedt	83.3901
Petri dish (35 mm)	Sarstedt	82.1135.500
Plastic pipette 3 mL	Pastette	LW4111
PCR tubes	Sarstedt	72.991.002

Pipette tips 10 μ l, 200 μ l, 1000 μ l	Sarstedt	701130, 70.760.002, 70.1186
Serological pipetts 10 ml, 25 ml	Sarstedt	86.1254.001 86.1685.001

3.8. Equipment

	Origin	Identifier
Agarose gel documentation device	Biozym	Azure 200
Agarose gel systems	Thermo Scientific	Owl Easycast B1
Benchtop centrifuge	Eppendorf	5417R
Camera	XIMEA	MQ003MG-CM
Confocal Microscope	Zeiss	LSM 800
Confocal Microscope	Leica	DM6 CFS
Electrophoresis power supply	BioRad	PowerPac Basic
Fluorescence-Stereomicroscope	Olympus	SZX16
Incubator	Velp Scientifica	FOC215L
Infrared filter	Thorlabs	FGL7806S
Microdisplay	Kopin	
Microinjector	World Precision Instr.	PV820
Microinjection molds	MDC, selfmade	-
Micro scale	Fisher Scientific	PAS214
Microwave	Exquisit	
Mini Vortex	Roth	HXH6.1
NanoDrop (Photometer)	Eppendorf	D30
Needle Puller	Narishige	PC-100
pH Meter	Mettler-Toledo	Five Easy
Pipette 10 μ l, 100 μ l, 200 μ l and 1000 μ l	Eppendorf	Research Plus
Pipetboy	Integra	Acu 2

PCR System	Eppendorf	6337000019
StepOnePlus Real-Time PCR System	Thermo Fisher	4376600
Rotor (rotator)	Stuart	SRT6
Scale	Kern	EW4200
Stereomicroscope	Leica	S6
Thermal Cycler (Thermoblock)	Eppendorf	5382000015
Waterbath	GFL	11347017J
Water-immersion Objective (HC Fluotar L 25x/0.95)	Leica	
Water-immersion Objective (W Plan-Apochromat 20x/1.0 DIC VIS-IR)	Zeiss	
Zebrafish aquatic housing system	Aqua Schwarz	
Zebrafish breeding tanks	Techniplast	

3.9. Softwares and algorithms

	Origin	Identifier
Adobe Illustrator	Adobe	https://www.adobe.com/products/illustrator.html
CMTK plugin	(Jefferis, 2018)	http://sites.imej.net/Jefferis
EthoVision XT version 8.5	Noldus	https://www.noldus.com/ethovision-xt
Fiji/ImageJ	NIH	https://fiji.sc/
Imaris version 10	Oxford Instruments	https://imaris.oxinst.com/
MATLAB	The MathWorks	https://www.mathworks.com/products/matlab.html
NoRMCorre algorithm	(Pnevmatikakis & Giovannucci, 2017)	https://github.com/flatironinstitute/NoRMCorre

Prism version 9	GraphPad Software	https://www.graphpad.com/scientific-software/prism/
PsychoPy version 2.0	Open Science Tools	https://www.psychopy.org/
QuickFigures plugin	(Mazo, 2021)	https://github.com/grishkam/QuickFigures

3.10. Zebrafish lines and maintenance

Zebrafish were kept under standard conditions at 28.5°C on a 14 hours/10 hours light/dark cycle. Embryos and larvae were grown in Danieau's medium (58 mM NaCl, 0.7 mM KCl, 0.4 mM MgSO₄, 0.6 mM Ca(NO₃)₂, 5 mM HEPES, pH adjusted to 7) at a density of approximately 40 fish in a 90 mm plastic Petri dish.

All animal procedures were conducted in accordance with institutional (Max Delbrück Center for Molecular Medicine), State (LAGeSo Berlin) and German ethical and animal welfare guidelines and regulations, and according to protocols approved by LAGeSo.

Unless otherwise stated, experiments were performed at 7 dpf. After the procedures, larvae were euthanized, following anesthesia with 0.168 mg/ml tricaine, using hypothermic exposure (ice bath) for 20 minutes.

Sex of zebrafish cannot be determined at the developmental stages considered in this study. Animals were randomly assigned to experimental groups.

The following previously established transgenic lines were used in this study: *Tg[elav13:H2B-GCaMP6s]^{jf5}* (Freeman et al., 2014), *Tg[elav13:Gal4]^{nn6Tg}* (Kimura et al., 2008), *Tg[14XUAS:GCaMP6s]^{mpn101}* (Thiele et al., 2014), *Tg[atoh7:Gal4]^{js1992t}* (Del Bene et al., 2010), *Tg[5XUAS:EGFP]^{nkuasgfp1a}* (Asakawa et al., 2008), *Tg[th:Gal4-VP16]^{m1233}* (Fernandes et al., 2012), *Tg[UAS:EGFP-CAAX]^{m1230}* (Fernandes et al., 2012).

The *pcp4a^{md78}* mutant line was generated using the CRISPR/Cas9 technique. A guide RNA targeting the exon 2 of *pcp4a* was synthesized following an established protocol (Gagnon et al., 2014). In brief, target sites were selected using the online webtool CHOPCHOP (<https://chopchop.cbu.uib.no/>). A guide RNA (5'-GGAAGCATCAAACCCTCAGGTGG-3') designed to target exon 2 of *pcp4a*, was selected because of high specificity and because its target includes a restriction enzyme cutting site, allowing for easy genotyping. The sgRNA was synthesized by *in vitro* transcription of a construct containing 1) the T7 promoter for *in vitro* transcription, 2) the 20 base spacer region specific to the target site, 3) a 80 base constant region. To generate the mutant line, the sgRNA (100 ng/μl) and Cas9 protein (600 ng/μl) were microinjected in wild type embryos at one-cell stage. The injected embryos (F0 generation) were raised to adulthood in the Zebrafish facility at the Max Delbrück Center and screened for possible founders by finclipping. Fish carrying mutations were outcrossed to wild type to obtain embryos carrying only one copy of the mutated allele (F1 generation). These fish were also raised to adulthood and genotyped by Sanger sequencing to screen for mutations likely to generate a null allele. Founders were selected for an 8 bp deletion leading to a frameshift mutation and formation of a premature stop codon in exon 3. The protein, if produced, will be truncated and will not contain the calmodulin-interacting domain, and thus likely not functional. For genotyping the fish, the genomic region containing the *pcp4a^{md78}* mutation was amplified by PCR using the primers 5'-GAAAACAGACATCCCCGCTGTG-3' and 5'-CCCCACAAATCCAAAGACGTG-3', which in wild types produce a 632 bp DNA fragment. After digestion with the restriction enzyme Ddel (New England BioLabs, Cat# R0175L), the DNA fragment amplified from the wild type allele produces 2 bands of 484 bp and 148 bp. Since the mutant allele is missing the Ddel restriction site, an uncut band of 624 bp is produced.

3.11. Feeding protocol

At 5 dpf, clutchmates were split in separate 90 mm Petri dishes with Danieau's medium at a density of approximately 40 fish per dish. Larvae in the fed groups

were fed one time at 5 dpf (afternoon) and two times per day (morning and afternoon) from 6 dpf with dry food (SDS-100, Special Diets Services). The medium was changed prior to each feeding to avoid accumulation of uneaten food at the bottom of the dish. Fish in the food-deprived groups did not receive any food, and the medium was changed with the same timing and frequency as in the fed groups. Prior to experiments, gut content was inspected under a stereomicroscope to ensure that fish in the fed groups had ingested food. Although zebrafish larvae start to feed autonomously from 5 dpf, the fish can survive until 7 dpf with no food without showing any developmental problems, since at this stage they still receive nutrients from the residual yolk attached.

3.12. Behavioral assays

Experiments were performed in mutant larvae and wild-type siblings at the same time. Larvae were randomly distributed in the behavioral arenas to avoid positional effects. The behavioral setup was isolated from external stimuli: it was positioned on a vibration isolation table and shielded from external illumination. The light source was a computer screen placed underneath the recording arena. Fish were imaged using a high-speed camera (Ximea) placed above the chambers containing the larvae.

Assays for basal locomotion and behavioral choice were performed in 7 dpf free-swimming larvae.

3.12.1 Spontaneous locomotion

One hour prior to experiment, fish were transferred to a 12-wells plate with 2 ml of Danieau's medium in each well, which was kept in the fish incubator. The interval is necessary to avoid effects of the novel environment on spontaneous locomotion. The plate was then placed in the behavior-recording setup 10 minutes before the start of the experiment for the fish to adapt to the setup. Temperature during experiments was maintained constant at 28 ± 0.5 °C using

a custom-built temperature control chamber. Spontaneous locomotion was then imaged for 10 minutes at 40 Hz. For analysis, the software Ethovision XT 8.5 was used to track the fish trajectories and calculate the total distance travelled by each larva. Fish moving less than 1 mm/min were considered inactive and were excluded from the analysis.

3.12.2. Behavioral choice

After testing for spontaneous locomotion, behavioral choice was assessed using a previously established visual size discrimination assay (Barker & Baier, 2015; Filosa et al., 2016). Individual larvae were placed in custom-made transparent plastic chambers (100 X 12 mm) with 4 ml of Danieau's medium. Black circles of different sizes (1° to 30° of visual angle) moving at a constant speed of 33°/s on a white background were displayed on a computer screen positioned 1.5 cm underneath the fish. The speed and presentation mode (from below instead than above or from the side) of small stimuli were chosen to represent suboptimal prey-like stimuli in order to make them ambiguous during approach/avoidance decisions. Visual stimuli were generated with a custom-written script in PsychoPy v2.0 (Peirce et al., 2019). Circle sizes were calculated as degrees of the visual field occupied by the stimulus positioned right below a fish. Since the fish were freely moving, they were not always positioned in way to be able to detect the stimuli. Hence, the entire set of stimuli was repeated five times to maximize the number of stimulus-larvae interactions, with 2 minutes interval between each set. Locomotor responses to the visual stimuli were imaged at 60 Hz. Subsequently, they were manually scored as approaches (if the larvae swam toward an approaching visual stimulus with at least one swimming bout), avoidances (if the larvae performed at least one swimming bout to swim away from an approaching visual stimulus), or neutral interactions (when the larvae did not present any directed swimming) by an expert investigator blind to the identity of the experimental groups. The tendency of fish to approach or avoid circles was quantified using a valence index, calculated as:

$$\text{Valence index} = \frac{\text{Approaches} - \text{Avoidances}}{\text{Approaches} + \text{Avoidances}}$$

The valence index is positive when the fish preferentially approaches visual stimuli, and it is equal to 1 when 100% of the interactions are approaches. It is negative when the fish preferentially avoid visual stimuli, and it is equal to -1 when 100% of the interactions are avoidances. The general efficiency of larva-stimulus interactions was quantified using an activity index, calculated as:

$$\text{Activity index} = \frac{\text{Approaches} + \text{Avoidances}}{\text{Approaches} + \text{Avoidances} + \text{Neutral interactions}}$$

The activity index is equal to 0 if 100% of the interactions are neutral, and to 1 if all the interactions are either approaches or avoidances.

3.12.3. Optomotor response (OMR)

The OMR assay to measure visual acuity was performed in 5 dpf head-fixed larvae. The fish were mounted dorsal-side-up in a 6 cm transparent plastic Petri dish in 2% low-melting point agarose and covered with Danieau's medium. The agarose was cut below the swimming bladder with a scalpel blade to free the tail. The fish were left to recover for 30 minutes. Black and white gratings with bars of different sizes (1° to 10° of visual angle) moving forward at a constant speed of 60°/s were displayed on a computer screen positioned 1.5 cm beneath the fish. The gratings were generated using a custom-written code in PsychoPy v2.0 (Peirce et al., 2019). Bar sizes were calculated as degrees of the visual field occupied by the grating positioned right below a fish. Larvae were illuminated from above using a custom-built infrared LED ring. An infrared filter (780 nm LP, Thorlabs) was positioned in front of the camera to block visible light coming from the computer screen displaying the moving gratings. The optomotor responses of the fish to the moving bars were recorded for 30 seconds at 250 Hz. For each swimming bout episode, amplitude and duration of the bouts were manually measured using ImageJ. The fish occasionally

performed also vigorous attempts to free itself from the agarose, called 'struggles', which were differentiated from regular swimming bouts based on the tail angle ($> 90^\circ$) and were not included in the analysis.

3.13. qRT-PCR

Larvae were euthanized and their brains were manually dissected using fine dissection forceps (Dumont) in a 35 mm Petri dish with ice-cold PBS, which bottom was coated with 5% agarose in PBS. Ten brains from 7 dpf larvae were pooled for each sample. For the group treated with forskolin, and the related control, ten whole 5 dpf larvae were pooled for each sample. Samples were mechanically homogenized in Trizol and stored at -80°C . Total RNA was extracted by 1:5 chloroform purification, followed by precipitation with 1:1 isopropanol, 1:10 NaOAc and 0.5 mg/ml glycogen. All centrifugations were done at 4°C . The RNA pellet was then washed two times in ice-cold 75% ethanol and resuspended in RNase/DNase-free water. A DNase I treatment was used to prevent genomic DNA contamination, followed by an additional purification with 1:1 phenol-chloroform-isoamylalcohol. After precipitation with 1:10 LiCl and 2.5:1 ethanol 100% overnight at -20°C , total RNA was washed with ice-cold 75% ethanol and resuspended in RNase/DNase-free water. RNA concentration and quality was checked using a Nanodrop spectrophotometer (Eppendorf). cDNA was synthesized using the Superscript III First-Strand Synthesis kit (Life Technologies) using oligodT primers, following the manufacturer's instructions. After cDNA synthesis, RNase H treatment was used to digest the RNA template. The cDNA was then purified by phenol-chloroform-isoamylalcohol followed by isopropanol precipitation. The sample was then resuspended in RNase/DNase-free water, and cDNA concentration and quality were measured with a Nanodrop spectrophotometer. qRT-PCR was performed using Luna Universal qPCR Master Mix (New England BioLabs) in a StepOnePlus Real-Time PCR System (Applied Biosystem), following manufacturers' instructions. *pcp4a* mRNA was amplified using the primers 5'-CTCAGGTGGACAAGACCCATC-3' and 5'-ATCCCCCTGCCCTAAATGTG-3',

with an annealing temperature of 55°C. Each biological replica was run in triplicate, 10 ng of cDNA were used for each reaction. The housekeeping β -*actin* mRNA was used as endogenous control (using the primers 5'-GTCCCTGTATGCCTCTGGT-3' and 5'-AAGTCCAGACGGAGGATG-3' for its amplification). For each biological replica, two pools of brains or larvae were collected from the same clutch of fish: one subjected to experimental treatment and one as a control for normalization. Gene expression was normalized on the control from the same clutch using the $2^{-\Delta\Delta C_t}$ method (Gibson et al., 1996). Different biological replicas were obtained from different clutches.

3.14. Pharmacology

Wild type clutchmate larvae were split in equal numbers into two different Petri dish just before drug application. The drugs were dissolved in Danieau's medium, where the fish were incubated. The following treatments were used: 1.5 μ M fluoxetine hydrochloride (Sigma, Cat# PHR1394) for 4 hours, 10 μ M donepezil hydrochloride (Fisher, Cat# 458050010) with 0.1% DMSO for 24 hours, 50 μ M apomorphine hydrochloride (AbCam, Cat# ab269887) with 0.1% DMSO for 2 hours, 50 μ M SKF-38393 hydrochloride (MedChem Express, Cat# HY-12520A) with 0.1% DMSO for 4 hours, 16.7 μ M quinpirole hydrochloride (Sigma, Cat# Q102) with 0.1% DMSO for 3 hours, 10 μ M forskolin (Sigma, Cat# F6886) with 0.1% DMSO for 1 hour. Control groups were incubated in Danieau's medium with 0.1% DMSO, with the exception of the control group for fluoxetine treatment, which was incubated only in Danieau's medium.

For the treatment combining quinpirole with forskolin, fish were first incubated in 16.7 μ M quinpirole hydrochloride with 0.1% DMSO. After two hours, 10 μ M forskolin with 0.1% DMSO was added to the medium. Fish were incubated in both drugs for one additional hour.

3.15. *In situ* hybridization

In situ hybridization to detect *pcp4a*, *gad1b*, *vglut2*, *drd2a* and *drd2b* transcripts was performed using third-generation *in situ* hybridization chain reaction (HCR) v.3.0 (Choi et al., 2018). All the probes and fluorophore-conjugated hairpins were purchased from Molecular Instruments Inc. *vglut2* probes recognized both zebrafish *vglut2* paralogs *slc17a6a* and *slc17a6b*. *In situ* HCR v.3.0 was performed following the manufacturer's protocol. The fish were kept always in the dark to preserve endogenous fluorescence signal. 7 dpf larvae were fixed overnight in 4% PFA in PBS at 4°C, followed by washes in PBS and incubation in 100% methanol at -20°C for at least 10 minutes. Fish were rehydrated with serial solutions of methanol/PBT (PBS + 0.1% Tween20) and then washed several times in PBT. Larvae were then permeabilized with proteinase K (10 µg/ml) for 15-30 minutes, followed by postfixation in 4% PFA. After several washes in PBT, fish were pre-hybridized in probe hybridization buffer (Molecular Instruments) at 37°C for 30 minutes. Larvae were then incubated in probe hybridization buffer with 4 nM of each probe at 37°C overnight. The next morning, fish were washed several times with probe wash buffer (Molecular Instruments) at 37°C and in 5X SSCT (SSC + 0.1% Tween20) at room temperature. They were then incubated in amplification buffer (Molecular Instruments) for 30 minutes. The fluorophore-conjugated hairpins were snap-cooled at 95°C for 90 seconds, followed by cooling at room temperature in the dark. The larvae were then incubated in amplification buffer with 30 nM of each fluorophore-conjugated hairpin at room temperature. After washes in 5X SSCT, larvae were immediately mounted in 1.5% low-melting point agarose, covered in PBS and imaged with a Leica DM6 CFS confocal microscope a 25X water-immersion objective (HC Fluotar L 25X/0.95, Leica Microsystems).

Volume rendering of confocal stacks of the tectum and mapping of position of *pcp4a*⁺ PVNs (Figure 6B) was performed with the software Imaris using the 'spots' feature.

3.16. Immunohistochemistry

Immunohistochemistry was performed following an established protocol (Corradi et al., 2022). 7 dpf larvae were fixed overnight in 4% PFA in PBST (PBS + 0.3% Triton) at 4°C. The next morning, fish were washed several times in PBST, and incubated in 150 mM Tris-HCl (pH = 9) for 5 minutes at room temperature, followed by 15 minutes at 70°C. After a wash in PBST, larvae were incubated in Trypsin EDTA (Sigma, diluted 1:20 in PBST) for 40 minutes on ice. Trypsin was washed out with PBST. After 1 hour of blocking at room temperature in blocking solution (5% goat serum, 1% BSA, 1% DMSO in PBST), fish were incubated with primary antibodies, each diluted 1:500 in blocking solution for 96 hours at 4°C. Primary antibodies against the following antigens were used: GFP (Invitrogen, Cat# A10262), total ERK (tERK; Cell Signaling, Cat# 4696), phosphorylated ERK (pERK; Cell Signaling, Cat# 4370). Afterward, larvae were washed several times in PBST. After 1 hour of blocking at room temperature in blocking solution, fish were incubated in Alexa Fluor secondary antibodies, each diluted 1:300 in blocking solution for 48 hours at 4°C. The following Alexa Fluor secondary antibodies were used: α -chicken-AF488 (ThermoFisher, Cat# A11039), α -mouse-AF647 (Cell Signaling, Cat# 4410S), α -rabbit-AF555 (Cell Signaling, Cat# 4413S). Larvae were then washed several times in PBST and mounted in 1.5% low-melting point agarose for imaging. Images of the samples were acquired using a Leica DM6 CFS confocal microscope with a 25X water-immersion objective (HC Fluotar L 25X/0.95, Leica Microsystems). The same acquisition parameters were applied to all the larvae to be able to compare fluorescence intensities between fish. GFP-positive cells in *th:gal4-VP16; UAS:EGFP-CAAX* larvae were selected to measure the fluorescent intensities of pERK and tERK immunostainings by manually drawing ROIs in ImageJ. Dopaminergic cluster identity of each individual neuron was determined following the nomenclature used in (Kastenhuber et al., 2010). The cumulative percentage of pERK/tERK values was calculated for each cluster for each larva and then averaged across fish.

3.17. *In vivo* calcium imaging

7 dpf larvae used for *in vivo* calcium imaging were homozygous *mitfa*^{w2/w2} mutants lacking skin melanophores (Lister et al., 1999) to avoid pigmentation to interfere with the imaging. Larvae were mounted in 1% low-melting point agarose in Danieau's medium containing the myorelaxant pancuronium bromide (0.3 mg/ml, Sigma) in a small plastic Petri dish and covered with Danieau's medium. Pancuronium bromide was used to paralyze the fish and minimize motion artifacts during imaging. Black circles of different sizes (1° to 30° of visual angle), moving at a constant speed (4.4°/s) on a grey background, were displayed on a microdisplay (Kopin) on one side of the fish. The stimuli were generated with a custom-written script in PsychoPy. Neuronal responses to the visual stimuli were imaged in the contralateral side of the tectum using a confocal microscope (Zeiss LSM 880 NLO) with a 20X water-dipping objective (W Plan Aplanachromat 20X/1.0 DIC VIS-IR, Zeiss). Time series of single planes calcium signals were acquired at 4 Hz with an image pixel size of 1 μm^2 . The code for stimuli presentation was triggered from the microscope by the start of acquisition. This way, stimuli with the same size were presented always at the same timeframe in all the recordings. Three to four z-planes were acquired for each fish at different depths in the tectum to have a representative sample of the entire tectal population. Since PVNs size selectivity may vary with their location, utmost care was paid to image at similar depths in all larvae.

Raw images were first x-y motion corrected using the NoRMCorre algorithm in Matlab (Pnevmatikakis & Giovannucci, 2017). Slow x-y drifts in the image are generally a result of agarose dynamics due to the laser heat or osmotic adjustment to the Danieau's medium. To minimize these movements, fish were mounted and covered with buffer at least 30 minutes before imaging. This also allowed for a recovery of the fish from the mounting stress.

Regions of interest (ROIs) corresponding to single neurons were drawn manually in ImageJ. GCaMP6s fluorescence intensity, measured as the mean grey value for each ROI, was normalized as $\Delta F/F_0 = (F - F_0) / F_0$ where F is the fluorescence at each time point and F_0 is the average baseline fluorescence (10 frames preceding the stimulus presentation). A neurons was considered

responding to a stimulus if the calcium peak corresponding to stimulus presentation was higher than two standard deviation of the baseline. The size tuning of neurons was measured as WMR angles, calculated as weighted sums of visual stimulus sizes, to which neuronal responses were non-zero:

$$\text{WMRangle} = \sum_{i=1}^n w_i * x_i$$

where x_i are the angular sizes of the visual stimuli and w_i are the weights calculated as:

$$w_i = \left(\frac{\Delta F}{F_0}\right)_i / \sum_{i=1}^n \left(\frac{\Delta F}{F_0}\right)_i$$

To analyze the response to visual stimuli in the RGC terminals in the tectal neuropil, a pixel-wise analysis based on a regression model was performed using a code in Python (Filosa et al., 2016; Miri et al., 2010). A linear regression model composed of six variables, corresponding to the individual responses for the different visual stimulus sizes, and by a constant term, was used to represent the temporal series for each pixel. The regressor functions were obtained from the convolution of the waveforms of the stimulus presence with a GCaMP6s kernel, whose $t_{\text{off}} = 1.8$ s was based on the coefficient of determination R^2 . The distribution of T scores for different sizes of the stimuli were averaged across different trials (Figure 13C). Corrected distributions were obtained by subtracting a term, equal to 3 SD, accounting for changes in fluorescence in absence of stimulation. The number of pixels activated by presentation of visual stimuli was quantified by calculating the integrals of the corrected distributions.

In calcium imaging recordings, tectal PVNs expressing *pcp4a* were identified *post mortem* using an approach similar to the MultiMAP method (Lovett-Barron et al., 2017). *In vivo* Ca^{2+} imaging was performed in a selected set of z-planes at different depths in the tectum to record activity of tectal neurons in response to visual stimuli in *elavl3:H2B-GCaMP6s* larvae, expressing the calcium sensor GCaMP6s panneuronally. Then, stacks of images of the whole tectum

contralateral to the eye receiving visual stimulation was acquired with a 1 μm z-step. Each stack was centered around an individual Ca^{2+} imaging z-plane to allow for easy identification of the imaging plane during subsequent analysis, and was taken immediately after Ca^{2+} imaging to minimize possible z-shifts due to agarose movements. Minimal x-y shifts between the same plane in the calcium imaging timelapse and in the stack often occurred due to slow agarose drifting movements and were manually corrected in ImageJ using the 'translate' function to ensure accurate cell identification. Immediately after imaging, the larvae were euthanized and fixed in 4% PFA in PBS overnight at 4°C. *In situ* HCR was then performed to detect *pcp4a* mRNA, using the protocol described above. Special care was taken to keep the fish always in the dark throughout the protocol to preserve endogenous GCaMP6s signal. After *in situ* HCR, a stack of images of the residual GCaMP6s signal and the *pcp4a in situ* HCR signal was acquired from the same tectum with 1 μm z-step on a confocal microscope (Zeiss LSM 880 NLO) with a 20X water-immersion objective (W Plan Aplanachromat 20X/1.0 DIC VIS-IR, Zeiss). The stack imaged post-fixation was registered to the stack acquired during live imaging, using the GCaMP6s fluorescence signal in the two datasets to guide the alignment, with the CMTK plugin in ImageJ (Jefferis, 2018). The registration parameters used were: -awr 010203 -T 4 -X 200 -C 4 -G 160 -R 5 -A '--accuracy 0.4' -W '--accuracy 0.4'. The z-planes containing the neurons whose activity was recorded during the *in vivo* calcium imaging session were identified in the registered stack: they usually corresponded to the central image of the stack, since the live imaging template was acquired centered on the calcium imaging plane. In case minimal z-shifts occurred, the correct z-plane was identified thanks to the specific SINS localization pattern in the neuropil in each plane. Accuracy of the registration was checked manually by merging the *in vivo* calcium imaging recording to the corresponding z-plane in the registered post-fixation stack in ImageJ. The shift between the GCaMP6s signal in the two images was consistently well under the average cell nucleus diameter (5 μm), ensuring accurate cell identification (Figure 9D). Neurons were considered positive for *pcp4a* if the *in situ* signal occupied at least 50% of the perimeter of the nuclei labeled by H2B-GCaMP6s. In case of uncertainty, z-planes below and above the imaging plane were

checked in the registered stack. The same criteria were applied to check whether neurons were positive for *gad1b* or *drd2*.

For the experiment testing the effect of CaMKII inhibition on the activity of *pcp4a+* PVNs, 7 dpf *elavl3:H2B-GCaMP6s* food-deprived larvae were treated with the CaMKII inhibitor KN93 (5 μ M, Adooq Bioscience, Cat#A13276-5) with 0.1% DMSO in Danieau's medium for 3 hours prior to experiment. The control group was incubated with 0.1% DMSO in Danieau's medium for the same period of time. Activity of *pcp4a+* PVNs in response to visual stimuli was recorded using *in vivo* calcium imaging as described above, with the drug still in the solution.

For the experiments testing the effect of dopaminergic D2-like receptor signaling on the activity of *pcp4a+* PVNs, responses to visual stimuli were first recorded using *in vivo* calcium imaging in 7 dpf *elavl3:H2B-GCaMP6s* food-deprived larvae, as described above. The fish, still embedded in agarose, were then incubated for 3 hours in Danieau's medium containing 16.7 μ M quinpirole hydrochloride (Sigma, Cat# Q102). The control group was incubated in Danieau's medium for the same period of time. Larvae were then transferred again under the microscope, with the drug still in the solution, and responses to visual stimuli were recorded a second time from the same z-planes containing the PVNs imaged during the first session. The planes were identified based on the characteristic SInS localization pattern in the neuropil. *Post mortem* identification of *pcp4a+* neurons and analyses of GCaMP6s signal were then performed as described above.

3.18. Statistical analysis

Statistical significance was determined using one-sample t tests, two-tailed Student's t tests, two-way ANOVA, and nested two-way ANOVA in GraphPad Prism (GraphPad, version 9). Normal distribution of data was verified with the Shapiro-Wilk test before performing t tests. p values from multiple Student's t tests were corrected using the Bonferroni-Holm method. Statistical tests were considered significant if $p < 0.05$. Significance level was indicated in the graphs

as: * $p < 0.05$, ** $p < 0.01$, *** $p < 0.001$, n.s. = not significant. Data were represented as mean \pm SEM.

3.19. Graphics

All the figures in the dissertation were created in Adobe Illustrator. Representative confocal images were generated in ImageJ using the QuickFigures plugin (Mazo, 2021). 3D volume reconstructions were made in Imaris. All graphs were generated in GraphPad Prism version 9.

4. Results

4.1. *pcp4a* expression

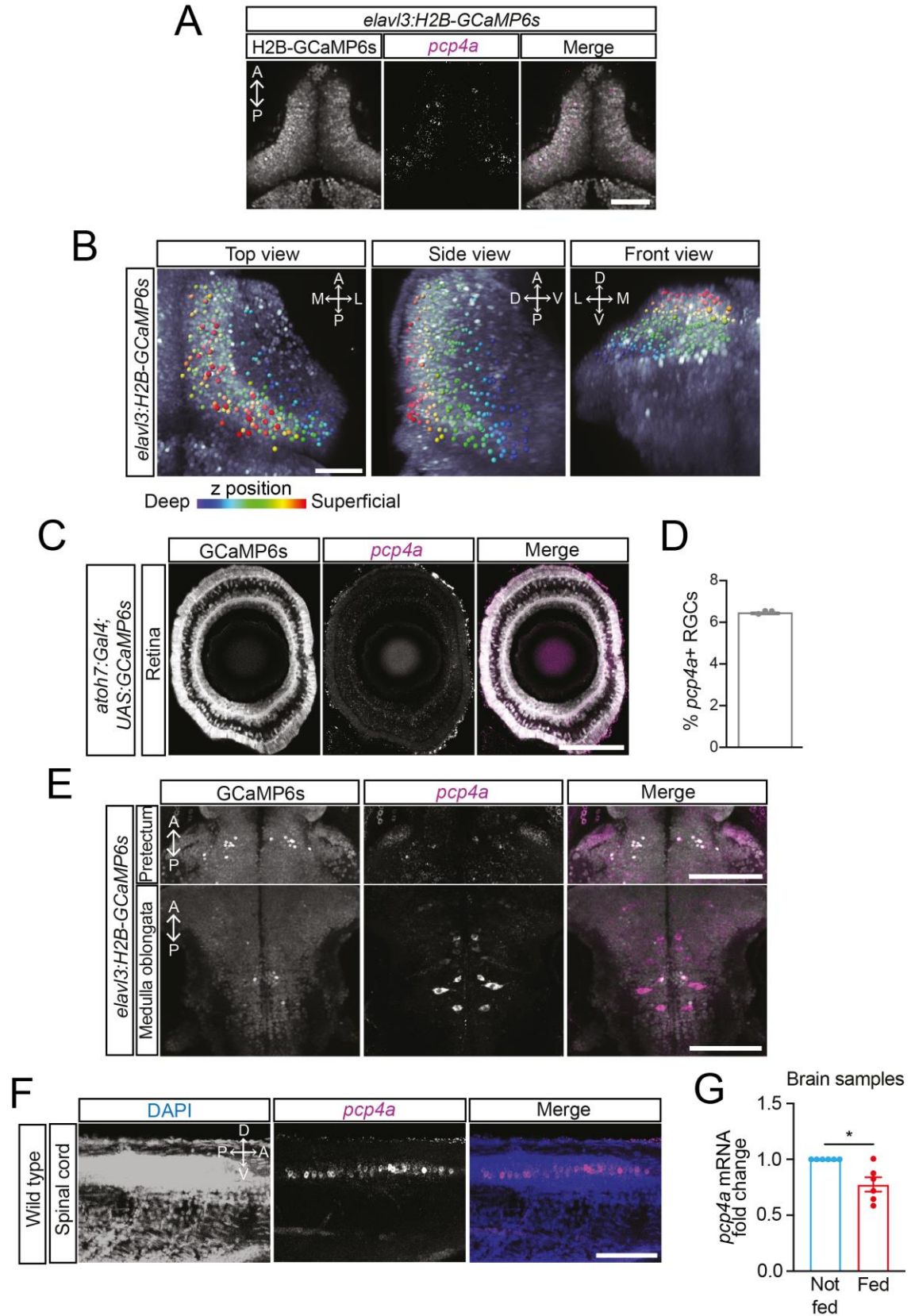


Figure 6: *pcp4a* expression in the central nervous system

A. Confocal images of the optic tectum of a 7 dpf *elavl3:H2B-GCaMP6s* larva. Nuclei of neurons are labeled with GCaMP6s and *pcp4a* mRNA localization is revealed by *in situ* HCR. Scale bar: 50 μ m. **B.** Top, side and front views of a 3D-rendered volume of the tectum of a 7 dpf *elavl3:H2B-GCaMP6s* larva. Spheres label *pcp4a*⁺ PVNs location, identified by *in situ* HCR and color-coded according to depth. Scale bar: 50 μ m. **C.** Confocal images showing localization of *pcp4a* mRNA in the retina of a 7 dpf *ato7:Gal4;UAS:GCaMP6s* larva. Scale bar: 100 μ m. **D.** Bar graph depicting average percentage of *pcp4a*⁺ RGCs in the retina. n = 3 larvae. **E.** Confocal images showing localization of *pcp4a* mRNA in the pretectum and medulla oblongata of a 7 dpf *elavl3:H2B:GCaMP6s* larva. Scale bar: 100 μ m. **F.** Confocal images showing expression of *pcp4a* in the ventral spinal cord of 7 dpf wild-type fish. Scale bar: 100 μ m. **G.** Bar graph depicting fold change of *pcp4a* mRNA levels in the brain of 7 dpf wild-type fed larvae versus food-deprived fish. n = 6 biological replica for each condition. Ten brains were pooled for each replica. One sample t test: p = 0.02. Abbreviations: A, anterior; D, dorsal; L, lateral; M, medial; P, posterior; V, ventral.

I first checked the expression pattern of *pcp4a* in 7 dpf zebrafish larvae by performing *in situ* hybridization to localize *pcp4a* mRNA. The results showed that *pcp4a* has sparse expression in the optic tectum (Figure 6A). *pcp4a*⁺ PVNs do not present any particular gradient along the dorso-ventral or medio-lateral axis (Figure 6B). The stainings also show *pcp4a* expression in the retina (Figure 6C) in a subset of RGCs (around 6%, Figure 6D), amacrine and bipolar cells. In the central nervous system, *pcp4a* is also expressed in the pretectum, the reticulospinal network in the medulla oblongata (Figure 6E) and the spinal cord (Figure 6F).

The previous proteomic study conducted in whole larva showed a decreased abundance of Pcp4a in fed fish (Figure 5B). To confirm if the same change happens in the brain, I measured *pcp4a* mRNA levels in brain samples from 7 dpf fed and food-deprived siblings by reverse transcription-quantitative polymerase chain reaction (RT-qPCR). *pcp4a* mRNA levels were 25% lower in samples from fed larvae compared to non-fed siblings (Figure 6G). This suggests that feeding decreases *pcp4a* expression in the brain through a transcriptional mechanism.

4.2. Role of *pcp4a* in the modulation of behavioral choice

To analyze the role of *pcp4a* in regulating decision-making, I looked at the effect of a lack of *pcp4a*. For this purpose, I generated a mutant line employing CRISPR/Cas9 technique. I used a guide RNA targeting exon 2 of *pcp4a* and selected founders carrying a 8 bp deletion (*md78* allele). This mutation induce a frameshift and a premature stop codon in exon 3. The resulting protein, if translated, would be missing the domain for binding to calmodulin and thus likely not functional (Figure 7A).

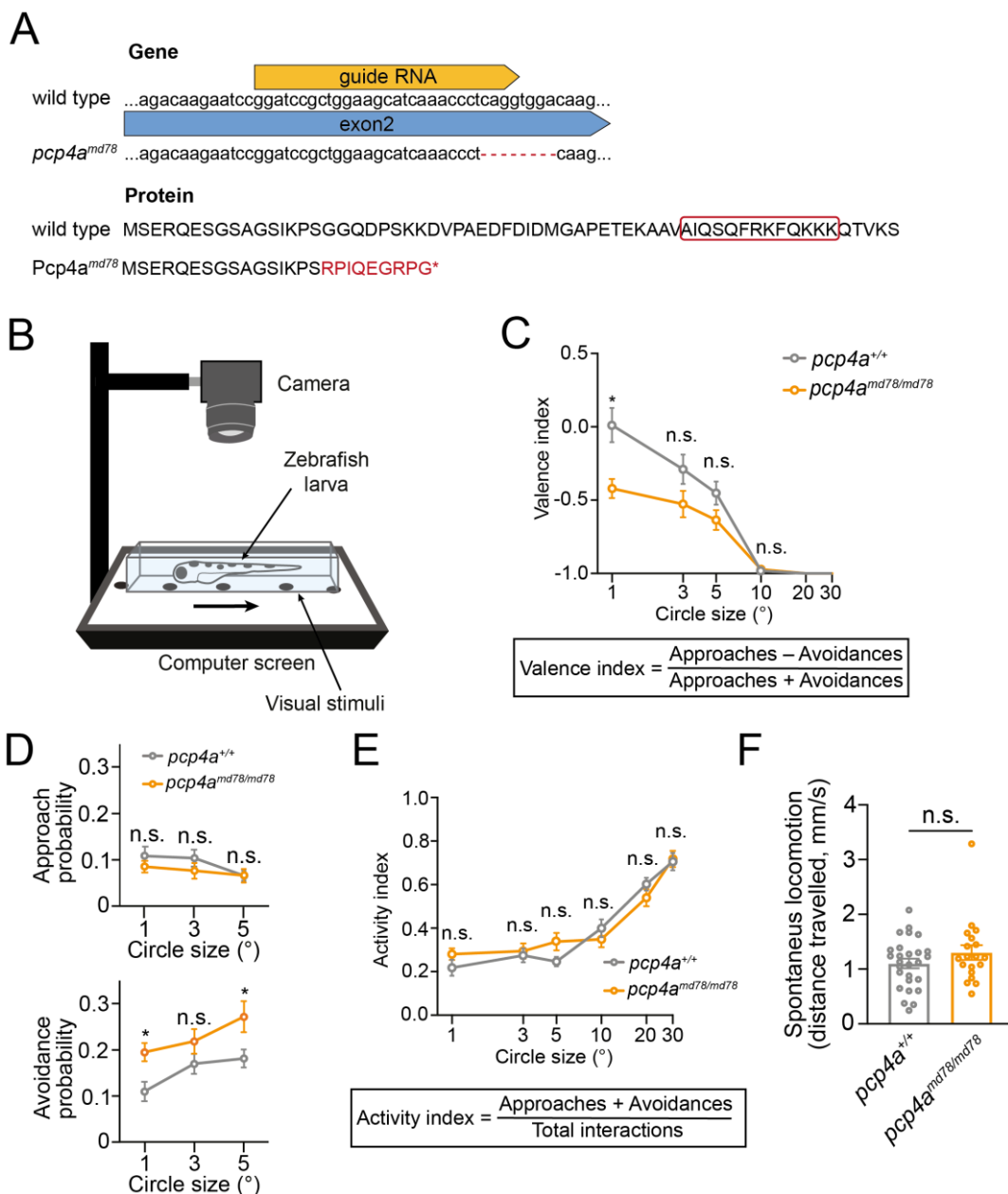


Figure 7: Mutating *pcp4a* alters behavioral choice

A. Schematic representation of the strategy employed to mutate *pcp4a* using the CRISPR/Cas9 technique. Using a guide RNA targeting exon 2 of *pcp4a*, I generated an 8 bp deletion resulting in a frame shift and the formation of an early stop codon in exon 3 (*md78* allele). If produced, the resulting short truncated protein would have a partially mutated sequence lacking the Calmodulin-interacting domain (labeled by the red box in the wild-type protein sequence). **B.** Schematic representation of the behavioral setup used for recording approach/avoidance decisions of zebrafish larvae. Circles of different sizes moving at constant speed were displayed on a computer screen positioned below small tanks containing single zebrafish larvae. Movements of the fish in response to the visual stimuli were recorded with a high-speed camera positioned above the tanks. **C.** Graph showing average valence indexes for different sizes of visual stimuli of 7 dpf food-deprived *pcp4a*^{+/+} and *pcp4a*^{md78/md78} larvae. Two-tailed t test with Bonferroni-Holm correction: $p = 0.01$. **D.** Graphs showing approach (top) or avoidance (bottom) probability for small visual stimuli in 7 dpf food-deprived *pcp4a*^{+/+} and *pcp4a*^{md78/md78} larvae. Approach and avoidance probabilities were calculated as [approaches/(approaches + avoidances + neutral interactions)] or [avoidances/(approaches + avoidances + neutral interactions)], respectively. Two-tailed test with Bonferroni-Holm correction. Approach probability: $p = 0.02$ (1°), $p = 0.04$ (5°). **E.** Graph showing average activity indexes for different sizes of visual stimuli of 7 dpf food-deprived *pcp4a*^{+/+} and *pcp4a*^{md78/md78} larvae. Two-tailed t test with Bonferroni-Holm correction. In (C-E) $n_{pcp4a+/+} = 22$ larvae, $n_{pcp4amd78/md78} = 18$ larvae. **F.** Bar graph showing average spontaneous locomotion of 7 dpf food-deprived *pcp4a*^{+/+} and *pcp4a*^{md78/md78} larvae. $n_{pcp4a+/+} = 27$ larvae, $n_{pcp4amd78/md78} = 19$ larvae. Two-tailed t test.

To study behavioral choice in mutant fish lacking Pcp4a, I performed a size discrimination assay in freely swimming larvae previously employed in other studies (Barker & Baier, 2015; Filosa et al., 2016). Black circles of different sizes moving at constant speed are displayed on a screen underneath the fish. The locomotor response of the fish to the visual stimuli is recorded with a high speed camera (Figure 7B). Behavioral responses were categorized as approach, if the fish performed small bouts oriented towards the circle; avoidance, if the fish performed a stereotypical escape maneuver; or neutral interactions if the fish did not show any active response to the stimulus. Small circles are likely perceived as preys and approached while large ones should

be perceived as predators and avoided. However, as the stimuli do not perfectly mimic natural cues, the choice can be less straightforward, allowing to discern subtle differences in decision-making. By counting the number of approaches toward versus avoidances of circles of different sizes, it is possible to measure the tendency of the fish to take risks during foraging.

I first performed the experiment in food-deprived larvae since they normally have higher levels of Pcp4a (Figure 5B) and thus I expected that differences in the mutant would be enhanced. The tendency to approach or avoid a stimulus of a particular size was measured by the valence index, calculated as:

$$\text{Valence index} = \frac{\text{Approaches} - \text{Avoidances}}{\text{Approaches} + \text{Avoidances}}$$

The valence index is positive when fish preferentially approach and negative when fish preferentially perform avoidances.

Food-deprived homozygous mutant larvae showed decreased valence index for small stimuli (Figure 7C) due to increased avoidance of small stimuli (Figure 7D), while the approach probability did not change compared to wild-type siblings (Figure 7D). The behavioral choice displayed by mutant larvae closely resemble the one shown by fed larvae (Filosa et al., 2016). Thus, food-deprived larvae lacking Pcp4a phenocopy fed larvae, suggesting that Pcp4a indeed plays a role in modulation of decision-making behavior by feeding state.

The tendency of the fish to actively respond to stimuli of different size was measured by the activity index, calculated as:

$$\text{Activity index} = \frac{\text{Approaches} + \text{Avoidances}}{\text{Total interactions}}$$

There was no difference in the number of active responses to visual cues in mutant compared to wild-type siblings (Figure 7E), meaning that the mutation does not impair neuronal circuits for visuomotor transformation. Moreover, homozygous mutant fish do not show alterations of locomotion in basal conditions, suggesting lack of Pcp4a does not lead to general locomotor impairments (Figure 7F).

To further ensure that lack of Pcp4a does not affect detection of visual stimuli, we measured visual acuity of mutant larvae using an optomotor response assay. In this behavioral test, the fish is mounted in a head-fixed preparation in agarose, while its tail is free to move. Black and white gratings moving forward

at constant speed are projected on a screen below the fish. Since this is perceived by the fish as if the ground beneath is moving, like it happens when water flow wash the fish away in a natural environment, it will try to swim to maintain the same relative position. Since the tail is free from the agarose, it is possible to infer the effort the fish put in by measuring different parameters related to swim bouts. This behavior is affected by impairment of visual or locomotor function. Using gratings with bars of different width allow to highlight differences in visual acuity. There was no significant difference in the amplitude (Figure 8A), duration (Figure 8B) or number of swim bouts (Figure 8C) in response to gratings of small and large size in 5 dpf mutant larvae, suggesting that lack of Pcp4a does not lead to changes in visual acuity.

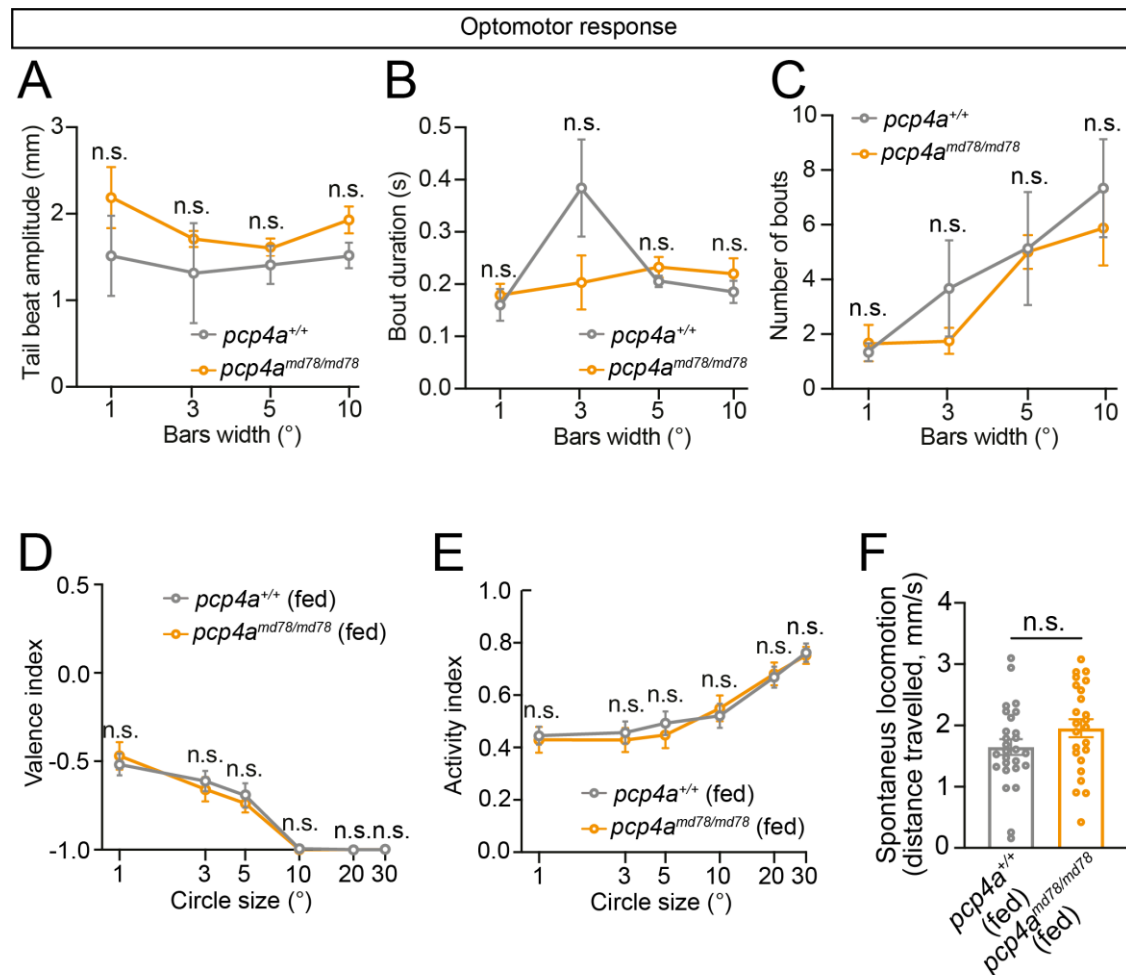


Figure 8: Behavioral performance of *pcp4a* mutants

A – C. Graphs depicting tail beat amplitude (A), bout duration (B) and number of bouts (C) during optomotor response performed by 5 dpf food-deprived *pcp4a*^{+/+} and *pcp4a*^{md78/md78} fish. $n_{pcp4a+/+} = 10$ larvae, $n_{pcp4amd78/md78} = 9$ larvae. Two-tailed t test with Bonferroni-Holm correction. **D, E.** Graphs showing average valence indexes (D) or activity indexes (E) for different sizes of visual stimuli of 7 dpf fed *pcp4a*^{+/+} and *pcp4a*^{md78/md78} larvae. $n_{pcp4a+/+} = 26$ larvae, $n_{pcp4amd78/md78} = 22$ larvae. Two-tailed t test with Bonferroni-Holm correction. **F.** Bar graph showing average spontaneous locomotion of 7 dpf fed *pcp4a*^{+/+} and *pcp4a*^{md78/md78} larvae. $n_{pcp4a+/+} = 27$ larvae, $n_{pcp4amd78/md78} = 24$ larvae. Two-tailed t test.

Finally, I checked the effect of *pcp4a* mutation on behavior in fed larvae. Fed 7dpf homozygous mutant larvae showed no significant difference in valence index (Figure 8D) compared to fed wild-type siblings. This confirm that lack of Pcp4a induce behavioral choice similar to what observed in fed larvae, which indeed have already low levels of Pcp4a. Moreover, mutant larvae showed no differences in activity index (Figure 8E) or spontaneous locomotion (Figure 8F), confirming that the mutation does not lead to general impairment of visuomotor circuits.

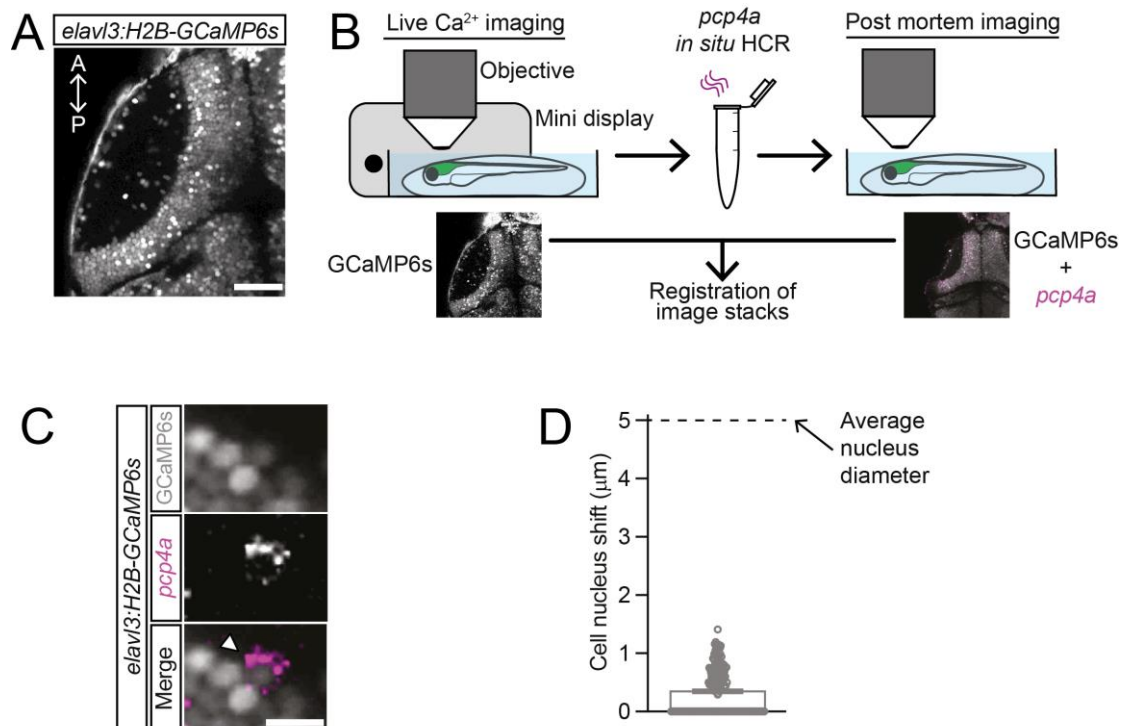
4.3. Tectal *pcp4a*⁺ neurons activity

4.3.1. Modulation of *pcp4a*⁺ tectal neurons activity by feeding state

I then investigated if *pcp4a* regulates decision-making behavior by affecting processing of visual stimuli in the optic tectum. For this purpose, I characterized the response to visual stimuli of tectal *pcp4a*-expressing neurons. Since there is no transgenic line labeling specifically *pcp4a*⁺ neurons available, I first performed calcium imaging in a line with panneuronal nuclear expression of the calcium sensor GCaMP6s (*elavl3:H2B-GCaMP6s*) (Figure 9A) and then identified *pcp4a*⁺ neurons *post mortem* by *in situ* hybridization, following a protocol similar to a previously established one (Lovett-Barron et al., 2020) (Figure 9B). In brief, moving black circles of different sizes were displayed on a

small screen on the side of the fish, while imaging the activity of the neurons in the contralateral side of the optic tectum. Calcium imaging was performed on few planes at different depths in the optic tectum, followed by acquisition of a z-stack of the whole tectum. Fish were fixed immediately after imaging and *pcp4a* mRNA was detected by *in situ* hybridization using the hybridization chain reaction (HCR) technique (Choi et al., 2018). After staining, a z-stack of the *pcp4a in situ* signal and the residual GCaMP6s fluorescence signal was acquired. By registering the stack of the fixed GCaMP6s signal to the stack of the live GCaMP6s signal, it was possible to identify the *pcp4a*⁺ neurons in the calcium imaging planes (see Materials and Methods, section 3.17, for a detailed protocol) (Figure 9C).

The accuracy of the registration was checked rigorously to ensure correct cell identification. The shift between registered fixed and live GCaMP6s signal was consistently well under the average diameter of a nucleus (5 μm), making cell identification errors unlikely (Figure 9D,E).



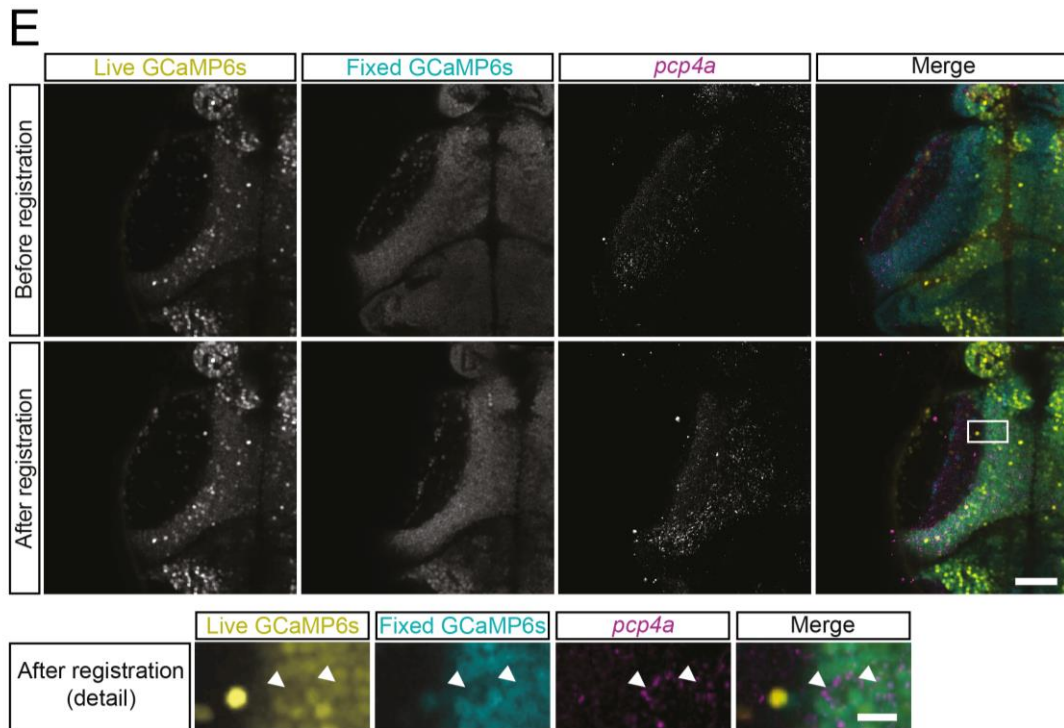


Figure 9: Calcium imaging strategy

A. Confocal image showing part of the tectum of a 7 dpf *elavl3:H2B-GCaMP6s* fish. Scale bar: 50 μm . **B.** Schematic representation of the strategy used to identify *pcp4a*+ neurons after *in vivo* calcium imaging. Visual stimuli (black circles of different sizes moving at constant speed on a grey background) were shown on a microdisplay to one eye of 7 dpf *elavl3:H2B-GCaMP6s* larvae embedded in agarose, while performing calcium imaging of their contralateral tectum. After fixation and *in situ* HCR to detect *pcp4a* mRNA, a confocal image stack was acquired and aligned to the one taken during *in vivo* calcium imaging to identify *pcp4a*+ neurons. **C.** Confocal images showing localization in a 7 dpf *elavl3:H2B-GCaMP6s* larva of *pcp4a* mRNA, detected with *in situ* HCR, and GCaMP6s signal acquired during *in vivo* Ca^{2+} imaging. The images were taken from the image stack obtained after aligning the *in vivo* and *post mortem* stacks. The white arrowhead points to a *pcp4a*+ PVN. Scale bar: 10 μm . **D.** Graph showing quantification of the shift of cell nuclei between *in vivo* and *post mortem* images after registration. $n = 168$ neurons randomly selected from 3 fish. **E.** Confocal images showing GCaMP6s signal before (live GCaMP6s, average projections of a Ca^{2+} imaging timelapse of a single z-plane) and after fixation (fixed GCaMP6s, corresponding z-plane of the fixed and stained sample), and *pcp4a* mRNA localization (detected by *in situ* HCR) in a 7 dpf *elavl3:H2B-GCaMP6s* larva, before and after registration of the *in vivo* and fixed confocal images using the CMTK algorithm. At the bottom, high magnification images of the area marked by the white rectangle in the top

panel are shown. Scale bars, 50 μm (top panel) or 10 μm (bottom panel). Note that the registration is very efficient in the PVL, while the neuropil region of the two images does not align well due to severe morphological alterations caused by the *in situ* HCR protocol.

pcp4a⁺ neurons represent around 10% of the total tectal PVNs (Figure 10D). The majority of *pcp4a*⁺ neurons respond to both small ($\leq 5^\circ$) and large ($\geq 10^\circ$) stimuli ('dual' responding neurons), while only around 10% of *pcp4a*⁺ PVNs are selective for large stimuli. Neurons tuned to small stimuli only are rare in this population (Figure 10A). In average, the amplitude of the response to large stimuli is greater than the response to small (Figure 10B). Given the heterogeneity in tuning properties of these neurons, we defined the tuning size of each neuron as weighted mean response (WMR) angle, which correspond to the average size of the stimulus each neuron responds to, weighted for the amplitude of the response to each stimulus (see Materials and Methods, section 3.17, for details).

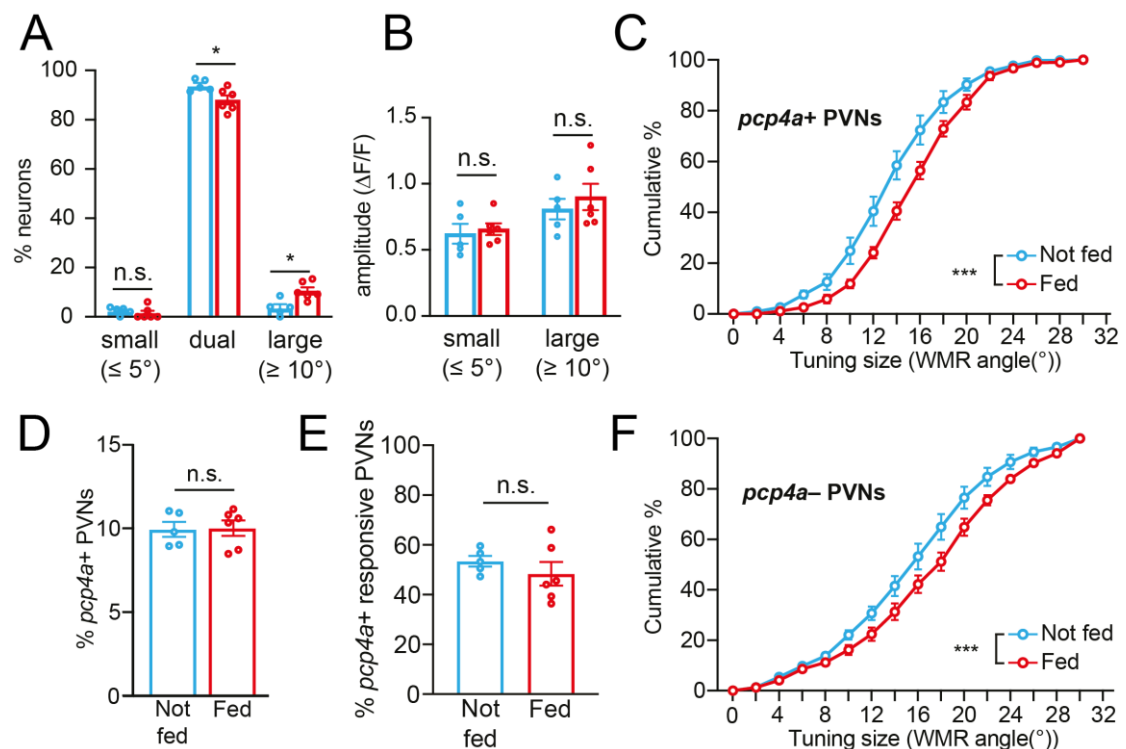


Figure 10: Feeding alters tuning properties of *pcp4a*+ PVNs

A. Bar graph showing proportion of size-selective *pcp4a*+ PVNs in food-deprived and fed 7 dpf *elavl3:H2B-GCaMP6s* larvae. $n_{\text{fed}} = 6$ fish, $n_{\text{not-fed}} = 5$ fish. Two-tailed t test with Bonferroni-Holm correction: dual, $p = 0.04$; large, $p = 0.03$. **B.** Bar graph showing average normalized amplitude ($\Delta F/F$) of responses to small or large visual stimuli in *pcp4a*+ PVNs in food-deprived and fed 7 dpf *elavl3:H2B-GCaMP6s* larvae. $n_{\text{fed}} = 6$ fish, $n_{\text{not-fed}} = 5$ fish. Two-tailed t test. **C.** Graph depicting cumulative percentages of WMR angles of *pcp4a*+ PVNs in food-deprived and fed 7 dpf *elavl3:H2B-GCaMP6s* larvae. $n_{\text{fed}} = 6$ fish, $n_{\text{not-fed}} = 5$ fish. Two-way ANOVA: $p < 0.0001$. **D.** Bar graph showing average percentages of *pcp4a*+ PVNs. $n_{\text{fed}} = 6$ fish, $n_{\text{not-fed}} = 5$ fish. Two-tailed t test. **E.** Bar graph showing average proportion of *pcp4a*+ PVNs responsive to visual stimuli in 7 dpf fed and not-fed *elavl3:H2B-GCaMP6s*. $n_{\text{fed}} = 6$ fish, $n_{\text{not-fed}} = 5$ fish. Two-tailed t test. **F.** Graph depicting cumulative percentages of WMR angles of *pcp4a*- PVNs in food-deprived and fed 7 dpf *elavl3:H2B-GCaMP6s* larvae. $n_{\text{fed}} = 6$ fish, $n_{\text{not-fed}} = 5$ fish. Two-way ANOVA: $p < 0.0001$.

To elucidate the effect of feeding state on *pcp4a*+ PVNs activity I imaged both fed and food-deprived siblings. In fed larvae, the response profile shifted towards large stimuli, as evident from the cumulative distribution of the tuning size (Figure 10C).

Since there is no difference in the proportion of *pcp4a*+ PVNs (Figure 10D) or the percentage of *pcp4a*+ PVNs responding to visual stimuli (Figure 10 E), the shift in the response profile is unlikely due to changes in the expression pattern or in the activation or silencing of large neuronal populations. Instead, it may be explained by an alternative recruitment of different neuronal subpopulations or by changes in the size tuning of individual neurons.

Finally, *pcp4a*-negative PVNs are also preferentially tuned to large stimuli in fed larvae (Figure 10F), similar to what was previously shown in (Filosa et al., 2016). This result suggests that *pcp4a* may not be the only molecular pathway regulating feeding state-dependent PVNs activity and thus behavioral choice. Since decision-making during feeding behavior plays such a crucial role for survival, it is reasonable to hypothesize that it must be finely regulated by multiple parallel and complementary pathways.

4.3.2. Role of *pcp4a* in modulation of tectal neurons activity

To investigate whether the shift in the response profile induced by feeding is due to change in the levels of Pcp4a, I analyzed the response to visual stimuli of *pcp4a*⁺ PVNs in the mutant. Since *pcp4a* mRNA is still produced in the mutant, it is still possible to identify *pcp4a*⁺ neurons by *in situ* hybridization. *pcp4a*⁺ PVNs in food-deprived mutant larvae displayed a shift in the response profile towards large stimuli compared to food-deprived wild-type siblings (Figure 11A), similar to what observed in fed larvae (Figure 10C). This suggest that the observed changes in tuning properties are indeed due to the decrease in Pcp4a levels induced by feeding. There was no difference in the number of *pcp4a*⁺ PVNs (Figure 11B) or the proportion of *pcp4a*⁺ neurons responding to visual stimuli (Figure 11C), suggesting that the mutation does not alter development of tectal neurons. Interestingly, the mutation has a negligible effect on the response profile of *pcp4a*-negative neurons (Figure 11D), indicating that *pcp4a* acts mainly in a cell-autonomous way and has limited effect on other neuronal subpopulations through intratectal circuits.

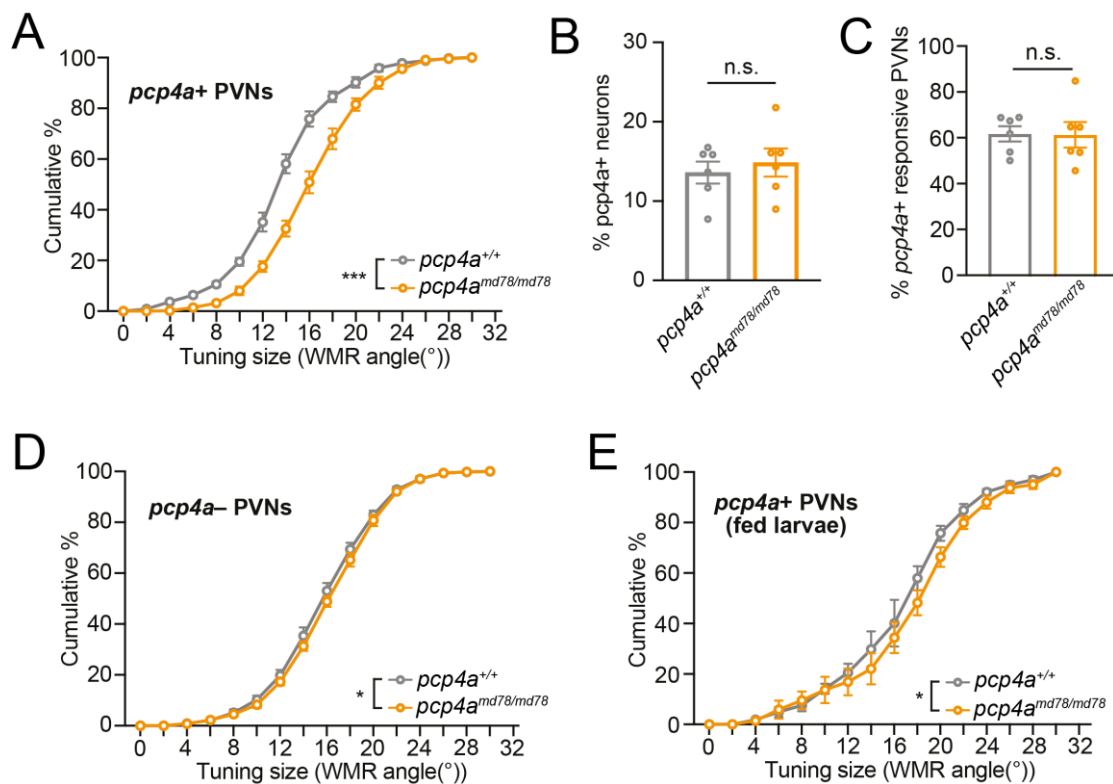


Figure 11: Mutating *pcp4a* alters tuning properties of *pcp4a*+ PVNs

A. Graphs depicting cumulative percentages of WMR angles of *pcp4a*+ PVNs in food-deprived 7 dpf *elavl3:H2B-GCaMP6s; pcp4a^{+/+}* and *elavl3:H2B-GCaMP6s; pcp4a^{md78/md78}* larvae. n = 6 larvae per group. Two-way ANOVA: p < 0.0001. **B.** Bar graph showing average percentages of *pcp4a*+ PVNs. n = 6 fish per group. Two-tailed t test. **C.** Bar graph showing average percentages of *pcp4a*+ PVNs responsive to visual stimuli in unfed 7 dpf *elavl3:H2B-GCaMP6s; pcp4a^{+/+}* and *elavl3:H2B-GCaMP6s; pcp4a^{md78/md78}* larvae. n = 6 larvae per group. Two-tailed t test. **D.** Graphs depicting cumulative percentages of WMR angles of *pcp4a*- PVNs in food-deprived 7 dpf *elavl3:H2B-GCaMP6s; pcp4a^{+/+}* and *elavl3:H2B-GCaMP6s; pcp4a^{md78/md78}* larvae. n = 6 larvae per group. Two-way ANOVA: p = 0.01. **E.** Graphs depicting cumulative percentages of WMR angles of *pcp4a*+ PVNs in fed 7 dpf *elavl3:H2B-GCaMP6s; pcp4a^{+/+}* and *elavl3:H2B-GCaMP6s; pcp4a^{md78/md78}* larvae. n = 5 larvae per group. Two-way ANOVA: p = 0.03.

In fed larvae, the mutation has a smaller effect on the response profile (Figure 11E) than the one observed in food-deprived larvae (Figure 11A), as expected from the lower amount of Pcp4a in fed larvae. This small effect is likely the reason the mutation was unable to induce significant changes in behavioral choice in fed larvae (Figure 8D).

SINs, whose soma is located in the superficial layers of the neuropil (Figure 12A), are known to regulate PVNs size selectivity (Del Bene et al., 2010). Since around 20% of SINs express *pcp4a* (Figure 12B), I investigated if the changes observed in the PVNs response profile may result from the effect of the mutation on SINs activity. Unfortunately, it was not possible to analyze the response of *pcp4a*+ SINs only, because neuropil morphology is harshly deformed by the HCR protocol and the registration algorithm does not work as well as in the PVL (Figure 9E). Hence, I analyzed the effect of *pcp4a* mutation on the response profile of the total SINs population. There was no significant change in the proportion of SINs responding to visual stimuli in food-deprived mutant larvae (Figure 12C) and SINs response profile showed no difference compared to wild-type siblings (Figure 12D), indicating that changes in Pcp4a levels likely do not affect activity of SINs.

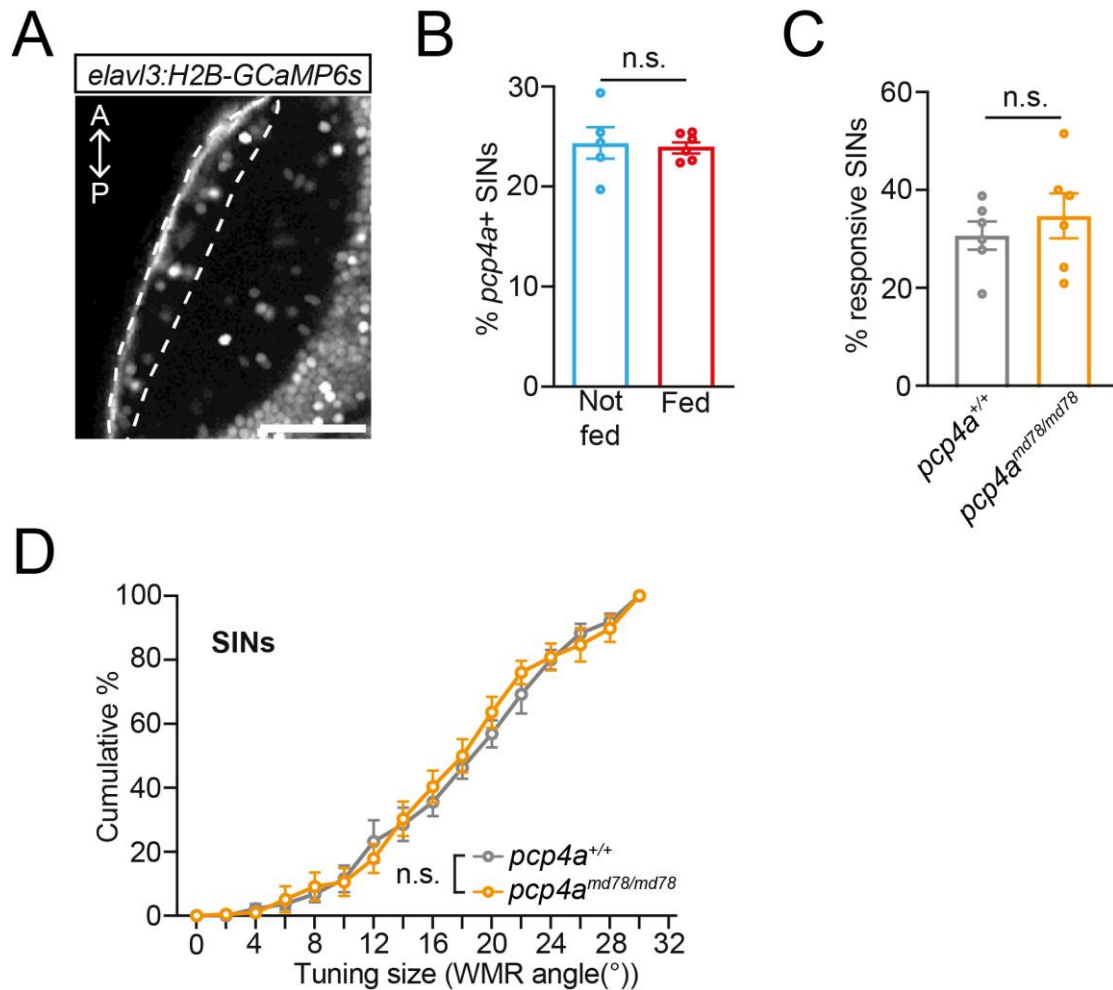


Figure 12: Mutating *pcp4a* does not alter tuning properties of SINs

A. Confocal image showing SINs in the tectum of a 7 dpf *elavl3:H2B-GCaMP6s* larva. The dashed white line demarcates the neuropil region containing SINs soma. Scale bar: 50 μ m. **B.** Bar graph showing average percentages of *pcp4a*⁺ SINs in fed and food-deprived larvae. $n_{\text{fed}} = 6$ fish, $n_{\text{not-fed}} = 5$ fish. Two-tailed t test. **C.** Bar graph showing average percentage of SINs responsive to visual stimuli in 7 dpf *elavl3:H2B-GCaMP6s; pcp4a*^{+/+} and *elavl3:H2B-GCaMP6s; pcp4a*^{md78/md78} larvae. $n = 6$ larvae per group. Two-tailed t test. **D.** Graph depicting cumulative percentages of WMR angles of SINs in food-deprived 7 dpf *elavl3:H2B-GCaMP6s; pcp4a*^{+/+} and *elavl3:H2B-GCaMP6s; pcp4a*^{md78/md78} larvae. $n = 6$ larvae per group. Two-way ANOVA.

Since *pcp4a* is expressed also in a small subset of retinal ganglion cells (RGCs) (Figure 6D), I looked at the response to visual stimuli at the RGC axon terminals in the tectum neuropil. For this purpose, I used a transgenic line expressing

GCaMP in RGCs and their tectal projection (*atoh7:Gal4;UAS:GCaMP6s*) (Figure 13A). There was no significant difference in the number of pixels active in response to stimuli of different sizes in food-deprived mutant larvae (Figure 13B,C), suggesting the shift in PVNs response profile is not due to a change in the input from RGCs.

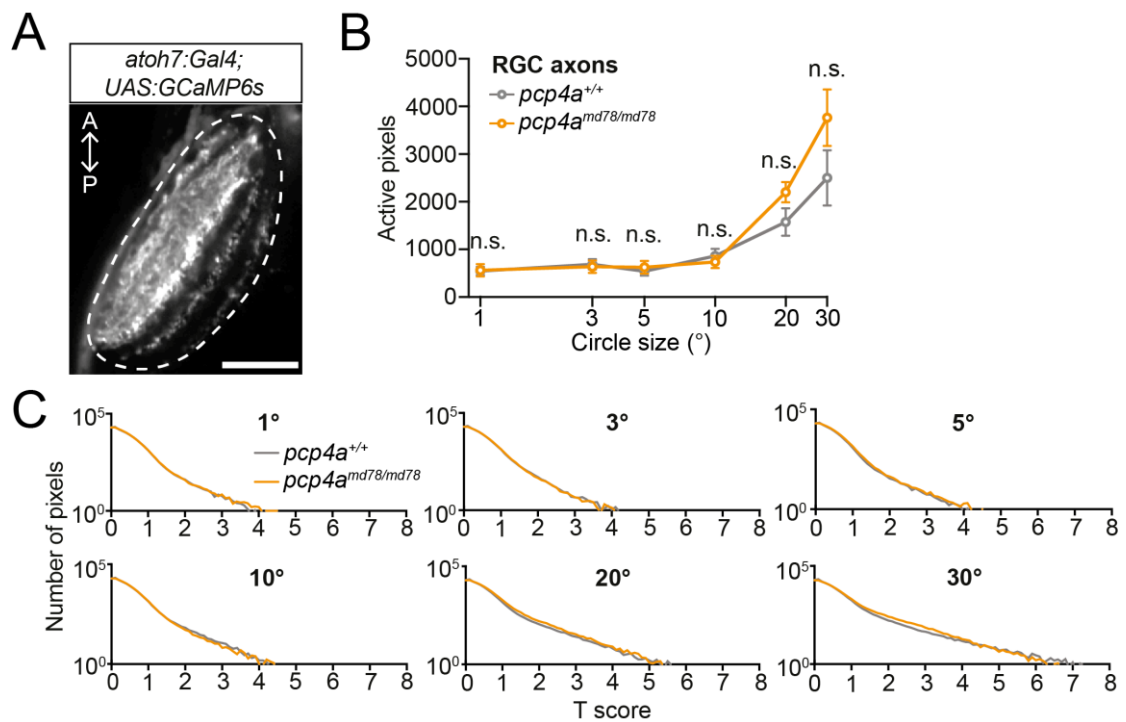


Figure 13: Mutating *pcp4a* does not alter responses to visual stimuli at RGC terminals

A. Confocal image showing the tectal neuropil, labeled by retinal ganglion cell axons, of a 7 dpf *atoh7:Gal4; UAS:GCaMP6s* larva. The dashed white line marks the borders of the neuropil region. Scale bar: 50 μ m. A, anterior; P, posterior. **B.** Graph showing average numbers of active pixels in RGC axons of food-deprived 7 dpf *atoh7:Gal4; UAS:GCaMP6s; pcp4a^{+/+}* and *atoh7:Gal4; UAS:GCaMP6s; pcp4a^{md78/md78}* larvae in response to visual stimuli of different sizes. $n_{pcp4a^{+/+}} = 14$ larvae, $n_{pcp4a^{md78/md78}} = 9$ larvae. Two-tailed t test with Bonferroni-Holm correction. **C.** Graphs depicting distribution of T scores obtained with the pixel-wise analysis based on a regression model to analyze responses of RGC axons to visual stimuli of different sizes in 7 dpf *atoh7:Gal4; UAS:GCaMP6s; pcp4a^{+/+}* and *atoh7:Gal4; UAS:GCaMP6s; pcp4a^{md78/md78}* larvae (see Materials and Methods for details). $n_{pcp4a^{+/+}} = 14$ larvae, $n_{pcp4a^{md78/md78}} = 9$ larvae.

I next investigated how Pcp4a is able to affect neuronal activity through cell-autonomous mechanisms by examining its downstream targets. The mammalian PCP4 is known to inhibit CaM-dependent enzymes such as CaMKII and NOS (Slemmon et al., 1996). In particular, CaMKII plays a well-studied role in synaptic plasticity (Yasuda et al., 2022). To analyze how CaMKII mediates the effect of Pcp4a on PVNs activity, I analyzed the response of *pcp4a*⁺ PVNs to visual stimuli in food-deprived wild type and mutant larvae treated with the CaMKII inhibitor KN-93. The results showed that CaMKII inhibition in the mutant is able to rescue the effect of the mutation on the response profile (Figure 14), suggesting that Pcp4a indeed controls the tuning properties of tectal neurons through CaMKII. KN-93 treatment in wild-type food-deprived larvae did not induce an additional shift of the response profile towards small stimuli, suggesting starvation-induced elevation of Pcp4a levels is sufficient to saturate CaMKII inhibition.

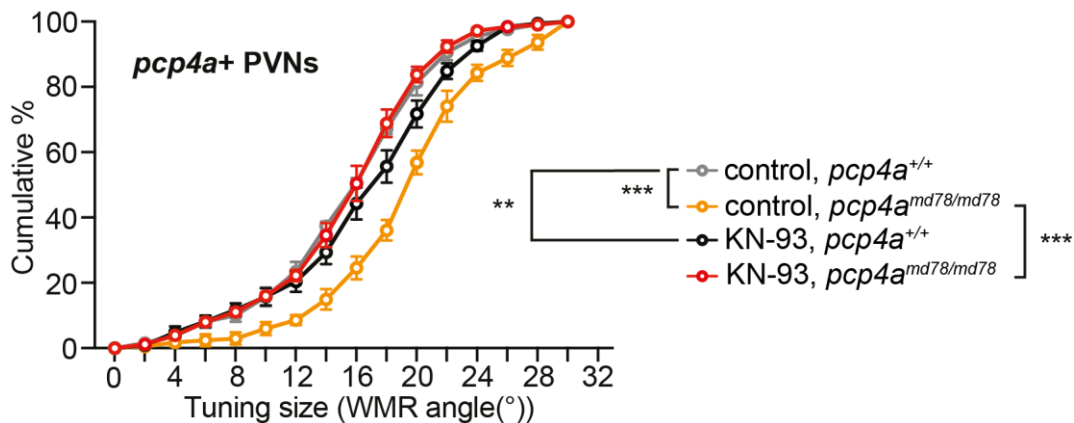


Figure 14: Inhibition of CaMKII reverts the effect of *pcp4a* mutation on *pcp4a*⁺ PVNs activity

Graph depicting cumulative percentages of WMR angles of *pcp4a*⁺ PVNs in food-deprived 7 dpf *elavl3:H2B-GCaMP6s; pcp4a*^{+/+} and *elavl3:H2B-GCaMP6s; pcp4a*^{md78/md78} larvae, treated with the CaMKII inhibitor KN-93 or control solution. $n_{\text{control_pcp4a}^{+/+}} = 5$ fish, $n_{\text{control_pcp4amd78/md78}} = 4$ fish, $n_{\text{KN-93_pcp4a}^{+/+}} = 6$ fish, $n_{\text{KN-93_pcp4amd78/md78}} = 6$ fish. Two-way ANOVA: control *pcp4a*^{+/+} vs control *pcp4a*^{md78/md78}, $p < 0.0001$; control *pcp4a*^{+/+} vs KN-93 *pcp4a*^{+/+}, $p = 0.002$; control *pcp4a*^{md78/md78} vs KN-93 *pcp4a*^{md78/md78}, $p < 0.0001$.

4.4. Neuromodulation upstream *pcp4a*

4.4.1 Neurotransmitter systems upstream of *pcp4a*

The effect of internal states on processing of sensory cues is often mediated by neuromodulators. Hence, I decided to identify which neuromodulatory system mediates the effect of feeding state on *pcp4a* expression by pharmacologically activating different neurotransmitter pathways and measuring *pcp4a* mRNA levels in brain samples by RT-qPCR.

I first tested the effect of serotonin receptor activation, since it was previously shown that starvation activates serotonergic neurons in the raphe, which project to the optic tectum and regulate activity of PVNs (Filosa et al., 2016). I activated serotonergic signaling in fed larvae by treating them with the serotonin reuptake inhibitor fluoxetine, resulting in an increase in *pcp4a* mRNA levels (Figure 15A). However, the effect was relatively small, suggesting that serotonin may not be the only neurotransmitter involved in the regulation of *pcp4a* expression.

Hence, I analyzed other neuromodulatory systems involved in decision-making. First, I focused my attention on dopamine: since feeding increases dopamine release (Zhang et al., 2022), I activated dopaminergic signaling in food-deprived larvae first using the non-selective agonist apomorphine, which induced a significant decrease of *pcp4a* mRNA to levels similar to what observed in fed larvae (Figure 15B), suggesting that dopamine is indeed modulating *pcp4a* expression. Dopamine receptors can be divided in two main categories: D1-like (D1 and D5), which activates adenylate cyclase, and D2-like receptors (D2, D3 and D4), which inhibits adenylate cyclase (Beaulieu & Gainetdinov, 2011). To better understand which receptor subtype is mediating the effect of dopamine on *pcp4a* expression, I activated dopaminergic signaling in food-deprived larvae first using the D1-like selective agonist SKF-38393, which did not show any effect (Figure 15C). On the contrary, treating food-deprived larvae with the D2-like selective agonist quinpirole decreased *pcp4a* levels significantly (Figure 15D). This means that dopamine regulates *pcp4a* expression by signaling through D2-like receptors.

Since cholinergic signaling has also been shown to regulate the effect of dopamine on some aspects of decision-making (Kenny & Markou, 2006), I also activated cholinergic signaling in food-deprived larvae by treating them with the acetylcholine esterase inhibitor donepezil, with no effect on *pcp4a* expression levels (Figure 15E).

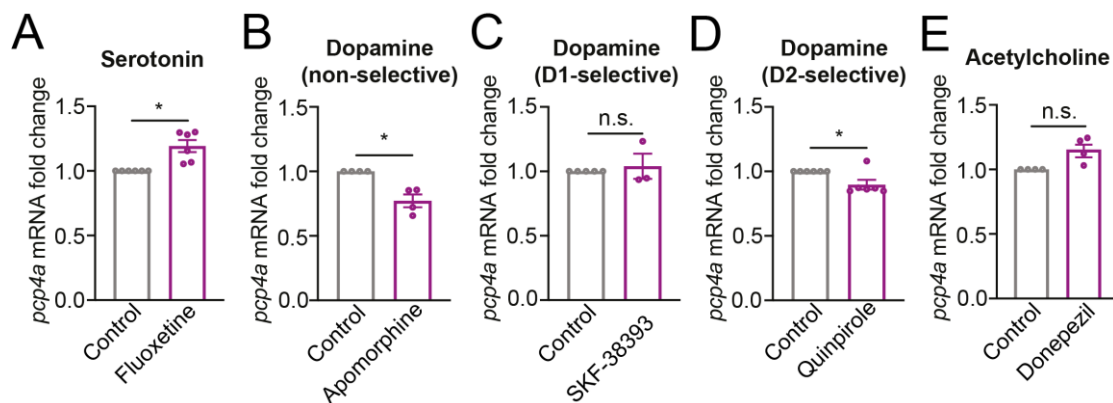


Figure 15: Serotonergic and dopaminergic signaling regulate expression of *pcp4a*

A – E. Bar graphs showing average *pcp4a* mRNA fold change in brain samples from 7 dpf wild-type larvae fed and treated with the selective serotonin reuptake inhibitor fluoxetine (A), or food deprived and treated with the non-selective dopamine agonist apomorphine (B), the D1-like selective agonist SKF-38393 (C), the D2-like selective agonist quinpirole (D), or the Acetylcholinesterase inhibitor donepezil (E). mRNA levels were normalized to control (non-treated) clutchmates. $n = 6$ in (A, D), $n = 4$ in (B, E), $n = 3$ in (C). n indicates number of biological replicas (pool of ten brains per replica). One-sample t test: $p = 0.01$ (A), $p = 0.02$ (B), $p = 0.04$ (D).

4.4.2. Food-dependent activation of dopaminergic neurons

I then tested if feeding activates dopaminergic neurons in zebrafish larvae. In zebrafish, dopaminergic neurons are located in distinct nuclei in the telencephalon, pretectum, posterior tuberculum and hypothalamus. Sparse dopaminergic neurons are also present in the optic tectum and in the retina (Kastenhuber et al., 2010).

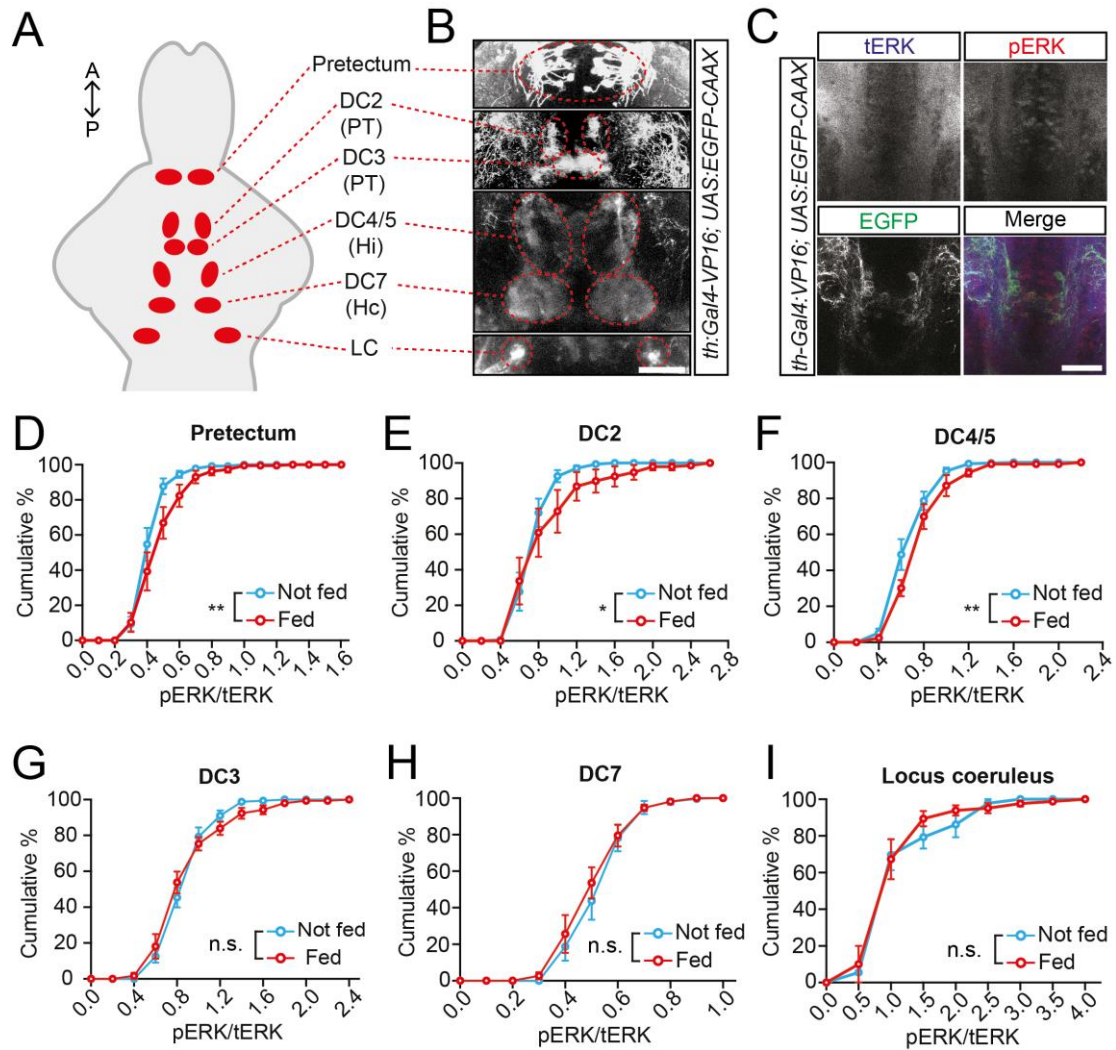


Figure 16: Feeding increase activity in distinct dopaminergic nuclei

A, B. Schematic representation (A) and confocal image of a 7 dpf *th:gal4-VP16; UAS:EGFP-CAAX* larva (B) showing localization of dopaminergic and noradrenergic (locus coeruleus) neuronal clusters. Scale bar in (B): 50 μ m. **C.** Confocal images of a 7 dpf *th:gal4-VP16; UAS:EGFP-CAAX* larva immunostained with antibodies against GFP, pERK, and tERK. The DC2, DC3, and DC4/5 clusters of dopaminergic neurons are visible in the images. Scale bar: 50 μ m. **D – I.** Graphs depicting cumulative percentages of pERK/tERK values in dopaminergic neurons in the prepectum (D), or in the DC2 (E), DC4/5 (F), DC3 (G), DC7 (H) clusters or in the locus coeruleus (I) in fed or food-deprived 7 dpf *th:gal4-VP16; UAS:EGFP-CAAX* larvae. $n_{\text{not-fed}} = 9$ (D, E, G – I) or $n_{\text{not-fed}} = 10$ (F); $n_{\text{fed}} = 9$ (D, E) or $n_{\text{fed}} = 10$ (F – I). Two-way ANOVA: $p = 0.005$ (D), $p = 0.03$ (E), $p = 0.002$ (F).

PT: posterior tuberculum, Hi: intermediate hypothalamus, Hc: caudal hypothalamus, LC: locus coeruleus.

I used a transgenic line labeling dopaminergic and noradrenergic neurons (*th:Gal4;UAS:EGFP-CAAX*). This line labels dopaminergic nuclei in the pretectum, posterior tuberculum (DC2, DC3), intermediate (DC4/5) and caudal (DC7) hypothalamus. It also labels the noradrenergic locus coeruleus (Figure 16A,B). To measure neuronal activity, I performed an immunostaining against pERK (Figure 16C). Extracellular signal-regulated kinase (ERK) is a protein that is phosphorylated upon neuronal activation (Rosen et al., 1994): measurement of pERK signal intensity, normalized with total ERK levels, has been proven to be a reliable indicator of neuronal activity (Randlett et al., 2015). Some dopaminergic nuclei, such as the prepectal one (Figure 16D), DC2 (Figure 16E) and DC4/5 nuclei (Figure 16F), were indeed more active in fed larvae compared to food-deprived siblings. Other nuclei, like the DC3 (Figure 16G), DC7 (Figure 16H) did not show any difference in activity. Moreover, feeding did not activate noradrenergic neurons in the locus coeruleus (Figure 16I), excluding the possibility that noradrenergic signaling may affect feeding state-dependent tectal activity.

4.4.2. Molecular signaling upstream *pcp4a*

Several dopaminergic nuclei (prepectum, DC1, DC2 and DC4/5) send direct projections to the optic tectum (Tay et al., 2011). Interestingly, several of these nuclei (prepectal, DC2, DC4/5) displayed increased activity in fed larvae. These results indicate that *pcp4a*⁺ PVNs may receive direct input from dopaminergic neurons, inducing feeding state-dependent transcriptional changes. To prove this hypothesis, I performed *in situ* HCR to detect expression of genes coding for dopaminergic receptors in tectal PVNs (Figure 17A). Indeed, I found that a fraction of *pcp4a*⁺ PVNs co-expressed either the *drd2a* or the *drd2b* isoform of the D2 receptor (Figure 17B). This suggests that dopamine may regulate transcription of *pcp4a* by direct signaling through D2 receptors expressed in *pcp4a*⁺ neurons.

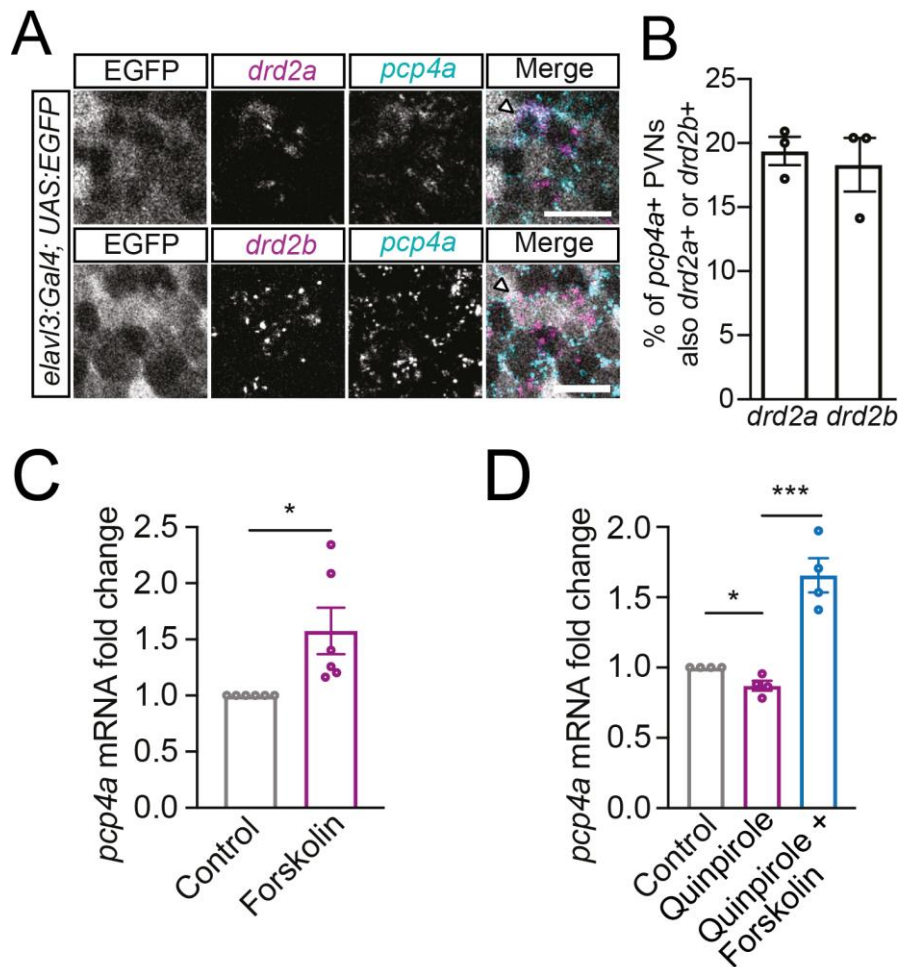


Figure 17: Dopaminergic signaling controls *pcp4a* transcription through regulation of cAMP levels

A. Confocal images of 7 dpf *elavl3:gal4; UAS:EGFP* larvae showing localization of *pcp4a*, *drd2a*, and *drd2b* mRNA, detected with *in situ* HCR, in GFP-labeled tectal PVNs. Scale bars: 10 μ m. **B.** Bar graph showing average percentages of *pcp4a*+ tectal neurons expressing either *drd2a* or *drd2b*. $n = 3$ larvae. **C, D.** Bar graphs showing average *pcp4a* mRNA fold change in 5 dpf wild-type fish treated with the adenylate cyclase activator forskolin (C), or in brain samples from 7 dpf wild-type larvae treated first with quinpirole for 2 hours, and then with quinpirole and forskolin for one further hour (D). mRNA levels were normalized to control (non-treated) clutchmates. $n = 6$ (C) or $n = 4$ (D) biological replicas (pool of ten larvae per replica) per group. One-sample t test: $p = 0.04$ (C), $p = 0.04$ (D, quinpirole). Two tailed t test: $p = 0.0008$ (D, quinpirole vs quinpirole + forskolin).

To validate this hypothesis, I looked into the signaling cascade downstream D2 receptors. Since it is known that D2 receptors are associated with a G-protein that inhibits adenylate cyclase and decrease cAMP levels (Beaulieu &

Gainetdinov, 2011), I tested whether increasing cAMP levels would induce *pcp4a* expression. Pharmacologically activating adenylate cyclase using forskolin indeed increased *pcp4a* mRNA levels (Figure 17C). I also confirmed that forskolin treatment rescues quinpirole-induced decrease of *pcp4a* levels (Figure 17D), indicating that cAMP acts downstream D2 receptors to regulate *pcp4a* transcription.

4.5. Effect of dopaminergic signaling on tectal neurons activity

Since results indicated that D2 receptors signaling regulates *pcp4a* expression in *pcp4a+* PVNs, I investigated how activation of dopaminergic signaling through D2 receptors affects PVNs activity. I performed calcium imaging on food-deprived larvae as previously described, then treated them with quinpirole for three hours and subsequently imaged again from the same planes. This strategy allowed to measure responses to visual stimuli from the same neurons before and after dopamine receptor activation. PVNs could be divided in three categories based on their response: neurons that respond to visual stimuli of any size both before and after treatment ('persistent'), neurons responding only during the first imaging session before drug treatment ('lost') or only after dopaminergic activation ('gained') (Figure 18A).

Quinpirole treatment shifts the response profile of *pcp4a+* neurons towards large stimuli (Figure 18B), similar to what observed in fed larvae. This suggests that dopamine mediates the effect of feeding on PVNs activity. Interestingly, many persistent neurons, responding to both small and large visual stimuli during the first imaging session, did not respond to small stimuli after quinpirole treatment (Figure 18C,D), suggesting that this selective suppression of neuronal responses may contribute to the shift in tuning size.

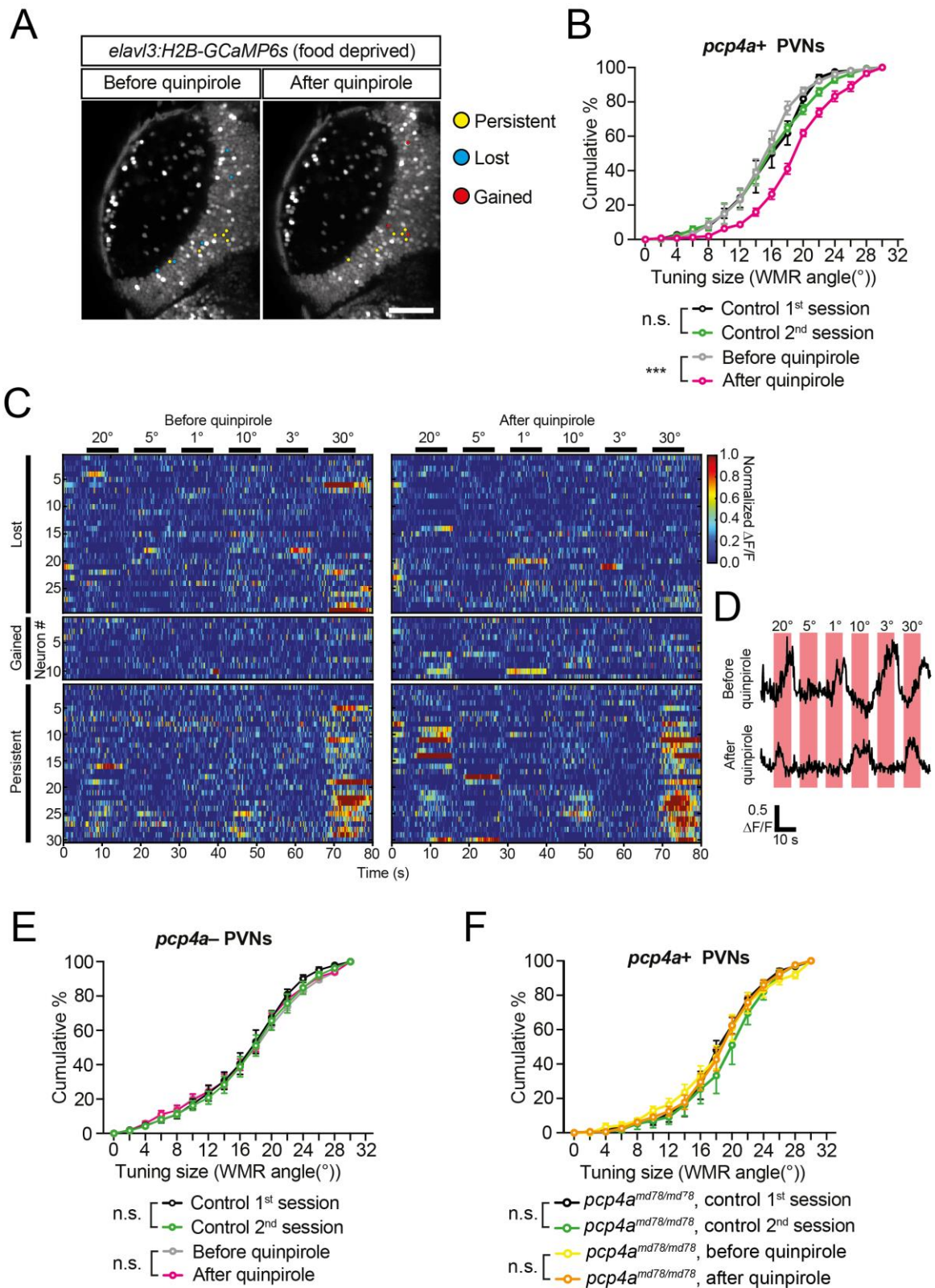


Figure 18: Dopaminergic signaling alters *pcp4a*⁺ PVNs tuning properties

A. Images showing part of the tectum of a 7 dpf *elav13:H2B-GCaMP6s* larva before and after treatment with the D2-like dopamine receptor agonist quinpirole. PVNs were classified as ‘persistent’ if they responded to visual stimuli of any size before and after

quinpirole treatment, 'lost' if they responded only in the first imaging session, and 'gained' if they responded only in the second imaging session. Scale bar = 50 μm . **B.** Graphs showing cumulative percentages of WMR angles of *pcp4a+* PVNs in food-deprived 7 dpf *elavl3:H2B-GCaMP6s* larvae before and after three hours treatment with quinpirole, or in control food-deprived 7 dpf *elavl3:H2B-GCaMP6s* fish not treated with quinpirole, but kept in agarose for the same duration of the drug treatment. $n = 5$ larvae per group. Two-way ANOVA: $p < 0.0001$. **C.** Heatmap showing activity of lost, gained and persistent *pcp4a+* PVNs in response to visual stimuli of different sizes in a 7 dpf *elavl3:H2B-GCaMP6s* larvae before and after treatment with quinpirole. **D.** Examples of traces of a persistent *pcp4a+* PVN which responded to both small and large visual stimuli before treatment with quinpirole, and only to large ones after. **E.** Graphs showing cumulative percentages of WMR angles of *pcp4a-* PVNs in food-deprived 7 dpf *elavl3:H2B-GCaMP6s* larvae before and after three hours treatment with quinpirole, or in control food-deprived 7 dpf *elavl3:H2B-GCaMP6s* fish not treated with quinpirole, but kept in agarose for the same duration of the drug treatment. $n = 5$ larvae per group. Two-way ANOVA. **F.** Graph showing cumulative percentages of WMR angles of *pcp4a+* PVNs in food-deprived 7 dpf *pcp4a^{md78/md78}; elavl3:H2B-GCaMP6s* larvae before and after three hours treatment with quinpirole and in untreated controls kept in agarose for the same duration of the drug treatment. $n_{\text{pcp4amd78/md78_control}} = 3$ fish, $n_{\text{pcp4amd78/md78_quinpirole}} = 4$ fish. Two-way ANOVA.

In control fish, which received no treatment, there was no difference in the response profile during the first and second imaging session three hours apart (Figure 18B). Quinpirole treatment also had no significant effect on *pcp4a-* negative neurons (Figure 18E), suggesting that dopamine affects mostly *pcp4a+* neurons activity.

Moreover, quinpirole treatment induced no additional alteration of *pcp4a+* PVNs response profile in homozygous mutants (Figure 18F), indicating Pcp4a mediates the effect of dopaminergic signaling on the tuning properties of tectal neurons.

To better understand how dopaminergic activation affect *pcp4a*+ PVNs activity and how this could influence tectal circuits, I investigated if *pcp4a*+ neurons have an excitatory or inhibitory profile. I found that the majority of *pcp4a*+ PVNs are excitatory, since they co-expressed the glutamatergic marker *vglut2*, while only around 30% co-expressed the gabaergic marker *gad1b* (Figure 19 A,B). I then investigated if dopaminergic signaling affects differentially the activity of the glutamatergic or gabaergic subpopulation.

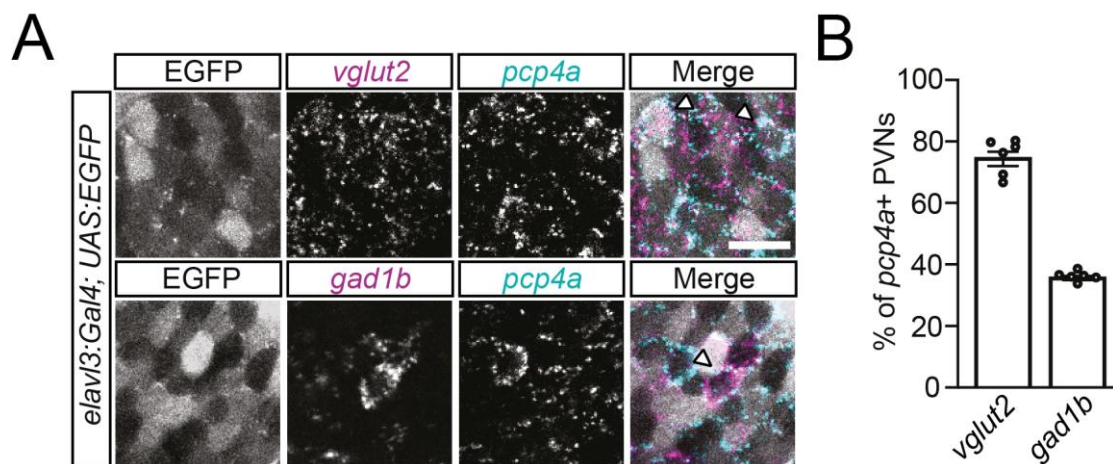


Figure 19: *pcp4a*+ PVNs express both glutamatergic and gabaergic markers

A. Confocal images showing localization of *pcp4a*, *vglut2*, and *gad1b* mRNA, detected with *in situ* HCR, in tectal PVNs (labeled by EGFP) in 7 dpf *elav13:gal4, UAS:EGFP* larvae. Scale bars = 10 μ m. **B.** Bar graph showing percentages of glutamatergic (*vglut2*+) or GABAergic (*gad1b*+) *pcp4a*+ PVNs. n = 6 larvae per group.

I first focused my attention on *pcp4a*+/*gad1b*+ PVNs. Quinpirole treatment induced a shift of the response profile towards large stimuli in the gabaergic subpopulation (Figure 20A).

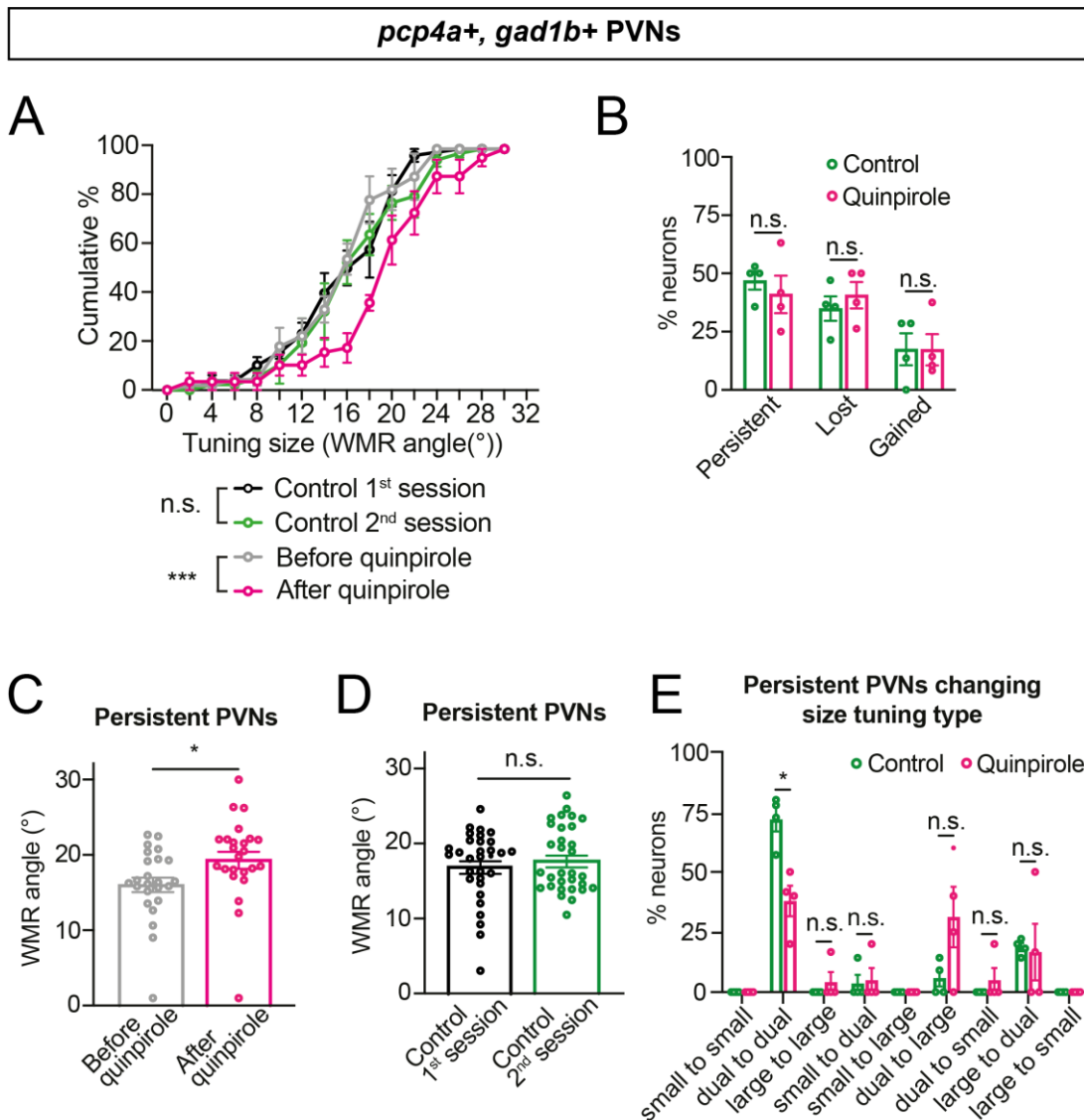


Figure 20: Dopaminergic signaling alters gabaergic *pcp4a+* PVNs size tuning properties

A. Graphs showing cumulative percentages of WMR angles of *pcp4a+/gad1b+* PVNs in food-deprived 7 dpf *elavl3:H2B-GCaMP6s* larvae before and after three hours treatment with quinpirole, or in control food-deprived 7 dpf *elavl3:H2B-GCaMP6s* fish not treated with quinpirole imaged in two consecutive sessions three hours apart. Data in these graphs are a subset of the data shown in Figure 18B. $n = 4$ larvae per group. Two-way ANOVA: $p < 0.0001$. **B.** Bar graph depicting percentages of *pcp4a+/gad1b+* PVNs, imaged in two sessions three hours apart, classified as persistent, lost, and gained in quinpirole-treated and untreated (control) 7 dpf *elavl3:H2B-GCaMP6s* larvae. $n = 4$ fish per group. Two-tailed t test with Bonferroni-Holm correction. **C, D.** Graph showing size tuning (WMR angle) of persistent *pcp4a+/gad1b+* PVNs before and after quinpirole treatment (C), or before (1st session) or after three hours of permanence in agarose (2nd session) without drug treatment (D). $n_{\text{quinpirole}} = 24$ neurons

from 4 fish, $n_{\text{control}} = 31$ neurons from 4 fish. Two-tailed paired t test: $p = 0.03$ (C). **E.** Graph displaying percentages of persistent *pcp4a+/gad1b+* PVNs changing response type in the two imaging sessions. Small, neurons responding to circles $\leq 5^\circ$; large, neurons responding to circles $\geq 10^\circ$; dual, neurons responding to both types of stimuli. $n = 4$ larvae per group. Two-tailed t test with Bonferroni-Holm correction: $p = 0.04$ (dual to dual).

Since the experimental strategy employed allowed to image responses from the same neurons before and after the pharmacological treatment, I investigated if the shift in the response profile is due to activation of different subpopulations of neurons or to changes of size tuning of individual neurons. In the *gad1b+* subpopulation, there was no difference in the proportion of 'lost' or 'gained' neurons compared to control fish (Figure 20B), suggesting that there is no preferential activation or silencing of specific subpopulations by dopamine. However, in 'persistent' neurons there was an increased preference for larger stimuli of individual neurons (Figure 20C), which was not present in the control group (Figure 20D). Persistent neurons responding to both large and small stimuli during the first imaging session, did not respond to small objects after quinpirole treatment but were activated by large stimuli only (Figure 20E). These results indicate that in *pcp4a+* gabaergic PVNs dopaminergic signaling shifts size tuning of individual neurons towards large stimuli by suppressing the response to small visual stimuli in dual-responding neurons.

In *pcp4a+/gad1b-* PVNs, quinpirole treatment similarly induced a shift of the response profile towards large stimuli (Figure 21A).

In the glutamatergic (*gad1b-*) subpopulation there was an increased proportion of 'lost' neurons and a decreased proportion of 'gained' neurons compared to the control (Figure 21B). While there was no change in the average tuning size of 'lost' neurons compared to control (Figure 21C), 'gained' neurons displayed size tuning shifted toward larger stimuli (Figure 21D), possibly contributing to the shift in the total population.

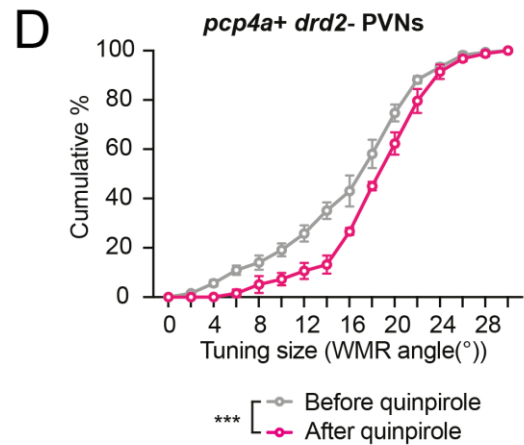
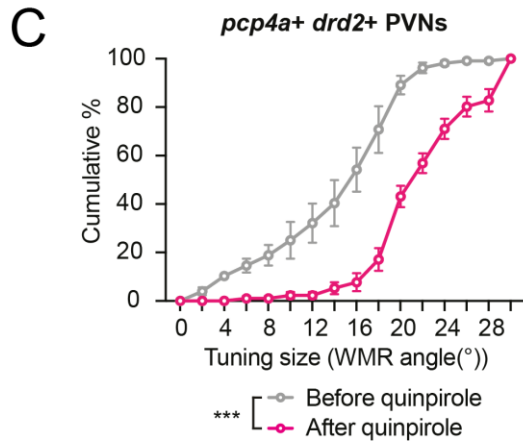
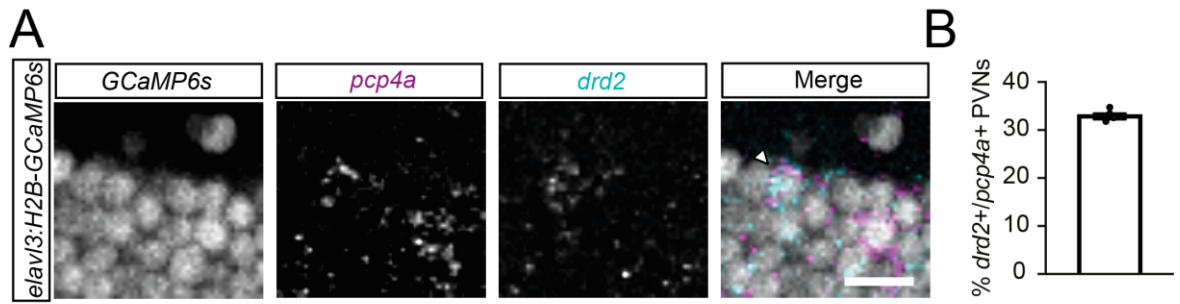
Similar to what observed for the *gad1b+* subpopulation, 'persistent' neurons increased their size preference for larger stimuli in the treated group (Figure 21E), but not in the controls (Figure 21F). Again, this was due to dual-

Figure 21: Dopaminergic signaling alters glutamatergic *pcp4a+* PVNs size tuning properties

A. Graph showing cumulative percentages of WMR angles of *pcp4a+/gad1b-* PVNs in food-deprived 7 dpf *elavl3:H2B-GCaMP6s* larvae before and after three hours treatment with quinpirole, or in control food-deprived 7 dpf *elavl3:H2B-GCaMP6s* fish not treated with quinpirole imaged in two consecutive sessions three hours apart. Data in these graphs are a subset of the data shown in Figure 18B. $n = 4$ larvae per group. Two-way ANOVA: $p < 0.0001$. **B.** Bar graph depicting percentages of *pcp4a+/gad1b-* PVNs, imaged in two sessions three hours apart, classified as persistent, lost, and gained in quinpirole-treated and untreated (control) 7 dpf *elavl3:H2B-GCaMP6s* larvae. $n = 4$ fish per group. Two-tailed t test with Bonferroni-Holm correction: $p = 0.002$ (lost), $p = 0.03$ (gained). **C, D.** Bar graphs depicting tuning size (WMR angle) of lost (C) or gained (D) *pcp4a+/gad1b-* PVNs in fish treated with quinpirole and untreated controls. $n_{\text{Lost-Control}} = 55$ neurons from 4 larvae, $n_{\text{Lost-Quinpirole}} = 76$ neurons from 4 larvae, $n_{\text{Gained-Control}} = 82$ neurons from 4 larvae, $n_{\text{Gained-Quinpirole}} = 34$ neurons from 4 larvae. Nested two-way ANOVA: $p = 0.03$ (D). **E, F.** Graph showing size tuning (WMR angle) of persistent *pcp4a+/gad1b-* PVNs before and after quinpirole treatment (E), or before (1st session) or after three hours of permanence in agarose (2nd session) without drug treatment (F). $n_{\text{quinpirole}} = 77$ neurons from 4 fish, $n_{\text{control}} = 110$ neurons from 4 fish. Two-tailed paired t test: $p < 0.0001$ (E). **G.** Graph displaying percentages of persistent *pcp4a+/gad1b-* PVNs changing response type in the two imaging sessions. Small, neurons responding to circles $\leq 5^\circ$; large, neurons responding to circles $\geq 10^\circ$; dual, neurons responding to both types of stimuli. $n = 4$ larvae per group. Two-tailed t test with Bonferroni-Holm correction: $p = 0.0006$ (dual to large).

Taken together, these results suggest that dopamine affects *pcp4a+* PVNs response profile by suppressing the response to small stimuli in dual-responding glutamatergic and gabaergic neurons, and by activating a subpopulation of large-responding glutamatergic neurons.

Finally, I tested if dopamine influences the tuning properties of *pcp4a+* PVNs through direct signaling. For that purpose, I performed an *in situ* HCR recognizing both D2 receptor isoforms (*drd2a* and *drd2b*) after *in vivo* calcium imaging (Figure 22A). I confirmed that around a third of *pcp4a+* PVNs co-express at least one *drd2* isoform (Figure 22B).



pcp4a+ *drd2+* PVNs

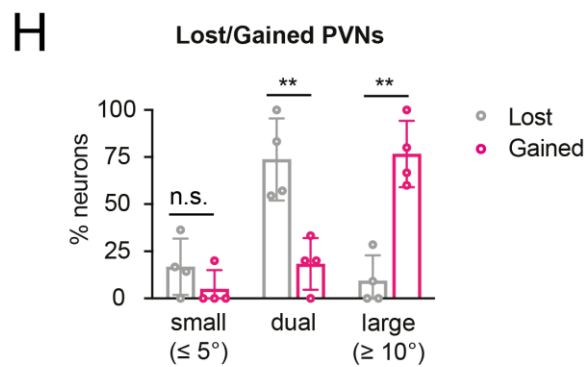
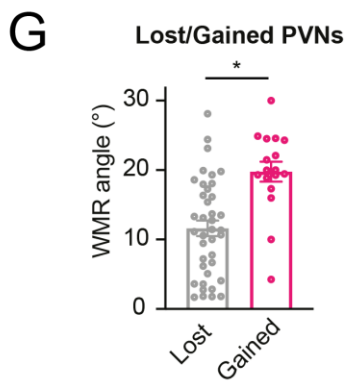
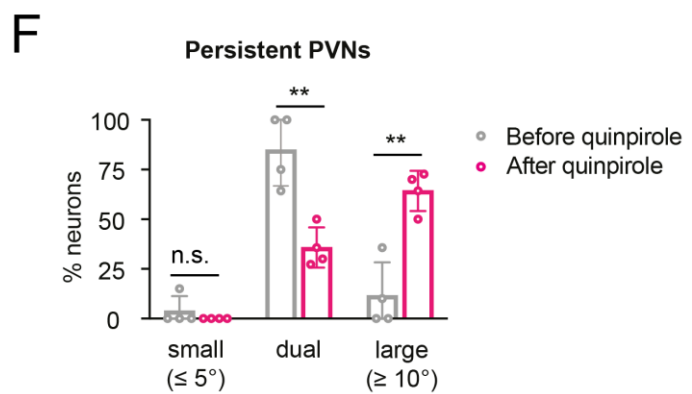
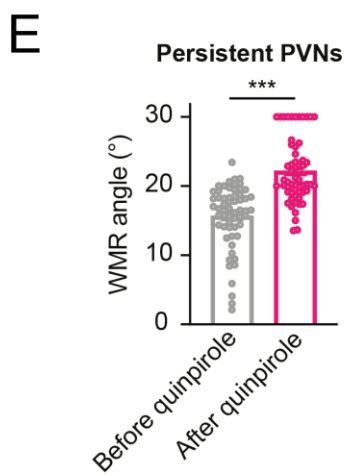


Figure 22: Dopaminergic signaling affects mainly size tuning properties of *pcp4a+* / *drd2+* PVNs

A. Confocal images showing localization of *pcp4a* and *drd2* mRNA, detected with *in situ* HCR, in tectal PVNs (labeled by H2B-GCaMP) in 7 dpf *elavl3:H2B-GCaMP6* larvae. Scale bars = 10 μ m. **B.** Bar graph showing percentages of *drd2+* *pcp4a+* PVNs. n = 4 larvae. **C, D.** Graphs showing cumulative percentages of WMR angles of *pcp4a+* and *drd2+* (C) or *pcp4a+* and *drd2-* (D) PVNs in food-deprived 7 dpf *elavl3:H2B-GCaMP6s* larvae before and after three hours treatment with quinpirole, or in control food-deprived 7 dpf *elavl3:H2B-GCaMP6s* fish not treated with quinpirole imaged in two consecutive sessions three hours apart. n = 4 larvae per group. Two-way ANOVA: p < 0.0001 (C), p < 0.0001 (D). **E.** Graph showing size tuning (WMR angle) of persistent *pcp4a+/drd2+* PVNs before and after quinpirole treatment. n = 59 neurons from 4 fish. Two-tailed paired t test: p < 0.0001. **F.** Bar graph showing proportion of size-selective persistent *pcp4a+/drd2+* PVNs in food-deprived 7 dpf *elavl3:H2B-GCaMP6s* larvae treated with quinpirole. n = 4 fish. Two-tailed t test with Bonferroni-Holm correction: dual, p = 0.01; large, p = 0.01. **G.** Graph showing tuning size (WMR angle) of lost and gained *pcp4a+/drd2+* PVNs in treated larvae. n_{Lost} = 39 neurons, n_{Gained} = 17 neurons from 4 fish. Nested two-way ANOVA: p = 0.01. **H.** Bar graph showing proportion of size-selective lost and gained *pcp4a+/drd2+* PVNs in food-deprived 7 dpf *elavl3:H2B-GCaMP6s* larvae treated with quinpirole. n = 4 fish. Two-tailed t test with Bonferroni-Holm correction: dual, p = 0.02; large, p = 0.004.

In *pcp4a+/drd2+* PVNs, quinpirole treatment induced an important shift of the response profile towards large stimuli (Figure 22C), showing a stronger effect compared to the total *pcp4a+* population (Figure 18B). *pcp4a+/drd2-* negative PVNs also responded more to large stimuli (Figure 22D), but the effect was much milder than in *drd2+* neurons, indicating that dopaminergic signaling affects *pcp4a+* PVNs activity mainly through a direct mechanism. It is also possible that some *drd2-* negative neurons may express the D3 dopaminergic receptor, which is also activated by quinpirole, accounting for the effect of the pharmacological treatment on this subpopulation. Persistent *drd2+* neurons showed a shift of size tuning toward large stimuli after treatment (Figure 22E), due to suppression of the response to small stimuli in dually-responding neurons (Figure 22F).

The proportion of gained neurons is smaller than lost ones and they show greater preference for large stimuli (Figure 22G). Analysis of size selectivity suggests the loss of a subpopulation of small- and dual- responding neurons and the activation of a large-responding subpopulation after treatment (Figure 22H).

These results further confirm that dopaminergic signaling decrease synaptic strength of small stimuli, mainly through a cell-autonomous mechanism.

5. Discussion

5.1. A model of the *pcp4a* pathway for feeding state-dependent modulation of behavioral choice

Fast and reliable decision-making is crucial for survival in a rapidly changing natural environment. Moreover, it needs to be attuned to the physiological needs of the animal to ensure the choice of optimal behavioral strategy to maintain body homeostasis. Studies in various animal models have uncovered the key role of neuromodulatory systems in mediating the effect of internal states on behavioral choice, however the molecular mechanisms downstream these neurotransmitters are still largely unknown. In this study we use the zebrafish as model organism to unveil the molecular components of a pathway mediating the effect of internal states on decision-making.

By employing a behavioral paradigm where the fish has to choose whether to approach or avoid moving visual stimuli of different sizes, mimicking either preys or predators, we identified the small cytoplasmic protein Pcp4a as a key player in feeding state-dependent modulation of behavioral choice. Feeding decreased Pcp4a expression through a transcriptional mechanism, as shown by mass spectrometry and RT-qPCR data. Food-deprived *pcp4a* mutant showed increased avoidance of small, prey-like stimuli in a size discrimination assay, thus phenocopying behavioral choice of fed larvae (Filosa et al., 2016). The subpopulation of neurons expressing *pcp4a* in the optic tectum, a brain region known to mediate the choice between approach and avoidance (Barker & Baier, 2015), responded preferentially to large visual stimuli in fed larvae compared to food-deprived larvae. This preference was also observed in *pcp4a* mutants, suggesting that changes in Pcp4a levels alters tuning properties of tectal neurons.

pcp4a levels are increased by serotonergic signaling and decreased by dopaminergic signaling through D2 receptors. Feeding increased activity of dopaminergic neurons in the pretectal, DC2 and DC4/5 nuclei, which send

direct projections to the optic tectum. A subpopulation of tectal *pcp4a*⁺ neurons expressed D2 receptors, which control *pcp4a* transcription through the cAMP signaling pathway. Indeed, dopaminergic signaling through D2 receptors shifted the response profile of *pcp4a*⁺ PVNs toward large stimuli, affecting mostly *pcp4a*⁺ neurons co-expressing *drd2*.

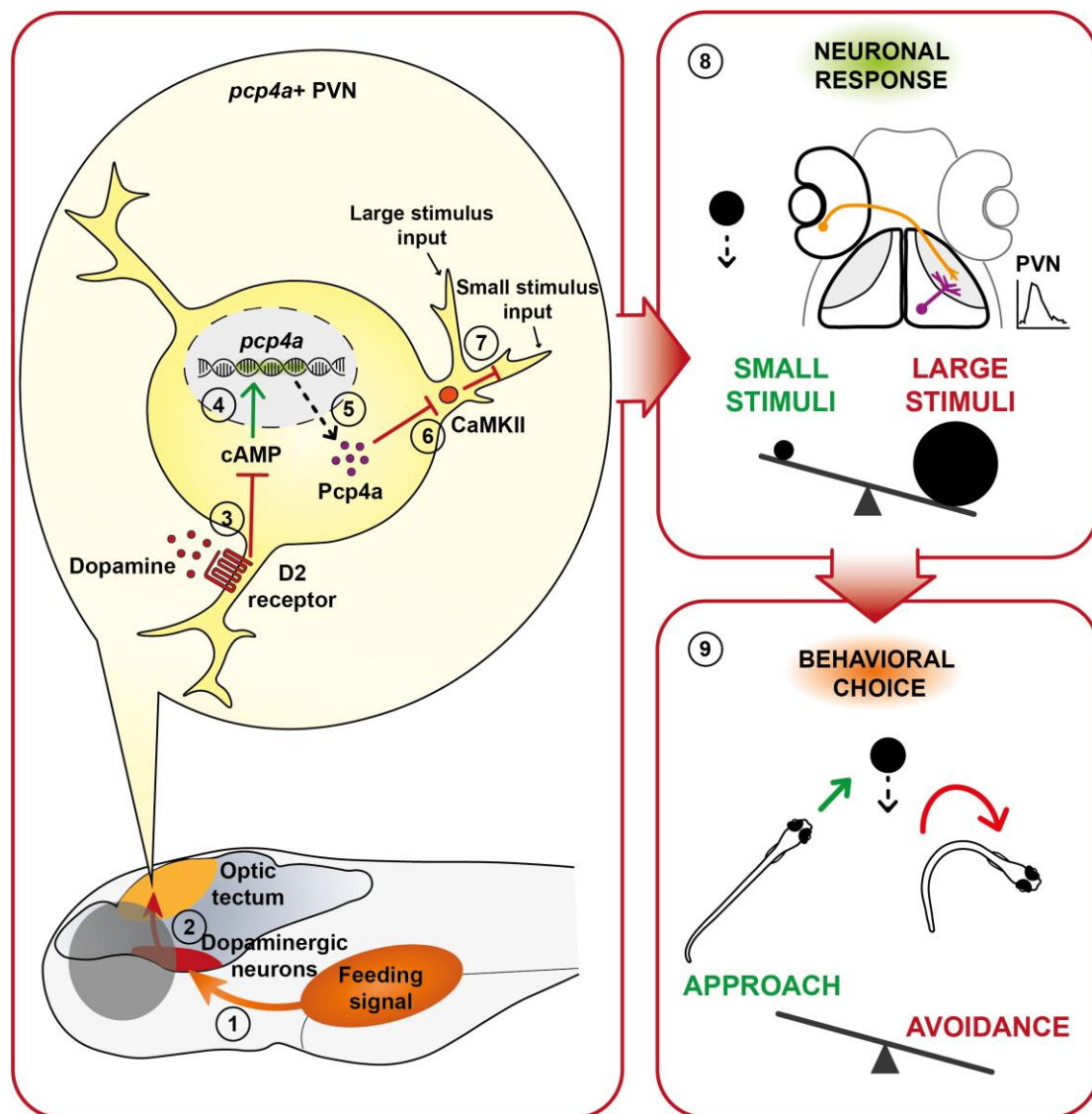


Figure 23: Model of the *pcp4a* pathway for feeding state-dependent modulation of behavioral choice

A feeding signal activates dopaminergic neurons in the pretectum and hypothalamus (1). These dopaminergic neurons send projections to tectal *pcp4a*⁺ PVNs (2). In *pcp4a*⁺ PVNs, dopaminergic signaling through D2 receptors decrease cAMP levels (3), which is a positive regulator of *pcp4a* transcription (4). As a result, feeding reduce

Pcp4a abundance (5), with subsequent increase in CaMKII activity (6). In these neurons, CaMKII acts on synaptic plasticity by decreasing the synaptic strength of small visual stimuli inputs (7). As a result, the response profile of tectal PVNs shifts toward large stimuli (8), ultimately inducing increased avoidance of small stimuli in behavioral choice during foraging (9).

Combined, the results depict a molecular pathway controlling feeding state-dependent regulation of decision-making behavior in zebrafish. In our model, feeding activates specific dopaminergic nuclei in the pretectum and hypothalamus. These dopaminergic neurons project to the optic tectum, where they form functional connections with *pcp4a*-expressing PVNs. Signaling through D2 receptors inhibits the downstream cAMP signaling pathway, resulting in decreased transcription of *pcp4a* in tectal *pcp4a+* PVNs. This leads to increased activity of CaM and consequently of its target enzyme CaMKII. CaMKII affects the tuning properties of dually responding *pcp4a+* neurons by decreasing synaptic strength of small visual stimuli. This leads to a shift of tectal neurons response profile towards large stimuli in a cell-autonomous way, ultimately resulting in a bias towards avoidance in behavioral choice during foraging (Figure 23).

The model elucidates how metabolic state affects decision-making by linking molecular and cellular events to behavior. The most evident gap is a description of how the changes in *pcp4a+* PVNs activity influence tectal circuits and ultimately lead to alteration in behavioral choice. I tried to gain insights on the possible neuronal circuits involved by investigating the neurotransmitter identity of *pcp4a+* PVNs and how dopaminergic signaling affects each subpopulation separately. Around 30% of *pcp4a+* PVNs are gabaergic, and in this population dopamine shift size tuning of individual neurons toward large stimuli by suppressing the response to small visual stimuli. Dopamine also decreases synaptic strength of small stimuli in glutamatergic neurons, which constitute the majority of *pcp4a+* PVNs, and additionally it recruits a small populations of glutamatergic neurons responding to large visual stimuli. Still, it was not possible to draw a definite conclusion about the possible circuit leading to the increase in avoidance of small stimuli.

To answer this question it would be necessary to use a transgenic line labeling *pcp4a*⁺ neurons to identify the downstream neuronal partners of *pcp4a*⁺ neurons and test the effects of optogenetic activation or inhibition of *pcp4a*⁺ neurons on approach and avoidance.

For this reason, during my doctoral studies I attempted to generate a zebrafish transgenic line labeling specifically *pcp4a*⁺ neurons. For this purpose, I employed several techniques: first I tried to insert randomly in the genome a construct containing the transcription factor Gal4 under the control of the *pcp4a* promoter region using a transposon-based transgenesis technique widely used in zebrafish (Tol2 transgenesis). This technique is fairly easy to employ but has the disadvantages of positional effects deriving from random insertion and also because it does not take into account the effect of distal enhancers on gene expression. To remedy these problems, I employed a CRISPR/Cas9-based targeted knock-in technique to insert the Gal4 coding sequence immediately upstream *pcp4a* gene, this way the transcription factor would have exactly the same regulatory elements as the gene (Kimura et al., 2014).

Unfortunately, I was unable to obtain a line with strong, specific labeling of *pcp4a*-expressing cells. In both transgenesis strategies, I obtained a very mosaic, weak labeling of just few cells per animal in the F1 generation, harboring stable integration of the transgene. Moreover, when I tried to validate the line by performing *in situ* hybridization to detect *pcp4a* mRNA, the labeled cells did not stain positive for *pcp4a*. Often, *pcp4a*-expressing neurons were adjacent to the labeled neuron, but the two signals were not overlapping (data not shown).

Due to these technical difficulties, I was not able to perform the experiments that would have allowed me to elucidate the neuronal circuit mediating the effect of tectal *pcp4a*⁺ neurons on behavioral choice, such as identifying their downstream partners and their role in approach and avoidance behavior.

5.2. Neuromodulatory systems regulating behavioral choice

A crucial point of this study is the critical role of neuromodulatory neurotransmitters in the regulation of decision-making. In particular, it elucidates the role of dopamine in modulation of feeding state-dependent behavioral choice. This function of the dopaminergic system is consistent with several studies in invertebrate models (Crossley et al., 2023; Rengarajan et al., 2019; Siju et al., 2021). Given that also in mammals dopamine is increased by food consumption (Zhang et al., 2022) and plays a well-known role in the regulation of decision-making (Rogers, 2011), it is reasonable to hypothesize that this function is conserved across the animal kingdom. That make this study especially valuable since it suggests that also the molecular pathway downstream dopamine may be conserved in mammals, where the molecular mechanisms underlying behavioral choice are largely unknown.

Studies in mammals on the neuromodulatory systems involved in decision-making have highlighted the opponency of serotonin and dopamine in the regulation of behavioral choice and learning (Boureau & Dayan, 2011). In the present study, by investigating the effect of neuromodulators on the neuronal circuits controlling behavioral choice in zebrafish, we show that dopamine biases responses of tectal neurons towards large, aversive stimuli. This would ultimately lead to a preference for avoidance in behavioral choice during foraging. Interestingly, in a previous study it was shown that serotonin bias tectal neurons responses towards small, prey-like stimuli (Filosa et al., 2016), which would ultimately lead to an increased approach during hunting. Hence, serotonin and dopamine play an opposite role in decision-making in a simple behavioral paradigm in zebrafish.

Although in mammals decision-making may engage more complex neuronal circuits and involve learning, the parallelism of the relationship between dopamine and serotonin suggests that the basic underlying mechanisms of neuromodulation are likely conserved. Hence, zebrafish is an attractive vertebrate model to study decision-making using simpler behavioral paradigms, while still maintaining translational potential.

Interestingly, the results suggest that serotonin and dopamine are not acting on the same downstream neurons but they employ different molecular pathways and specific mechanisms to bias neuronal responses. This is suggested by the fact that in fed larvae, *pcp4a*-negative neurons also show a shift of the response profile towards large, aversive stimuli compared to food-deprived siblings. This is in contrast to what observed in the *pcp4a* mutant, where the mutation did not affect *pcp4a*-negative neurons, suggesting the existence of other molecular pathways biasing the response of different tectal populations. In addition, pharmacological activation of the serotonergic system did not show a strong effect on *pcp4a* expression levels.

Moreover, while serotonin bias the response profile of tectal neurons towards prey-like cues by recruiting new subpopulations of small-responding neurons (Filosa et al., 2016), dopamine acts mainly by affecting the tuning properties of individual neurons, suppressing stimulus-specific inputs.

This suggests that dopamine acts primarily through the *pcp4a* pathway in a synapse-specific way, modulating the tuning specificity of *pcp4a*+ tectal neurons. Meanwhile, serotonin acts likely through another unknown molecular pathway, activating size-selective tectal neurons populations (Filosa et al., 2016).

The existence of parallel and complementary pathways regulating behavioral choice is likely of evolutionary importance, given the crucial role of foraging behavior for survival. The presence of several separate neuromodulatory mechanisms allows for a tight regulation of decision-making and grants redundancy to the system, ensuring reliable behavioral choice even if one of the regulatory components fails.

Since the opposite roles of dopamine and serotonin in the regulation of decision-making behavior are conserved in mammals, it suggests that the molecular pathways and the mechanism to modulate neuronal activity may also be conserved. This is especially interesting since the specific molecular pathways acting downstream neuromodulatory neurotransmitters are still unclear in mammals. This study provides some indications of the possible

neuronal mechanisms and candidate genes involved, offering a base for targeted studies in more complex behavioral paradigms in higher vertebrates.

5.3. Mechanisms for Pcp4a-dependent regulation of neuronal activity and behavioral switch

The results support the hypothesis that Pcp4a modulates PVNs activity through a cell autonomous mechanism. Indeed, *pcp4a* mutation affect mainly *pcp4a+* PVNs response profile and not much other populations of tectal neurons, such as *pcp4a-* PVNs and SINS. The mutation also does not affect the activity at the RGCs terminals in the neuropil, making it unlikely that the shift in the response profile of tectal neurons derive from alteration of the visual inputs. Moreover, pharmacological activation of dopaminergic signaling affect mostly *pcp4a+* neurons expressing *drd2* receptors, likely due to decrease in Pcp4a levels.

The reason why Pcp4a acts through a cell autonomous mechanism is probably linked to its function: Pcp4a is a small cytoplasmic protein that inhibits the activation of CaM following a calcium influx, thus inhibiting downstream enzymes involved in postsynaptic plasticity such as CaMKII. This would lead to mainly changes in the activity of neurons expressing *pcp4a*.

Several studies in zebrafish suggest that size selectivity of PVN is acquired from the size-selective inputs they receive from RGCs and refined by SINS (Förster et al., 2020). Ultimately, their tuning properties are a result of their connectivity. However, in this study we describe a class of neurons switching their tuning properties due to transcriptional changes resulting in synaptic plasticity.

It is important to note that the majority of *pcp4a+* neurons changing size tuning respond to both large and small visual stimuli. This class of neurons represents only a small minority of PVNs (around 3% according to our estimates), but it likely plays an important role in decision-making due to its specific properties. Since they receive inputs from both small and large visual stimuli, they may play a crucial role in the switch between approach and avoidance. Feeding

state induces stimulus-specific changes in the activity through a transcriptional mechanism, biasing behavioral choice towards the most advantageous strategy.

It would be interesting to investigate if similar classes of dual-responding neurons, mediating the switch between opposite behaviors depending on internal states, are also present in other vertebrate models.

The study also highlights the importance of small CaM-binding protein in regulating neuronal activity *in vivo*. Pcp4a is part of a larger family of small proteins inhibiting Ca²⁺ mediated activation of CaM that includes also Neurogranin and Neuromodulin among others (Slemmon et al., 1996). Although they have long been described and it is known they are widely expressed in the central nervous system (Represa et al., 1990; Slemmon et al., 2000), most research has been conducted *in vitro* and their role in regulation of neuronal excitability *in vivo* is understudied. Given their function in regulating the activity of important enzymes in calcium-dependent signal transduction such as CaMKII and NOS, a more detailed understanding of their mechanism of action is required.

In this study, we show that Pcp4a may have a synapse-specific effect on neuronal excitability, changing neuronal response in a stimulus-specific way. This could be achieved by targeting Pcp4a and/or CaMKII at specific synapses or by differential effect of Pcp4a on CaMKII depending on the type of stimulus inducing calcium influx. Studies have shown that different methods of stimulation have opposite effects on Pcp4a regulation of CaMKII activity (Johanson et al., 2000). It is also possible that Pcp4a may play a role in localizing CaM at specific synapses, since a similar function has been proposed for proteins belonging to the same family like Neuromodulin and Neurogranin (Gerendasy et al., 1994; Yuechueng & Storm, 1990).

This suggests an intriguing role for neurons responding to different stimulations to change their response depending on the levels of Pcp4a, ultimately leading to distinct behavioral responses. Since Pcp4a levels are tuned to the metabolic state of the individual, this is a mechanism to link behavioral choice to internal states.

How is Pcp4a affecting synaptic strength? It is unlikely due to structural changes at the synapses such as new synapse formation or pruning, since alteration of synaptic strength needs to be attuned to the metabolic state of the individual, which can fluctuate rather quickly. Consequently, synaptic properties should be able to switch within relatively fast timescales.

The results suggest that CaMKII is likely involved in this process downstream Pcp4a. It is known that CaMKII influence synaptic plasticity through phosphorylation of ion channels and receptors, and shuttling of postsynaptic components (Bayer & Schulman, 2019; Coultrap et al., 2011; Yasuda et al., 2022). Pcp4a-mediated changes in synaptic strength likely involve similar mechanisms.

Given the role played by the optic tectum in behavioral choice, most likely feeding state-dependent changes in tuning properties of *pcp4a*+ tectal neurons contributes to regulation of decision-making. However, we cannot exclude that *pcp4a* may influence decision-making also by affecting sensorimotor transformation in other brain structures, upstream or downstream of the tectum, since it is expressed also in the retina, pretectum and reticulospinal network.

5.4. Translational potential of this study

This study provides insights on the molecular and neuronal mechanisms underlying the regulation of decision-making by internal states and thus may offer interesting points for translational research. Moreover, identifying the molecular pathway computing valence of food-related cues may be important in the treatment of eating disorders, where the appetitive value of food is disconnected from the metabolic state of the individual and processing of food-related cues is altered (Brooks et al., 2011; García-García et al., 2013; Giel et al., 2011).

Additionally, in humans *PCP4* is located in chromosome 21 and thus is overexpressed in Down Syndrome patients. Moreover, the gene maps within

the Down Syndrome Critical Region (Chen et al., 1996) and is thus likely a major player in the symptomatology associated with the syndrome. Interestingly, obesity has a higher prevalence in these patients compared to the general population. The causes for this comorbidity are still unclear and generally attributed to metabolic dysfunction or parental dietary practices (Bertapelli et al., 2016). Based on the results of our study, it is possible that PCP4 overexpression in Down syndrome patients may alter their perception of food and facilitate the onset of obesity.

To the best of my knowledge, this study is the first to elucidate the molecular mechanisms controlling behavioral choice in a vertebrate model, and represents an important step towards understanding the molecular basis of decision-making in complex organisms. Given that molecular pathways underlying specific behaviors are fairly conserved among vertebrates, this could open research avenues for studies in mammals, including humans.

6. Bibliography

- Asakawa, K., & Kawakami, K. (2008). Targeted gene expression by the Gal4-UAS system in zebrafish. *Development, Growth & Differentiation*, *50*(6), 391–399. <https://doi.org/https://doi.org/10.1111/j.1440-169X.2008.01044.x>
- Asakawa, K., Suster, M. L., Mizusawa, K., Nagayoshi, S., Kotani, T., Urasaki, A., Kishimoto, Y., Hibi, M., & Kawakami, K. (2008). Genetic dissection of neural circuits by Tol2 transposon-mediated Gal4 gene and enhancer trapping in zebrafish. *Proceedings of the National Academy of Sciences*, *105*(4), 1255–1260. <https://doi.org/10.1073/pnas.0704963105>
- Aston-Jones, G., & Cohen, J. D. (2005). AN INTEGRATIVE THEORY OF LOCUS COERULEUS-NOREPINEPHRINE FUNCTION: Adaptive Gain and Optimal Performance. *Annual Review of Neuroscience*, *28*(1), 403–450. <https://doi.org/10.1146/annurev.neuro.28.061604.135709>
- Barker, A. J., & Baier, H. (2015). Sensorimotor decision making in the Zebrafish tectum. *Current Biology*, *25*(21), 2804–2814. <https://doi.org/10.1016/j.cub.2015.09.055>
- Bayer, K. U., & Schulman, H. (2019). CaM Kinase: Still Inspiring at 40. *Neuron*, *103*(3), 380–394. <https://doi.org/10.1016/j.neuron.2019.05.033>
- Beaulieu, J.-M., & Gainetdinov, R. R. (2011). The Physiology, Signaling, and Pharmacology of Dopamine Receptors. *Pharmacological Reviews*, *63*(1), 182. <https://doi.org/10.1124/pr.110.002642>
- Becchetti, A., & Amadeo, A. (2016). Why we forget our dreams: Acetylcholine and norepinephrine in wakefulness and REM sleep. *Behavioral and Brain Sciences*, *39*, e202. <https://doi.org/DOI: 10.1017/S0140525X15001739>
- Beppi, C., Straumann, D., & Bögli, S. Y. (2021). A model-based quantification of startle reflex habituation in larval zebrafish. *Scientific Reports*, *11*(1), 846. <https://doi.org/10.1038/s41598-020-79923-6>
- Bertapelli, F., Pitetti, K., Agiovlasis, S., & Guerra-Junior, G. (2016). Overweight and obesity in children and adolescents with Down syndrome—prevalence, determinants, consequences, and interventions: A literature review. *Research in*

Developmental Disabilities, 57, 181–192.

<https://doi.org/https://doi.org/10.1016/j.ridd.2016.06.018>

- Boureau, Y.-L., & Dayan, P. (2011). Opponency Revisited: Competition and Cooperation Between Dopamine and Serotonin. *Neuropsychopharmacology*, 36(1), 74–97. <https://doi.org/10.1038/npp.2010.151>
- Brockerhoff, S. E., Hurley, J. B., Janssen-Bienhold, U., Neuhauss, S. C., Driever, W., & Dowling, J. E. (1995). A behavioral screen for isolating zebrafish mutants with visual system defects. *Proceedings of the National Academy of Sciences*, 92(23), 10545–10549. <https://doi.org/10.1073/pnas.92.23.10545>
- Brooks, S., Prince, A., Stahl, D., Campbell, I. C., & Treasure, J. (2011). A systematic review and meta-analysis of cognitive bias to food stimuli in people with disordered eating behaviour. *Clinical Psychology Review*, 31(1), 37–51. <https://doi.org/https://doi.org/10.1016/j.cpr.2010.09.006>
- Burgess, C. R., Ramesh, R. N., Sugden, A. U., Levandowski, K. M., Minnig, M. A., Fenselau, H., Lowell, B. B., & Andermann, M. L. (2016). Hunger-Dependent Enhancement of Food Cue Responses in Mouse Postrhinal Cortex and Lateral Amygdala. *Neuron*, 91(5), 1154–1169. <https://doi.org/10.1016/j.neuron.2016.07.032>
- Burgess, H. A., & Granato, M. (2007). Sensorimotor Gating in Larval Zebrafish. *Journal of Neuroscience*, 27(18), 4984–4994. <https://doi.org/10.1523/JNEUROSCI.0615-07.2007>
- Burnett, C. J., Li, C., Webber, E., Tsaousidou, E., Xue, S. Y., Brüning, J. C., & Krashes, M. J. (2016). Hunger-Driven Motivational State Competition. *Neuron*, 92(1), 187–201. <https://doi.org/10.1016/j.neuron.2016.08.032>
- Chen, H., Bouras, C., & Antonarakis, S. E. (1996). Cloning of the cDNA for a human homolog of the rat PEP-19 gene and mapping to chromosome 21q22.2–q22.3. *Human Genetics*, 98(6), 672–677. <https://doi.org/10.1007/s004390050282>
- Choi, H. M. T., Schwarzkopf, M., Fornace, M. E., Acharya, A., Artavanis, G., Stegmaier, J., Cunha, A., & Pierce, N. A. (2018). Third-generation in situ hybridization chain reaction: multiplexed, quantitative, sensitive, versatile, robust. *Development*, 145(12). <https://doi.org/10.1242/dev.165753>

- Corradi, L., Zaupa, M., Sawamiphak, S., & Filosa, A. (2022). Using pERK immunostaining to quantify neuronal activity induced by stress in zebrafish larvae. *STAR Protocols*, 3(4), 101731.
<https://doi.org/https://doi.org/10.1016/j.xpro.2022.101731>
- Coultrap, S. J., Vest, R. S., Ashpole, N. M., Hudmon, A., & Bayer, K. U. (2011). CaMKII in cerebral ischemia. *Acta Pharmacologica Sinica*, 32(7), 861–872.
<https://doi.org/10.1038/aps.2011.68>
- Crossley, M., Staras, K., & Kemenes, G. (2023). A central control circuit for encoding perceived food value. *Science Advances*, 4(11), eaau9180.
<https://doi.org/10.1126/sciadv.aau9180>
- Deem, J. D., Faber, C. L., & Morton, G. J. (2022). AgRP neurons: Regulators of feeding, energy expenditure, and behavior. *The FEBS Journal*, 289(8), 2362–2381. <https://doi.org/https://doi.org/10.1111/febs.16176>
- Del Bene, F., Wyart, C., Robles, E., Tran, A., Looger, L., Scott, E. K., Isacoff, E. Y., & Baier, H. (2010). Filtering of Visual Information in the Tectum by an Identified Neural Circuit. *Science*, 330(6004), 669–673.
<https://doi.org/10.1126/science.1192949>
- Dunn, T. W., Gebhardt, C., Naumann, E. A., Riegler, C., Ahrens, M. B., Engert, F., & Del Bene, F. (2016). Neural Circuits Underlying Visually Evoked Escapes in Larval Zebrafish. In *Neuron* (Vol. 89, Issue 3, pp. 613–628).
<https://doi.org/10.1016/j.neuron.2015.12.021>
- Ek, F., Malo, M., Åberg Andersson, M., Wedding, C., Kronborg, J., Svensson, P., Waters, S., Petersson, P., & Olsson, R. (2016). Behavioral Analysis of Dopaminergic Activation in Zebrafish and Rats Reveals Similar Phenotypes. *ACS Chemical Neuroscience*, 7(5), 633–646.
<https://doi.org/10.1021/acscchemneuro.6b00014>
- Fernandes, A. M., Fero, K., Arrenberg, A. B., Bergeron, S. A., Driever, W., & Burgess, H. A. (2012). Deep Brain Photoreceptors Control Light-Seeking Behavior in Zebrafish Larvae. *Current Biology*, 22(21), 2042–2047.
<https://doi.org/10.1016/j.cub.2012.08.016>

- Filosa, A., Barker, A. J., Dal Maschio, M., & Baier, H. (2016). Feeding State Modulates Behavioral Choice and Processing of Prey Stimuli in the Zebrafish Tectum. *Neuron*, *90*(3), 596–608. <https://doi.org/10.1016/j.neuron.2016.03.014>
- Förster, D., Helmbrecht, T. O., Mearns, D. S., Jordan, L., Mokayes, N., & Baier, H. (2020). Retinotectal circuitry of larval zebrafish is adapted to detection and pursuit of prey. *ELife*, *9*, e58596. <https://doi.org/10.7554/eLife.58596>
- Frank, M. J., & O'Reilly, R. C. (2006). A Mechanistic Account of Striatal Dopamine Function in Human Cognition: Psychopharmacological Studies With Cabergoline and Haloperidol. *Behavioral Neuroscience*. <https://doi.org/10.1037/0735-7044.120.3.497.supp>
- Freeman, J., Vladimirov, N., Kawashima, T., Mu, Y., Sofroniew, N. J., Bennett, D. V., Rosen, J., Yang, C.-T., Looger, L. L., & Ahrens, M. B. (2014). Mapping brain activity at scale with cluster computing. *Nature Methods*, *11*(9), 941–950. <https://doi.org/10.1038/nmeth.3041>
- Gagnon, J. A., Valen, E., Thyme, S. B., Huang, P., Akhmetova, L., Pauli, A., Montague, T. G., Zimmerman, S., Richter, C., & Schier, A. F. (2014). Efficient mutagenesis by Cas9 protein-mediated oligonucleotide insertion and large-scale assessment of single-guide RNAs. *PloS One*, *9*(5), e98186. <https://doi.org/10.1371/journal.pone.0098186>
- Gahtan, E., Tanger, P., & Baier, H. (2005). Visual Prey Capture in Larval Zebrafish Is Controlled by Identified Reticulospinal Neurons Downstream of the Tectum. *The Journal of Neuroscience*, *25*(40), 9294. <https://doi.org/10.1523/JNEUROSCI.2678-05.2005>
- García-García, I., Narberhaus, A., Marqués-Iturria, I., Garolera, M., Rădoi, A., Segura, B., Pueyo, R., Ariza, M., & Jurado, M. A. (2013). Neural Responses to Visual Food Cues: Insights from Functional Magnetic Resonance Imaging. *European Eating Disorders Review*, *21*(2), 89–98. <https://doi.org/https://doi.org/10.1002/erv.2216>
- Gaudry, Q., & Kristan, W. B. (2009). Behavioral choice by presynaptic inhibition of tactile sensory terminals. *Nature Neuroscience*, *12*(11), 1450–1457. <https://doi.org/10.1038/nn.2400>

- Gerendasy, D. D., Herron, S. R., Watson, J. B., & Sutcliffe, J. G. (1994). Mutational and biophysical studies suggest RC3/neurogranin regulates calmodulin availability. *Journal of Biological Chemistry*, *269*(35), 22420–22426.
- Gibson, U. E., Heid, C. A., & Williams, P. M. (1996). A novel method for real time quantitative RT-PCR. *Genome Research*, *6*(10), 995–1001.
<https://doi.org/10.1101/gr.6.10.995>
- Giel, K. E., Teufel, M., Friederich, H.-C., Hautzinger, M., Enck, P., & Zipfel, S. (2011). Processing of pictorial food stimuli in patients with eating disorders—A systematic review. *International Journal of Eating Disorders*, *44*(2), 105–117.
<https://doi.org/https://doi.org/10.1002/eat.20785>
- Gillette, R., Huang, R.-C., Hatcher, N., & Moroz, L. L. (2000). Cost-benefit analysis potential in feeding behavior of a predatory snail by integration of hunger, taste, and pain. *Proceedings of the National Academy of Sciences*, *97*(7), 3585–3590.
<https://doi.org/10.1073/pnas.97.7.3585>
- Heap, L. A., Vanwalleghem, G. C., Thompson, A. W., Favre-Bulle, I., Rubinsztein-Dunlop, H., & Scott, E. K. (2018). Hypothalamic projections to the optic tectum in larval zebrafish. *Frontiers in Neuroanatomy*, *11*(January), 1–12.
<https://doi.org/10.3389/fnana.2017.00135>
- Helmbrecht, T. O., dal Maschio, M., Donovan, J. C., Koutsouli, S., & Baier, H. (2018). Topography of a Visuomotor Transformation. *Neuron*, *100*(6), 1429–1445.e4.
<https://doi.org/https://doi.org/10.1016/j.neuron.2018.10.021>
- Hirayama, K., & Gillette, R. (2012). A neuronal network switch for approach/avoidance toggled by appetitive state. *Current Biology*, *22*(2), 118–123. <https://doi.org/10.1016/j.cub.2011.10.055>
- Howe, K., Clark, M. D., Torroja, C. F., Torrance, J., Berthelot, C., Muffato, M., Collins, J. E., Humphray, S., McLaren, K., Matthews, L., McLaren, S., Sealy, I., Caccamo, M., Churcher, C., Scott, C., Barrett, J. C., Koch, R., Rauch, G.-J., White, S., ... Stemple, D. L. (2013). The zebrafish reference genome sequence and its relationship to the human genome. *Nature*, *496*(7446), 498–503.
<https://doi.org/10.1038/nature12111>
- Inagaki, H. K., Panse, K. M., & Anderson, D. J. (2014). Independent, reciprocal neuromodulatory control of sweet and bitter taste sensitivity during starvation in

- Drosophila. *Neuron*, 84(4), 806–820.
<https://doi.org/10.1016/j.neuron.2014.09.032>
- Irons, T. D., Kelly, P. E., Hunter, D. L., MacPhail, R. C., & Padilla, S. (2013). Acute administration of dopaminergic drugs has differential effects on locomotion in larval zebrafish. *Pharmacology Biochemistry and Behavior*, 103(4), 792–813.
<https://doi.org/https://doi.org/10.1016/j.pbb.2012.12.010>
- Jefferis, G. (2018). *IGS (CMTK) Image Registration Tools Classic MacOSX GUI*. Zenodo. <https://doi.org/10.5281/zenodo.1193268>
- Johanson, R. A., Sarau, H. M., Foley, J. J., & Slemmon, J. R. (2000). Calmodulin-Binding Peptide PEP-19 Modulates Activation of Calmodulin Kinase II & In Situ; *The Journal of Neuroscience*, 20(8), 2860.
<https://doi.org/10.1523/JNEUROSCI.20-08-02860.2000>
- Kastenhuber, E., Kratochwil, C. F., Ryu, S., Schweitzer, J., & Driever, W. (2010). Genetic dissection of dopaminergic and noradrenergic contributions to catecholaminergic tracts in early larval zebrafish. *Journal of Comparative Neurology*, 518(4), 439–458. <https://doi.org/10.1002/cne.22214>
- Kenny, P. J., & Markou, A. (2006). Nicotine Self-Administration Acutely Activates Brain Reward Systems and Induces a Long-Lasting Increase in Reward Sensitivity. *Neuropsychopharmacology*, 31(6), 1203–1211.
<https://doi.org/10.1038/sj.npp.1300905>
- Kettunen, P. (2020). Calcium Imaging in the Zebrafish. In Md. S. Islam (Ed.), *Calcium Signaling* (pp. 901–942). Springer International Publishing.
https://doi.org/10.1007/978-3-030-12457-1_36
- Kimura, Y., Hisano, Y., Kawahara, A., & Higashijima, S. (2014). Efficient generation of knock-in transgenic zebrafish carrying reporter/driver genes by CRISPR/Cas9-mediated genome engineering. *Scientific Reports*, 4, 6545.
<https://doi.org/10.1038/srep06545>
- Kimura, Y., Satou, C., & Higashijima, S. (2008). V2a and V2b neurons are generated by the final divisions of pair-producing progenitors in the zebrafish spinal cord. *Development*, 135(18), 3001–3005. <https://doi.org/10.1242/dev.024802>

- Kleerekoper, Q. K., & Putkey, J. A. (2009). PEP-19, an intrinsically disordered regulator of calmodulin signaling. *The Journal of Biological Chemistry*, *284*(12), 7455–7464. <https://doi.org/10.1074/jbc.M808067200>
- Kurniawan, I., Guitart-Masip, M., & Dolan, R. (2011). Dopamine and Effort-Based Decision Making. *Frontiers in Neuroscience*, *5*.
<https://www.frontiersin.org/articles/10.3389/fnins.2011.00081>
- LaBar, K. S., Gitelman, D. R., Parrish, T. B., Kim, Y. H., Nobre, A. C., & Mesulam, M. M. (2001). Hunger selectively modulates corticolimbic activation to food stimuli in humans. *Behavioral Neuroscience*, *115*(2), 493–500.
<https://doi.org/10.1037/0735-7044.115.2.493>
- Laing, B. T., Li, P., Schmidt, C. A., Bunner, W., Yuan, Y., Landry, T., Prete, A., McClung, J. M., & Huang, H. (2018). AgRP/NPY neuron excitability is modulated by metabotropic glutamate receptor 1 during fasting. *Frontiers in Cellular Neuroscience*, *12*(September), 1–13.
<https://doi.org/10.3389/fncel.2018.00276>
- Lee, S.-H., & Dan, Y. (2012). Neuromodulation of Brain States. *Neuron*, *76*(1), 209–222. <https://doi.org/https://doi.org/10.1016/j.neuron.2012.09.012>
- Leonard, B. E. (2007). HPA and Immune Axes in Stress: Involvement of the Serotonergic System. *Neuroimmunomodulation*, *13*(5–6), 268–276.
<https://doi.org/10.1159/000104854>
- Li, M., Zhao, L., Page-McCaw, P. S., & Chen, W. (2016). Zebrafish Genome Engineering Using the CRISPR/Cas9 System. *Trends in Genetics*, *32*(12), 815–827. <https://doi.org/10.1016/j.tig.2016.10.005>
- Lillesaar, C. (2011). The serotonergic system in fish. *Journal of Chemical Neuroanatomy*, *41*(4), 294–308.
<https://doi.org/https://doi.org/10.1016/j.jchemneu.2011.05.009>
- Lister, J. A., Robertson, C. P., Lepage, T., Johnson, S. L., & Raible, D. W. (1999). nacre encodes a zebrafish microphthalmia-related protein that regulates neural-crest-derived pigment cell fate. *Development*, *126*(17), 3757–3767.
<https://doi.org/10.1242/dev.126.17.3757>

- Lovett-Barron, M., Andalman, A. S., Allen, W. E., Vesuna, S., Kauvar, I., Burns, V. M., & Deisseroth, K. (2017). Ancestral Circuits for the Coordinated Modulation of Brain State. *Cell*, *171*(6), 1411-1423.e17. <https://doi.org/10.1016/j.cell.2017.10.021>
- Lovett-Barron, M., Chen, R., Bradbury, S., Andalman, A. S., Wagle, M., Guo, S., & Deisseroth, K. (2020). Multiple convergent hypothalamus-brainstem circuits drive defensive behavior. *Nature Neuroscience*, *23*(8), 959–967. <https://doi.org/10.1038/s41593-020-0655-1>
- Maaswinkel, H., & Li, L. (2003). Spatio-temporal frequency characteristics of the optomotor response in zebrafish. *Vision Research*, *43*(1), 21–30. [https://doi.org/https://doi.org/10.1016/S0042-6989\(02\)00395-4](https://doi.org/https://doi.org/10.1016/S0042-6989(02)00395-4)
- Matteucci, G., Guyoton, M., Mayrhofer, J. M., Auffret, M., Foustoukos, G., Petersen, C. C. H., & El-Boustani, S. (2022). Cortical sensory processing across motivational states during goal-directed behavior. *Neuron*, *110*(24), 4176-4193.e10. <https://doi.org/https://doi.org/10.1016/j.neuron.2022.09.032>
- Mazo, G. (2021). QuickFigures: A toolkit and ImageJ PlugIn to quickly transform microscope images into scientific figures. *PLOS ONE*, *16*(11), e0240280-. <https://doi.org/10.1371/journal.pone.0240280>
- Mione, M., Lele, Z., Kwong, C. T., Concha, M. L., & Clarke, J. D. (2006). Expression of *pcp4a* in subpopulations of CNS neurons in zebrafish. *The Journal of Comparative Neurology*, *495*(6), 769–787. <https://doi.org/10.1002/cne.20907>
- Miri, A., Daie, K., Burdine, R. D., Aksay, E., & Tank, D. W. (2010). Regression-Based Identification of Behavior-Encoding Neurons During Large-Scale Optical Imaging of Neural Activity at Cellular Resolution. *Journal of Neurophysiology*, *105*(2), 964–980. <https://doi.org/10.1152/jn.00702.2010>
- Miyazaki, K., Miyazaki, K. W., & Doya, K. (2011). Activation of Dorsal Raphe Serotonin Neurons Underlies Waiting for Delayed Rewards. *The Journal of Neuroscience*, *31*(2), 469. <https://doi.org/10.1523/JNEUROSCI.3714-10.2011>
- Mullins, M. C., Hammerschmidt, M., Haffter, P., & Nüsslein-Volhard, C. (1994). Large-scale mutagenesis in the zebrafish: in search of genes controlling development in a vertebrate. *Current Biology*, *4*(3), 189–202. [https://doi.org/10.1016/S0960-9822\(00\)00048-8](https://doi.org/10.1016/S0960-9822(00)00048-8)

- Muto, A., & Kawakami, K. (2013). Prey capture in zebrafish larvae serves as a model to study cognitive functions. *Frontiers in Neural Circuits*, 7. <https://www.frontiersin.org/articles/10.3389/fncir.2013.00110>
- Padilla, S. L., Qiu, J., Soden, M. E., Sanz, E., Nestor, C. C., Barker, F. D., Quintana, A., Zweifel, L. S., Rønnekleiv, O. K., Kelly, M. J., & Palmiter, R. D. (2016). Agouti-related peptide neural circuits mediate adaptive behaviors in the starved state. *Nature Neuroscience*, 19(5), 734–741. <https://doi.org/10.1038/nn.4274>
- Peirce, J., Gray, J. R., Simpson, S., MacAskill, M., Höchenberger, R., Sogo, H., Kastman, E., & Lindeløv, J. K. (2019). PsychoPy2: Experiments in behavior made easy. *Behavior Research Methods*, 51(1), 195–203. <https://doi.org/10.3758/s13428-018-01193-y>
- Pnevmatikakis, E. A., & Giovannucci, A. (2017). NoRMCorre: An online algorithm for piecewise rigid motion correction of calcium imaging data. *Journal of Neuroscience Methods*, 291, 83–94. <https://doi.org/https://doi.org/10.1016/j.jneumeth.2017.07.031>
- Preuss, S. J., Trivedi, C. A., Vom Berg-Maurer, C. M., Ryu, S., & Bollmann, J. H. (2014). Classification of object size in retinotectal microcircuits. In *Current Biology* (Vol. 24, Issue 20, pp. 2376–2385). <https://doi.org/10.1016/j.cub.2014.09.012>
- Randlett, O., Wee, C. L., Naumann, E. A., Nnaemeka, O., Schoppik, D., Fitzgerald, J. E., Portugues, R., Lacoste, A. M. B., Riegler, C., Engert, F., & Schier, A. F. (2015). Whole-brain activity mapping onto a zebrafish brain atlas. *Nature Methods*, 12(11), 1039–1046. <https://doi.org/10.1038/nmeth.3581>
- Rengarajan, S., Yankura, K. A., Guillermin, M. L., Fung, W., & Hallem, E. A. (2019). Feeding state sculpts a circuit for sensory valence in *Caenorhabditis elegans*. *Proceedings of the National Academy of Sciences*, 116(5), 1776–1781. <https://doi.org/10.1073/pnas.1807454116>
- Represa, A., Deloulme, J. C., Sensenbrenner, M., Ben-Ari, Y., & Baudier, J. (1990). Neurogranin: immunocytochemical localization of a brain-specific protein kinase C substrate. *The Journal of Neuroscience*, 10(12), 3782. <https://doi.org/10.1523/JNEUROSCI.10-12-03782.1990>

- Robles, E., Laurell, E., & Baier, H. (2014). The Retinal Projectome Reveals Brain-Area-Specific Visual Representations Generated by Ganglion Cell Diversity. *Current Biology*, 24(18), 2085–2096. <https://doi.org/https://doi.org/10.1016/j.cub.2014.07.080>
- Rogers, R. D. (2011). The Roles of Dopamine and Serotonin in Decision Making: Evidence from Pharmacological Experiments in Humans. *Neuropsychopharmacology*, 36(1), 114–132. <https://doi.org/10.1038/npp.2010.165>
- Rolls, E. T., Sienkiewicz, Z. J., & Yaxley, S. (1989). Hunger Modulates the Responses to Gustatory Stimuli of Single Neurons in the Caudolateral Orbitofrontal Cortex of the Macaque Monkey. *European Journal of Neuroscience*, 1(1), 53–60. <https://doi.org/https://doi.org/10.1111/j.1460-9568.1989.tb00774.x>
- Rosen, L. B., Ginty, D. D., Weber, M. J., & Greenberg, M. E. (1994). Membrane depolarization and calcium influx stimulate MEK and MAP kinase via activation of Ras. *Neuron*, 12(6), 1207–1221. [https://doi.org/10.1016/0896-6273\(94\)90438-3](https://doi.org/10.1016/0896-6273(94)90438-3)
- Scerbina, T., Chatterjee, D., & Gerlai, R. (2012). Dopamine receptor antagonism disrupts social preference in zebrafish: a strain comparison study. *Amino Acids*, 43(5), 2059–2072. <https://doi.org/10.1007/s00726-012-1284-0>
- Siju, K. P., De Backer, J.-F., & Grunwald Kadow, I. C. (2021). Dopamine modulation of sensory processing and adaptive behavior in flies. *Cell and Tissue Research*, 383(1), 207–225. <https://doi.org/10.1007/s00441-020-03371-x>
- Slemmon, J. R., Feng, B., & Erhardt, J. A. (2000). Small proteins that modulate calmodulin-dependent signal transduction: effects of PEP-19, neuromodulin, and neurogranin on enzyme activation and cellular homeostasis. *Molecular Neurobiology*, 22(1–3), 99–113. <https://doi.org/10.1385/MN:22:1-3:099>
- Slemmon, J. R., Morgan, J. I., Fullerton, S. M., Danho, W., Hilbush, B. S., & Wengenack, T. M. (1996). Camstatins Are Peptide Antagonists of Calmodulin Based Upon a Conserved Structural Motif in PEP-19, Neurogranin, and Neuromodulin *. *Journal of Biological Chemistry*, 271(27), 15911–15917. <https://doi.org/10.1074/jbc.271.27.15911>

- Sörensen, L. K. A., Bohté, S. M., Slagter, H. A., & Scholte, H. S. (2022). Arousal state affects perceptual decision-making by modulating hierarchical sensory processing in a large-scale visual system model. *PLOS Computational Biology*, *18*(4), e1009976-. <https://doi.org/10.1371/journal.pcbi.1009976>
- Tanaka, S. C., Shishida, K., Schweighofer, N., Okamoto, Y., Yamawaki, S., & Doya, K. (2009). Serotonin Affects Association of Aversive Outcomes to Past Actions. *The Journal of Neuroscience*, *29*(50), 15669. <https://doi.org/10.1523/JNEUROSCI.2799-09.2009>
- Tay, T. L., Ronneberger, O., Ryu, S., Nitschke, R., & Driever, W. (2011). Comprehensive catecholaminergic projectome analysis reveals single-neuron integration of zebrafish ascending and descending dopaminergic systems. *Nature Communications*, *2*(1), 171. <https://doi.org/10.1038/ncomms1171>
- Temizer, I., Donovan, J. C., Baier, H., & Semmelhack, J. L. (2015). A Visual Pathway for Looming-Evoked Escape in Larval Zebrafish. In *Current Biology* (Vol. 25, Issue 14, pp. 1823–1834). <https://doi.org/10.1016/j.cub.2015.06.002>
- Thiele, T. R., Donovan, J. C., & Baier, H. (2014). Descending Control of Swim Posture by a Midbrain Nucleus in Zebrafish. *Neuron*, *83*(3), 679–691. <https://doi.org/10.1016/j.neuron.2014.04.018>
- Thompson, A. W., Vanwalleghem, G. C., Heap, L. A., & Scott, E. K. (2016). Functional profiles of visual-, auditory-, and water flow-responsive neurons in the Zebrafish Tectum. *Current Biology*, *26*(6), 743–754. <https://doi.org/10.1016/j.cub.2016.01.041>
- van Staden, C., de Brouwer, G., Botha, T. L., Finger-Baier, K., Brand, S. J., & Wolmarans, D. (2020). Dopaminergic and serotonergic modulation of social reward appraisal in zebrafish (*Danio rerio*) under circumstances of motivational conflict: Towards a screening test for anti-compulsive drug action. *Behavioural Brain Research*, *379*, 112393. <https://doi.org/https://doi.org/10.1016/j.bbr.2019.112393>
- Vladimirov, N., Mu, Y., Kawashima, T., Bennett, D. V, Yang, C.-T., Looger, L. L., Keller, P. J., Freeman, J., & Ahrens, M. B. (2014). Light-sheet functional imaging in fictively behaving zebrafish. *Nature Methods*, *11*(9), 883–884. <https://doi.org/10.1038/nmeth.3040>

- Wei, P., Blundon, J. A., Rong, Y., Zakharenko, S. S., & Morgan, J. I. (2011). Impaired locomotor learning and altered cerebellar synaptic plasticity in *pep-19/PCP4*-null mice. *Molecular and Cellular Biology*, *31*(14), 2838–2844.
<https://doi.org/10.1128/MCB.05208-11>
- Wogar, M. A., Bradshaw, C. M., & Szabadi, E. (1993). Effect of lesions of the ascending 5-hydroxytryptaminergic pathways on choice between delayed reinforcers. *Psychopharmacology*, *111*(2), 239–243.
<https://doi.org/10.1007/BF02245530>
- Wullimann, M. F., & Mueller, T. (2004). Teleostean and mammalian forebrains contrasted: Evidence from genes to behavior. *Journal of Comparative Neurology*, *475*(2), 143–162. <https://doi.org/https://doi.org/10.1002/cne.20183>
- Xiong, L.-W., Kleerekoper, Q. K., Wang, X., & Putkey, J. A. (2010). Intra- and Interdomain Effects Due to Mutation of Calcium-binding Sites in Calmodulin *. *Journal of Biological Chemistry*, *285*(11), 8094–8103.
<https://doi.org/10.1074/jbc.M109.065243>
- Yasuda, R., Hayashi, Y., & Hell, J. W. (2022). CaMKII: a central molecular organizer of synaptic plasticity, learning and memory. *Nature Reviews Neuroscience*, *23*(11), 666–682. <https://doi.org/10.1038/s41583-022-00624-2>
- Yuechueng, L., & Storm, D. R. (1990). Regulation of free calmodulin levels by neuromodulin: neuron growth and regeneration. *Trends in Pharmacological Sciences*, *11*(3), 107–111. [https://doi.org/https://doi.org/10.1016/0165-6147\(90\)90195-E](https://doi.org/https://doi.org/10.1016/0165-6147(90)90195-E)
- Zhang, Q., Tang, Q., Purohit, N. M., Davenport, J. B., Brennan, C., Patel, R. K., Godschall, E., Zwiefel, L. S., Spano, A., Campbell, J. N., & Güler, A. D. (2022). Food-induced dopamine signaling in AgRP neurons promotes feeding. *Cell Reports*, *41*(9), 111718.
<https://doi.org/https://doi.org/10.1016/j.celrep.2022.111718>

Abbreviations

aa: aminoacids

AgRP: agouti-related peptide

***atoh7*:** atonal bHLH transcription factor 7

bp: base pair

BSA: bovine serum albumin

Ca²⁺: calcium

CaM: calmodulin

CaMKII: Ca²⁺/calmodulin-dependent kinase II

cAMP: cyclic adenosine monophosphate

cDNA: complementary DNA

CNS: central nervous system

CRISPR/Cas9: Clustered Regularly Interspaced Short Palindromic Repeats/CRISPR-associated protein 9

DAPI: 4',6-diamidin-2-phenylindol

DMSO: dimethylsulfoxide

dpf: days post fertilization

***drd2*:** dopamine receptor 2

EGFP: enhanced green fluorescent protein

***elavl3*:** ELAV like neuron-specific RNA binding protein 3

ERK: extracellular signal-regulated kinase

fps: frames per second

***gad1b*:** glutamate decarboxylase 1b

GECI: genetically encoded calcium indicator

GFP: green fluorescent protein

HCR: hybridization chain reaction

h: hour

Hc: caudal hypothalamus

Hi: intermediate hypothalamus

hpf: hours post fertilization

HPI: hypothalamic-pituitary-interrenal gland

iTB: ipsilateral tectobulbar tract

LC: locus coeruleus
LTD: long-term depression
LTP: long-term potentiation
mRNA: messenger RNA
nMLF: nucleus of the medial longitudinal fasciculus
NOS: nitric oxide synthase
OMR: optomotor response
PBS: phosphate buffer saline
Pcp4a: Purkinje cell protein 4a
PFA: paraformaldehyde
PCR: polymerase chain reaction
PT: posterior tuberculum
PVL: periventricular layer
PVN: periventricular neuron
PVPN: periventricular projection neuron
qRT-PCR: quantitative reverse transcription polymerase chain reaction
RGC: retinal ganglion cell
ROI: region of interest
SEM: standard error of the mean
sgRNA: small guide RNA
SIN: superficial interneuron
SSC: saline sodium citrate
th: tyrosine hydroxylase
UAS: upstream activation sequence
WMR: weighted mean response
vglut2: vesicular glutamate transporter 2

Figures

<i>Figure 1: Gal4/UAS system</i>	15
<i>Figure 2: Approach and avoidance behavior in zebrafish</i>	17
<i>Figure 3: Neuronal circuits in the optic tectum in zebrafish</i>	18
<i>Figure 4: Visuomotor transformations underlying approach and avoidance</i>	20
<i>Figure 5: Feeding decrease abundance of Pcp4a</i>	23
<i>Figure 6: pcp4a expression in the central nervous system</i>	48
<i>Figure 7: Mutating pcp4a alters behavioral choice</i>	50
<i>Figure 8: Behavioral performance of pcp4a mutants</i>	53
<i>Figure 9: Calcium imaging strategy</i>	55
<i>Figure 10: Feeding alters tuning properties of pcp4a+ PVNs</i>	57
<i>Figure 11: Mutating pcp4a alters tuning properties of pcp4a+ PVNs</i>	59
<i>Figure 12: Mutating pcp4a does not alter tuning properties of SInS</i>	61
<i>Figure 13: Mutating pcp4a does not alter responses to visual stimuli at RGCs terminals</i>	62
<i>Figure 14: Inhibition of CaMKII reverts the effect of pcp4a mutation on pcp4a+ PVNs activity</i>	63
<i>Figure 15: Serotonergic and dopaminergic signaling regulate expression of pcp4a</i>	65
<i>Figure 16: Feeding increases activity in distinct dopaminergic nuclei</i>	66
<i>Figure 17: Dopaminergic signaling controls pcp4a transcription through regulation of cAMP levels</i>	68
<i>Figure 18: Dopaminergic signaling alters pcp4a+ PVNs tuning properties</i>	70
<i>Figure 19: pcp4a+ PVNs express both glutamatergic and gabaergic markers</i>	72
<i>Figure 20: Dopaminergic signaling alters gabaergic pcp4a+ PVNs size tuning properties</i>	73
<i>Figure 21: Dopaminergic signaling alters glutamatergic pcp4a+ PVNs size tuning properties</i>	75
<i>Figure 22: Dopaminergic signaling affects mainly size tuning properties of pcp4a+ / drd2+ PVNs</i>	77
<i>Figure 23: Model of the pcp4a pathway for feeding state-dependent modulation of behavioral choice</i>	81